THE IMPACT OF 2000-2050 CLIMATE CHANGE ON OZONE AND SECONDARY ORGANIC AEROSOL IN CHINA

LIU QIAN

Ph.D

The Hong Kong Polytechnic University

2014

The Hong Kong Polytechnic University
Department of Civil and Environmental Engineering

THE IMPACT OF 2000-2050 CLIMATE CHANGE ON OZONE AND SECONDARY ORGANIC AEROSOL IN CHINA

By
LIU QIAN

A thesis submitted in partial fulfillment of
the requirements for the degree of
Doctor of Philosophy

July 2013

CERTIFICATE OF ORGINALITY

I hereby declare that this thesis is my own work and that, to the best of my knowledge and belief, it reproduces no material previously published or written, nor material that has been accepted for the award of any other degree or diploma, except where due acknowledgement has been made in the text.

_________________________________ (Signed)

LIU QIAN________________________ (Name of student)

Abstract

Significant changes in global climate could affect the meteorological conditions in the future. The emission reduction policies aimed at reducing the negative impacts of air pollution should account for this potential change. Thus, this study uses air quality model system WRF/Chem to evaluate the impact of changes in climate, biogenic emission and anthropogenic emission on surface ozone (O_3) and secondary organic aerosol (SOA) concentrations based on coupled global climate model−regional climate and chemistry model approach (GCM−CTM).

The first concern of this study is to assess the WRF/Chem's ability in simulating the meteorological and chemical variables over China. The simulation has been implemented over East China domain and run for April 2008. The comparison between modeled and measured meteorological fields, hourly O_3 mixing ratios illustrates that the model well captured the real condition. The results show that the simulated near surface temperature and wind speed are all slightly higher than the observed data, with mean bias of 0.7 °C and 2.1 m s^{-1}, respectively. Hourly O_3 at 8 monitoring stations exhibits a correlation with observations among 0.57 to 0.80, and the mean biases are among -12.0 to 11.3 ppb.

Then a series of numerical experiments are conducted to investigate the relative contributions of climate and emission change to surface O_3 over South China for the period of October in 2005-2007 and 2055-57. WRF/Chem was driven by the outputs

of Community Climate System Model version 3 (CCSM3). The change of climate and biogenic emission can result in a change of -5 to 5 ppb of afternoon surface O_3 mixing ratios, with an average of 1.6 ppb over the land region in South China. Our analysis suggests that the anthropogenic emissions have greater impact on the change of surface O_3 concentration (12.8 ppb) over South China compared to climate change. The combined effect of climate and emission can increase afternoon mean surface O_3 over South China by an average of 18.2 ppb in the land region.

With WRF/Chem updated with the parameterization scheme for the isoprene SOA formation, the sensitivities of biogenic SOA concentration to changes in climate and biogenic emissions over China are investigated under IPCC A1B and B1 scenarios using the same approach. Projected changes in regional climate, the subsequent changes in biogenic emissions and BSOA concentrations are scenarios dependent. Under A1B scenario, significant increase of biogenic isoprene and monoterpenes emission occurs over South, Southwest, and Northeast China. In response to the change in climate and biogenic emissions, the surface BSOA concentration increases 0.22 $\mu g\ m^{-3}$ over China, with the highest increase up 1.2 $\mu g\ m^{-3}$ occurring over the South China and Central China. The simulations predict that the mean surface BSOA concentration increases 0.26 $\mu g\ m^{-3}$ over China under B1 scenario. Over Southeast China, a significant increase of biogenic monoterpenes emission is observed over Southwest China (32.7%). As a result, highest increases in MSOA levels were simulated over Sichuan province, with peaks exceeding 1.0 $\mu g\ m^{-3}$.

PUBLICATIONS

Liu, Q., Lam, K.S., Jiang, F., Wang, T.J., Xie, M., Zhuang, B.L., Jiang, X.Y., A numerical study of the impact of climate and emission changes on surface ozone over South China in autumn time in 2000–2050, Atmospheric Environment, 76, 227–237, 2013.

Nie, W., Wang, T., Wang, W.X., Wei, X.L., **Liu, Q**., Atmospheric concentrations of particulate sulfate and nitrate in Hong Kong during 1995–2008: Impact of local emission and super-regional transport, Atmospheric Environment, 76, 43–51, 2013.

Zhuang B.L., **Liu Q**., Wang T.J., Yin, C.Q., Li, S., Xie, M., Jiang, F., Mao, H.T., Semi-direct and indirect climate effects of fossil fuel black carbon aerosol over China, Theoretical and Applied Climatology, DOI: 10.1007/s00704-013-0862-8, 2013.

Jiang, F., Zhou, P., **Liu, Q**., Wang, T.J., Zhuang, B.L., Wang, X.Y., Modeling tropospheric ozone formation over East China in springtime, Journal of Atmospheric Chemistry, 69, 303–319, 2012.

Wei X.L., **Liu Q**., Lam K.S., Wang, T.J., Impact of precursor levels and global warming on peak ozone concentration in Pearl River Delta Region of China, Advances in Atmospheric Sciences, 29(3), 635–645, 2012.

Jiang F., **Liu Q**., Huang, X.X., Wang, T.J., Zhuang B.L., Xie, M., Regional Modeling of Secondary Organic Aerosol over China by Using WRF/Chem, Journal of Aerosol Science, 43, 57–73, 2012.

Liu Q., LAM K.S., Modeling the impact of 2000-2050 climate and emission changes on surface ozone over South China in autumn time, 2012 American Geophysical Union Fall Meeting, San Francisco, December 3 –7, 2012.

ACKNOWLEDGEMENTS

I would like to express my deepest gratitude to my supervisor Dr. K.S. Lam for his constant encouragement, guidance, and providing me with an excellent atmosphere for doing research. I appreciate his vast knowledge and skill in many areas, and his assistance in writing thesis.

Very special thanks go out to Prof. Wang Tijian and Dr. Xie Min of Nanjing University for their suggestion on regional climate and chemistry modeling.

I must thank my friends, particularly Jiang Fei, Ling Zhenhao, and Xu Yue for their support and care helped me overcome setbacks and stay focused on my graduate study.

I would also like to thank my family for their support through my entire life and in particular, I must acknowledge my husband without whose love and encouragement, I would not have finished this thesis.

CONTENTS

LIST OF FIGURE

LIST OF TABLE

Nomenclature

Symbol	**Description**
A1	The A1 storyline and scenario family describes a future world of very rapid economic growth, global population that peaks in mid-century and declines thereafter, and the rapid introduction of new and more efficient technologies. Major underlying themes are convergence among regions, capacity building and increased cultural and social interactions, with a substantial reduction in regional differences in per capita income. The A1 scenario family develops into three groups that describe alternative directions of technological change in the energy system. The three A1 groups are distinguished by their technological emphasis: fossil intensive (A1FI), non-fossil energy sources (A1T), or a balance across all sources (A1B) (where balanced is defined as not relying too heavily on one particular energy source, on the assumption that similar improvement rates apply to all energy supply and end use technologies). (IPCC, 2001)
A2	The A2 storyline and scenario family describes a very heterogeneous world. The underlying theme is self-reliance and preservation of local identities. Fertility patterns across regions converge very slowly, which results in continuously increasing population. Economic development is primarily regionally oriented and per capita economic growth and technological change more fragmented and slower than other storylines. (IPCC, 2001)
AGL	Above Ground Level
ALM	ALM region stands for the rest of the world and corresponds to developing countries in Africa, Latin America, and Middle East. (IPCC, 2000)
API	Alpha-pinene & other cyclic terpenes with one double bond
AQO	Air Quality Objective
AR4	Fourth Assessment Report
ARW	Advanced Research WRF
ASIA	ASIA region stands for all developing countries in Asia (excluding the Middle East). (IPCC, 2000)
AVHRR	Advanced Very High Resolution Radiometer
B1	The B1 storyline and scenario family describes a convergent world with the same global population, that peaks in midcentury and declines thereafter, as in the A1 storyline, but with rapid change in economic structures toward a service and information economy, with reductions in material intensity and the introduction of clean and resource-efficient technologies. The emphasis is on global solutions to economic, social and environmental sustainability,

	including improved equity, but without additional climate initiatives. (IPCC, 2001)
B2	The B2 storyline and scenario family describes a world in which the emphasis is on local solutions to economic, social and environmental sustainability. It is a world with continuously increasing global population, at a rate lower than A2, intermediate levels of economic development, and less rapid and more diverse technological change than in the B1 and A1 storylines. While the scenario is also oriented towards environmental protection and social equity, it focuses on local and regional levels. (IPCC, 2001)
BC	Black Carbon
BSOA	Biogenic Secondary Organic Aerosol
BSOC	Biogenic Secondary Organic Carbon
Ca	Calcium
CAM3	Community Atmosphere Model version 3
CBMZ	Carbon-Bond Mechanism version Z
CCSM3	Community Climate System Model version 3
CFC-12	Dichlorodifluoromethane
CH_3SO_3	Methanesulfonate
CH_4	Methane
CL	Chloride
CLM3	Land Surface Model version 3
CMAQ	Congestion Mitigation and Air Quality
CO	Carbon Monoxide
CO_2	Carbon Dioxide
CO_3	Carbonate
COE	Correlation Coefficient
CSIM5	Community Sea Ice Model version 5
CTM	Chemistry Transport Model
DEV	Developing Countries
EC	Elemental Carbon
FTIR	Fourier Transform Infrared Spectroscopy
GC/MS	Gas Chromatograph-Mass Spectrometer
GCM	General Circulation Model
GOCART	Goddard Chemistry Aerosol Radiation and Transport
GRIB	Gridded Binary or General Regularly-distributed Information in Binary form
HKEPD	Hong Kong Environmental Protection Department
HNO_3	Nitric Acid
HR	Hit Rate
IND	Developed Countries
INTEX-B	Intercontinental Chemical Transport Experiment-Phase B
IPCC	Intergovernmental Panel on Climate Change
ISOA	Isoprene secondary Organic Aerosol

LAI	Leaf Area Index
LIM	d-Limonene & other cyclic diene terpenes
LS/MS	Liquid chromatography–mass spectrometry
MADE	Modal Aerosol Dynamics Model for Europe
MAE	Mean Absolute Error
MB	Mean Bias
MEGAN2.04	Model of Emissions of Gases and Aerosols from Nature version 2.04
MM5	PSU/NCAR mesoscale model
MOSAIC	Model for Simulating Aerosol Interactions and Chemistry
MOZART4	Model for Ozone And Related Chemical Tracers version 4
MSOA	Monoterpenes Secondary Organic Aerosol
MYJ	Mellor–Yamada–Janjic
Na	Sodium
N_2O	Nitrous Oxide
NCAR	National Center for Atmospheric Research
NCEP	National Centers for Environmental Prediction
NetCDF	Network Common Data Form
NH_4	Ammonium
NMVOC	Non-Methane Volatile Organic Compounds
NO	Nitrogen Monoxide
NO	Nitric Oxide
NO_2	Nitric Dioxide
NO_3	Nitrate
NOAA	National Oceanic and Atmospheric Administration
Noah/LSM	Noah Land Surface Model
NO_x	Nitrogen Oxides
O_3	Ozone
OC	Organic Carbon
OECD90	OECD90 region groups together all member countries of the Organization for Economic Cooperation and Development as of 1990, the base year of the participating models. (IPCC, 2000)
PAN	Peroxyacetyl Nitrate
PBL	Planetary Boundary Layer
PBLH	Planetary Boundary Layer Height
PFT	Plant Functional Type
PM10	Particular Matter with diameter less than 10 μm
PM2.5	Particular Matter with diameter less than 2.5 μm
POA	Primary Organic Aerosol
POC	Primary Organic Carbon
POP	Parallel Ocean Program version 1.4.3
PPFD	Photosynthetic Photon Flux Density
PRD	Pearl River Delta
RACM	Regional Atmospheric Chemistry Mechanism

RADM2	Regional Acid Deposition Model 2
RAIN	Precipitation
RAQMS	Real-time Air Quality Modeling System
REF	REF region consists of countries undergoing economic reform and groups together the East and Central European countries and the Newly Independent States of the former Soviet Union. (IPCC, 2000)
RH2	2-m Relative Humidity
RMSE	Root Mean Square Error
RRTM	Rapid Radiative Transfer Model
SO_2	Sulfur Dioxide
SO_4	Sulfate
SOA	Secondary Organic Aerosol
SOC	Secondary Organic Carbon
SORGAM	Secondary Organic Aerosol Model
SRES	Special Report on Emissions Scenarios
STE	Stratosphere-Troposphere Exchange
SWDOWN	Downward Solar Radiation
T2	2-m Temperature
TAR	Third Assessment Report
ToF-AMS	Time-of-Flight Aerosol Mass Spectrometer
TRACE-P	Transport and Chemical Evolution over the Pacific
UCM	Urban Canopy Model
USGS	U.S. Geological Survey
VOCs	Volatile Organic Compounds
WD10	10-m Wind Direction
WPS	WRF Preprocessing System
WRF	Weather Research and Forecasting
WRF/Chem	Weather Research and Forecast model coupled with Chemistry
WS10	10-m Wind Speed
WSM3	WRF Single-Moment 3-class scheme
WSM5	WRF Single-Moment 5-class scheme
WSM6	WRF Single-Moment 6-class scheme

Chapter 1 Introduction

1.1 Background

Air pollution is one of the most important and challenging issues for mega cities in the world. With rapid urbanization and industrial development in recent years, highly elevated ozone (O_3) and aerosol concentrations were frequently reported in megacities including Beijing, Shanghai, and the Pearl River Delta (PRD) regions (Chan and Yao, 2008). It was reported that PM10 concentrations in Beijing exceeded the China's Grade-2 Standard (1-day average of 150μg m-3) on more than 100 days per year during the period of 1999 - 2005 (Gao et al., 2011b). PRD has experienced severe photochemical pollution with surface O_3 levels frequently exceeding the Hong Kong Air Quality Objective (AQO, 1-h average 240 μg m^{-3} or 120 ppb) since the 1990s, especially in autumn with northerly winds and clear sky conditions (Huang et al., 2005; Ling et al., 2013).

Many studies have pointed out that air pollution can exert detrimental effects on human health, plants and ecosystems (Bell et al., 2005; Emberson et al., 2003). In order to protect public health, Chinese government officials have implemented a variety of policies to reduce emissions and ambient concentrations of precursors. However, other than precursor emissions, meteorological factors such as temperature, water vapor, precipitation, cloud cover, wind speed, and mixing depth are also directly or indirectly responsible for the change of atmospheric composition in the boundary layer. Climate change induced by greenhouse gases could significantly affect the meteorological conditions in the future. The changes in meteorological factors could directly affect the air quality through the processes of emission, chemical transformation, transport, and deposition. Besides, the changes in climate are likely to alter the vegetation and land covers which could further influence air quality via altering biogenic emissions and dry deposition. Those potential changes should be taken into account when implementing the emission reduction policies aiming at reducing the negative impacts of air pollution. Increasing efforts has been devoted to explore those potential changes and their roles in air quality. The sensitivities of O_3 air quality to climate change have been investigated extensively in a number of studies since 1990s, although only a few of them reported the important responses of aerosols to climate change.

Surface O_3 is formed by photochemical reactions involving carbon monoxide (CO), volatile organic compounds (VOCs) in the presence of nitrogen oxides (NO_x=NO + NO_2) under the sunlight. Jacob et al. (2009) reviewed a large number of studies and concluded that there are three common approaches to investigate the response of O_3 air quality to climate change. The first method is to study the statistical correlation between O_3 concentrations and meteorological variables which establishes an observational basis for diagnosing this effect. This approach analyzes long-term trends of O_3 concentrations and constructs empirical models for O_3 forecasts (Lin et al., 2001; Camalier et al., 2007). The other two approaches use numerical model. One approach explores the impact of climate change on regional O_3 by using regional climate chemistry model through perturbing individual meteorological and emission variables (Steiner et al., 2006; Dowson, et al., 2007a; Millstein et al., 2009). In the early development stage, most researches started with exploring the impact of temperature on the photochemistry of O_3. A number of them have directly pointed out that there is a positive correlation between O_3 concentration in lower troposphere and temperature (Jacob et al., 1993; Sillman and Samson, 1995). Johnson et al. (2005) summarized the possible influence on surface O_3 in the future due to the changes in meteorological factors. The other approach is using chemistry transport model (CTM) driven by the outputs of global circulation model (GCM). With global climate and chemistry modeling, Wu et al. (2008a) estimated the future changes in surface O_3 concentrations as a result of future climate and anthropogenic emission changes. Hogrefe et al. (2004) reported the first study applied the coupled GCM, regional climate model and regional CTM to address the climate change influences on surface O_3 concentrations in eastern US. Jiang et al. (2008b) evaluated the impacts of climate and land use change on surface O_3 in Houston through a modeling system of a global climate model and Weather Research and Forecast model coupled with Chemistry (WRF/Chem).

Atmospheric aerosol is defined as solid or liquid particles suspending in the air, including sulfate (SO_4), ammonium (NH_4), nitrate (NO_3), organic carbon (OC), elemental carbon (EC), crustal dust and sea salt. They are emitted directly from natural and anthropogenic sources or produced in the atmosphere through the condensation of low-volatile trace gases. Due to the varieties of aerosol components and the complex coupling between aerosol and meteorological variables, observed correlations approach is barely using in aerosol studies (Jacob et al., 2009). That leaves numerical experiment as a better choice to study of the response of aerosol to climate change. Dawson et al. (2007b) examined the individual effects of temperature, absolute humidity, mixing height, wind speed, etc., on PM2.5 concentrations in east US through perturbing meteorological parameters in regional CTM. There are also a few global and regional GCM-CTM studies examine the impact of climate change on aerosol concentrations (Tagaris and Kanakidou, 2007; Avise et al., 2009). They concluded that precipitation and water vapor are the most important factors. Increasing biogenic emissions in the future could be another important factor affecting secondary organic aerosol (SOA) and PM $_{2.5}$ concentrations. The impact of future climate change and the subsequent changes in biogenic emissions on SOA formation in global and regional scales have been estimated by Heald et al. (2008), Zhang et al. (2008c) and Jiang et al (2010c). It is indicated that the changes in temperature, radiation and biogenic emission play a relatively important role in SOA formation.

1.2 Aim and Objectives

The aim of this study is to gain some understanding of the potential impacts of climate change on regional air quality in China, which would help air quality managers consider this potential change when implementing policies aimed at reducing the detrimental effects of O_3 and SOA.

There are three major objectives:

1. To evaluate the performance of the regional climate chemistry model (WRF/Chem) based on present data;
2. To explore the impact of future climate change and the parallel changes in anthropogenic emissions on surface O_3 by applying regional climate and chemistry transport model driven by future global climate model outputs;
3. To investigate the responses of SOA formation to future climate change and the subsequent changes in biogenic emissions in regional scale.

1.3 Outline

This report will cover seven chapters:

1) The first chapter introduces the background of air quality and the significance of this study.

2) Chapter 2 briefly reviews literatures of O_3 and SOA chemistry, future changes in air pollution meteorology, and general approaches adopted to examine the impact of climate change on O_3 and SOA.

3) Chapter 3 provides the methodologies adopted in this study including model description, improvement, and data set.

4) The impacts of biogenic emissions and anthropogenic sources on O_3 formation over East China in spring time are examined in Chapter 4 using regional chemical transport model (WRF/Chem).

5) Chapter 5 investigates the impact of climate and emission changes on surface O_3 over South China in autumn time using the coupled GCM and regional climate and chemistry model (CCSM-WRF/Chem).

6) Chapter 6 discusses the effect of climate and biogenic emissions changes under different scenarios on biogenic SOA over China in summer time using CCSM-WRF/Chem model system.

7) The key findings and interpretations of this study and a few recommendations for further research are concluded in Chapter 7.

Chapter 2 Literature review

This chapter reviews the background of climate change, O_3 and SOA. The literature review begins with an introduction of O_3 chemistry and O_3 pollution study in Sections 2.1. Section 2.2 describes the SOA formation, properties and modeling schemes. In section 2.3, basic information on climate change that has a general effect on air quality was introduced. Then, three common methods used in examining the climate change effect on surface O_3 studies during the past 30 years were summarized in section 2.4. Section 2.5 concludes this chapter by addressing the niche of this study.

2.1 O_3 air quality

2.1.1 O_3 chemistry

O_3 is a reactive oxidant trace gas in the atmosphere, most of which (90%) is found in the stratosphere where it blocks harmful solar ultraviolet radiation from reaching the ground. As compared with the stratosphere, O_3 concentrations in the troposphere (0 -10 km in altitude) are very low. However, tropospheric O_3 plays a key role in climate change and air quality (NRC, 1991). It not only determines the oxidizing capacity of the atmosphere but also acts as an infrared absorber in the atmosphere (Lelieveld and Dentener, 2000; Staehelin et al., 2001).

In the troposphere, O_3 is formed by photochemical reactions involving CO, VOCs in the presence of NO_x under the sunlight. Another source of the tropospheric O_3 is stratospheric O_3 transported down across the tropopause. The formation of O_3 is associated with two major classes of precursors: NO_x and VOCs. The reactions of VOCs or CO with the OH radical **[R1, R2]** initiate the photochemical reactions. Then NO is converted to NO_2 through the reactions with HO_2 or RO_2 radical **[R3, R4]**. Through reactions of R5 and R6, O_2 combines the atomic oxygen generated by NO_2 to create O_3 **[R5, R6]**.

(R1) $VOCs + OH \rightarrow RO_2 + H_2O$

(R2) $CO + OH \rightarrow HO_2 + CO_2$

(R3) $RO_2 + NO \rightarrow RO + NO_2$

(R4) $HO_2 + NO \rightarrow OH + NO_2$

(R5) $NO_2 + hv \rightarrow NO + O$

(R6) $O + O_2 + M \rightarrow O_3 + M$

The hydroxyl radical is one of the key reactive species in the process of O_3 formation in the troposphere. It can oxidize VOCs, methane or CO to form HO_2, RO_2 radicals. Without the hydroxyl radical, O_3 formed through the reactions **[R5, R6]** can be quickly regenerated to NO_2 via **[R7]** resulting in no net O_3 formation.

(R7) $O_3 + NO \rightarrow O_2 + NO_2$

The termination of this process includes the self-reaction of peroxy radicals **[R8, R9]**, the nitric acid forming reaction **[R10]**, the reaction of RO_2 with NO to form alkyl nitrates **[R11]** and the reversible formation of Peroxyacetyl nitrates (PANs) **[R12]**. The decomposition of PANs is highly temperature dependent. So the PANs in the upper troposphere are quite stable which can undergo long range transport and thus commonly act as a reservoir for NO_x.

(R8) $HO_2 + HO_2 \rightarrow H_2O_2 + O_2$

(R9) $RO_2 + HO_2 \rightarrow ROOH + O_2$

(R10) $OH + NO_2 \rightarrow HNO_3$

(R11) $RO_2 + NO \rightarrow RONO_2$

(R12) $CH_3C(O)OO + NO_2 \leftrightarrow CH_3C(O)O_2NO_2$

The O_3 formation process is determined by the competition between VOCs and NO_x for the OH radical **[R1,R10]**. Under the high ratio of VOCs/NO_x, OH will mainly react with VOCs to form peroxy radicals which would facilitate the O_3 formation. While at a low ratio of VOCs/NO_x, the reaction between NO_x and OH predominates resulting in the decrease of OH and NO_x. Thus this reaction will retard the formation of O_3. When NO_x concentration continues decreasing to a very low value, self-reaction of peroxy radicals becomes the main termination pathway.

In general, the relation between O_3, NO_x and VOCs is complex: O_3 production does not increase linearly with an increase in the precursor concentrations. O_3 isopleth diagram (Figure 2.1) simply represents their relationship which shows peak O_3 concentrations as a function of initial amounts of NO_x and VOCs. Jeffries and Crouse (1990) generated this plot based on the simulations in Atlanta using Carbon Bond 4 chemical mechanism. As shown in the figure, the plot can be separated into two parts by the ridge line. Above the ridge line, at a high NO_x-to-VOCs ratio, the reduction of the VOCs concentration can lead to dramatically decrease of the O_3 concentration, which implies controlling VOCs would reduce O_3 concentrations. Below the ridge line, at a low NO_x-to-VOCs ratio, controlling the NO_x would reduce O_3 concentration. Therefore, the NO_x-to-VOCs ratio is a key factor to indicate the sensitivity of O_3 formation. The crossover point between these two regions depends on the amount and ratio of VOCs and NO_x as well as the production of peroxy radicals (Sillman et al., 1990; Thornton et al., 2002; Kleinman, 2005).

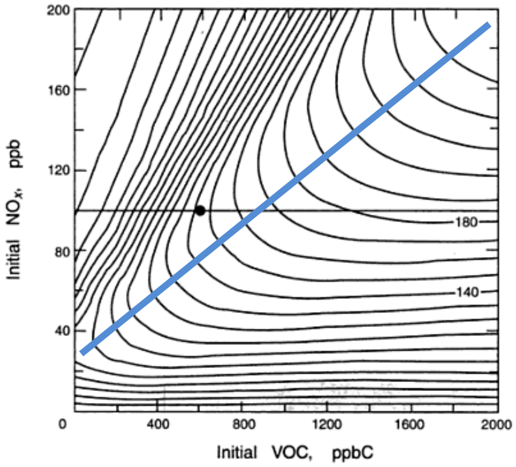

Figure 2.1 O_3 isopleth diagram for Atlanta (Adapted from Jeffries and Crouse, 1990)

2.1.2 O_3 air quality study

As a country with rapid urbanization and industrialization in recent years, O_3 pollution is of great concern in China. Chinese researchers have performed a number of field measurements and numerical studies to reveal the mechanism of O_3 formation, transport and deposition processes, especially in metropolitan areas including PRD, Beijing-Tianjing, and Yangze River Delta (YRD) (Chan and Yao, 2008). Severe air pollution with surface O_3 levels exceeding the AQO standard (1-h average of 240 μg m^{-3} or 120 ppb) were frequently observed in these regions since the 1990s (Huang et al., 2005; Ling et al., 2013).

Increasing emissions in O_3 precursors are identified to be the key factors influencing the ambient O_3 concentrations. A steep increase in NO_x emissions was indicated through both emission estimate on NO_x and satellite-sensed column concentrations of NO_2 in China (Zhang et al., 2007b; Zhang et al., 2009; Lamsal et al., 2011; Lin et al., 2010). Positive trends of ground-level O_3 concentrations were observed in both urban and rural areas of China. Due to the sharp rise in anthropogenic emissions since the 1990s, a steady increase trend in daytime O_3 was observed during 1991–2006 at a rural site in the YRD (Xu et al., 2008). By analyzing the data collected during MOZAIC (Measurement of O_3 and Water Vapor by Airbus In-Service Aircraft) campaign (with data concentrating in 1997 to 1998 and 2005), Ding et al. (2008) indicated that daytime O_3 concentrations in the lower troposphere of Beijing had increased by about 2% per year. Surface O_3 in the background atmosphere of South

China has seen its steady increase at an average rate of 0.58 ppbv yr^{-1} during the period of 1994−2007 as a result of the increasing NO_2 emissions in mainland China (Wang et al., 2009).

Seasonal patterns for surface O_3 were analyzed at both rural and urban areas in China. Monthly mean O_3 concentration was found to reach a narrow peak May or June and a sharp decrease in July and August at Lin'an in eastern China (Wang et al., 2001; Luo et al., 2000; Xu et al., 2008), a rural site at Shangdianzi in north China (Lin et al., 2008b), and three mountaintop sites in central China (Mount Tai, Mount Hua, and Mount Huang) (Li et al., 2007). In South China, observations at a coastal background site (Hok Tsui), a rural site (Jinguoling), a urban site (Luhu) and three suburban site (Tai O, Tung Chung and Wanqingsha) showed that the seasonal cycle of surface O_3 had a broad summer minimum and an autumn maximum (Lam et al., 2001; Wang et al., 2005a; Wang et al., 2009; Zheng et al., 2010). O_3 profiles recorded from MOZAIC Aircraft program taken in Beijing (Ding et al., 2008) and ozonesonde observations in Hong Kong (Liu et al., 2002) also showed that the minimum O_3 concentrations in the boundary layer occurring in July and August. He et al. (2008) suggested that the East Asia summer monsoon is the main reason resulting in the observed summer minimum in surface O_3 over the eastern China and the west Pacific region. On the contrary, a summertime maximum of surface O_3 during May–August was observed at Mt. Waliguan located in Qinghai province.

It is widely recognized that surface O_3 concentration is highly sensitive to the meteorological conditions. Besides the long-term trend and seasonal cycle analysis, roles of meteorological conditions in O_3 pollution were also investigated through intensive field campaigns. Typically, the studies pointed out that the O_3 episodes generally associated with warm weather, light winds, clear skies, and stagnating weather systems. From June 1999 to July 2000, field study of meteorological factors, air pollutants including O_3, CO, NO_x, and SO_2 was carried out at Lin'an in eastern China (Cheung et al., 2001). Analysis indicated that the large-scale stagnation, intense solar radiation, and minimum rainfall lead to the formation of serious O_3 pollution. In October 2004, Zhang et al. (2008b) conducted a comprehensive campaign (PRIDE-PRD2004) to deeply examine the characteristics of O_3 and its precursors in PRD. It is reported that in most of the sampling days, the O_3 mixing ratios at Xinken were higher than China's Grade III Standard (hourly average O_3 concentration at $200\mu g/m^3$). Meteorology analysis indicated that the high O_3 days over Xinken station were associated with inversion layers as well as quite specific vertical wind velocity profiles (Fan et al., 2008). A number of researches indicated that tropical cyclone located in the Northwestern Pacific Ocean or the South China Sea is the most important synoptic pattern for the occurrence of O_3 episodes in PRD region (Lam et al., 2005; Huang et al., 2005; Jiang et al., 2008a). Anticyclones located over mainland China to the north and troughs appearing over the South China Sea are also important synoptic patterns which facilitated the occurrence of O_3 episodes in PRD region (Huang et al., 2006; Jiang et al, 2010a). In autumn, particularly in the presence of high-pressure systems and distant tropical cyclones over the northwestern Pacific Ocean, the northerly winds and clear sky conditions are favor for the formation of severe regional pollutions.

The relationship between O_3 and its precursors (VOCs and NO_x) is another major science question that the campaigns tried to address. Previous studies showed that the formation of O_3 in PRD region is controlled by VOCs (Zhang et al., 2007a; Guo et al., 2009). Based on the observation based model (OBM), Zhang et al. (2007a) investigated ten O_3 episode cases occurring in autumn 2002 and pointed out that the formation of O_3 over Hong Kong was controlled by VOCs, especially the reactive aromatics. Field campaign of the main air pollutants was carried out between 22 October and 1 December 2007 at two sites in PRD (Guo et al., 2009). The difference in O_3 formation mechanisms between inland PRD region (WQS) and Hong Kong (TC) was examined. Remarkable differences in diurnal variations indicated that O_3 formation in Hong Kong is more sensitive to VOCs compared to the inland PRD region.

Chemical transport models including WRF/Chem, CMAQ, PATH are useful tools for exploring the characteristic of surface O_3 and its precursor and accessing different roles of atmospheric processes in O_3 formation on regional scale. Wang et al. (2005b) adopted a coupled regional climate and chemistry model to estimate the relatively importance of emissions from transportation, industry and power plant on ambient O_3,

NO_x, CO and VOC concentrations in PRD in March 2001. The results showed that the transportation emission was the dominant contributor for O_3 and its precursors. Huang et al. (2005) adopted three-dimensional air quality model to investigate O_3 production sensitivity to its precursors in an O_3 episode related to tropical cyclones. The simulation experiments indicate that the O_3 formation in PRD is limited by VOCs. The sensitivity of O_3 formation to biogenic VOC emissions was investigated through MM5-CMAQ model system (Wei et al., 2007). Using coupled MM5 and CMAQ model, Wang et al. (2010b) found the O_3 formation is controlled by VOCs in the central inland PRD, PRE, and surrounding coastal areas, but is controlled by NO_x in the rural southwestern PRD. With application of the similar model system, Kwok et al. (2010) simulated the O_3 concentrations at four months in 2004 over Hong Kong and PRD using the same air quality modeling system. The monthly mean simulated and observed O_3 concentrations were 43.6 ppb and 37.9 ppb in October 2004 at 6 HKEPD stations, which was higher than the other month (Jan, Apr, and Jul). The response of seasonal variations of boundary layer O_3 in East Asia to choice of chemical mechanisms, meteorological fields, boundary conditions, and model resolutions was evaluated by Lin et al. (2009a) using CMAQ. It is indicated that the accurate simulation of the East Asia summer monsoon is critical for conducting boundary layer O_3 modeling over China. WRF/Chem, a new generation of regional air quality modeling system, has been successfully applied to examine the spatiotemporal evolution of O_3 pollution (Jiang et al., 2008a). GEOS-CHEM, a global chemistry model, was applied to analyze the meteorological conditions and interoperate observations which suggested that the reduction in emissions of NO_x and VOCs in Beijing and surrounding areas accounted for 45% of the O_3 reduction during the Olympics Period (8–24 August, 2008) (Wang et al., 2010a).

2.2 SOA

Organic aerosol, a complex mixture of chemical compounds containing carbon–carbon bonds, can be primary (POA) or secondary (SOA). POA is directly emitted to the atmosphere from biogenic and anthropogenic sources, while SOA is formed through the oxidation of gas-phase precursors in the atmosphere (Alves and Pio, 2005; Wang et al., 2005c). It has been known that organic material generally accounts for 20–50% of the total fine particle (PM2.5) at continental mid-latitudes. The percentage can go up to 90% over tropical forest (Kanakidou et al., 2005). Organic aerosol has been associated with human health, atmospheric visibility, climate change, etc., and thus it has received more attention in recent years (Kanakidou et al., 2005; Mauderly and Chow, 2008).

In the past two decades, considerable efforts have been made to investigate SOA precursors, formation processes, and properties through laboratory experiment, field measurements and modeling studies (Odum et al., 1996; Pandis et al., 1992; Claeys et al., 2004). The SOA concentrations, chemical composition and their contributions to total OC were identified through field measurements of carbonaceous aerosols. The analytical techniques include EC tracer method, off-line method, and on-line method. The EC tracer method is an indirect method which could only estimate the total concentration of SOA. Offline technologies, including GC / MS (Kotianova et al., 2004), LC / MS (Anttila et al., 2005), NMR (Decesari et al., 2001), and FTIR (Sax et al., 2005; Polidori et al., 2008), usually provide specific information on individual SOA species and also functional groups. On-line techniques, including AMS (McKeown et al., 1991; Murphy et al., 2007) and TOF-AMS (Drewnick et al., 2005; DeCarlo et al., 2006), can provide near real-time data on certain level of chemical characterization but less specific information.

Through EC tracer method, Lim and Turpin (2002) estimated that SOA with a mean concentration of 3.9 ± 2.2 μgC m^{-3} constituted 46% of the total OC over the Atlanta area. Yu et al (2007) studied the observed samples at 142 observation stations of the United States in 2001. The annual mean concentration of secondary organic carbon (SOC) was 0.42 μgC m^{-3} over the continental United States, with the highest concentration in summer (0.63μgC m^{-3}) and the lowest concentration (0.13 μgC m^{-3}) in winter. Strader et al. (1999) estimated that the SOA concentrations were up to 15-20 μgC m^{-3} under appropriate conditions (such as clear skies, weak wind, etc.). Estimated SOC contributions to total OC in Berlin, Germany in 2010 were between 7% and 42% in PM10 and between 11% and 60% in PM1, which is slightly lower than observed in US- or Asian cities (Wagener, et al., 2012). In China, the compositions of carbonaceous aerosol at 14 cities were investigated by Cao et al.

(2007) during summer and winter seasons in 2003. It is estimated that SOC constituted 31.7% of total carbon in Chinese urban environments. Zhang et al. (2008a) investigated the EC and OC concentrations at 18 stations over different regions of China during 2006. The mean SOC to OC loading were estimated about 67% for the regional sites aerosols. PM2.5 samples observed at five sites of Beijing showed that organic aerosols constituted up to 42% of PM2.5 in winter and SOA was estimated at >50% and as high as 95% of total OC in summer (Dan et al., 2004).

According to the laboratory chambers, biogenic terpenes (Lee et al., 2006a; Lee et al., 2006b) and anthropogenic aromatics (Kleindienst et al., 2004) can be oxidized to form SOA. Recently, the results from both chamber experiments and field measurements have confirmed that isoprene is also an important precursor of SOA (Carlton et al., 2009). It is pointed out that the oxidation of isoprene can contribute to a significant amount of SOA especially under high NO_x experimental conditions. Applied with EC tracer and GC/MS method, Kleindienst et al. (2007) indicated that SOA formation from isoprene, α-pinene, β-caryophyllene, and toluene contributed significantly to the ambient OC concentrations. The environment factors including temperature, relative humidity, the pre-existing absorbing aerosol concentration, NO_x concentrations, and environmental pH could affect the formation of SOA. A number of smog chamber experiments and numerical simulations investigated the impact of individual factor on SOA concentrations (Cocker et al., 2001a; Cocker et al., 2001b; Jonsson et al.,2008; Presto et al.,2005; Ng et al., 2007; Lane et al., 2008; Song et al., 2007).

For SOA simulation, it is important to understand and illustrate the oxidation reactions of organic species in the gas-phase and their heterogeneous reactions, which generate low volatility organic compounds, and the conversion mechanism between the gas phase (low volatility organic compounds) and the particle phase (SOA). These processes are very complex and haven't been clearly understood so far. According to the data observed from chamber experiments and field measurement, the gas-particle partitioning theory has been developed to describe the SOA formation process (Pankow, 1994; Odum et al., 1996). It is addressed that a precursor VOC can be oxidized by the oxidants including OH radical, NO_3 radical and O_3 to form semi-volatile organic compounds. And then the gas-phase semi-volatile organic compounds can be transferred to the aerosol phase through the partitioning process (Seinfeld, et al., 1999). The partitioning of semi-volatile organic compounds between the gas phase (G_i) and the aerosol (Ai) is expressed as

$$\frac{A_i}{G_i} = M_0 K_{om,i} \qquad (1)$$

where M_0 is the mass concentration of the total pre-existing absorbing aerosol, $K_{om,i}$ is the partitioning coefficient.

$$K_{om,i} = \frac{1}{C^*_{sat,i}} = \frac{RT}{\gamma_i p_i^0 m_i 10^6} \qquad (2)$$

in which $C^*_{sat,i}$ is the saturation vapor concentration, R is the ideal gas constant, T is temperature (K), m_i is the molecular weight of the organic compound (g mol^{-1}), γ_i is the activity coefficient of compound, and p_i^0 is the sub-cooled liquid vapor pressure at the temperature T.

Based on the gas-particle partitioning theory, a 2-product partitioning approach was proposed by odum et al. (1997) to estimate the SOA chemical formation process. This approach is the most widely used method in SOA simulation. It is assumed that a precursor VOC can be oxidized by OH radical, NO_3 radical and O_3 to form only two semi-volatile organic compounds.

Both global and regional models applied with 2-product partitioning approach are conducted to study the SOA formation at different scales (Henze and Seinfeld, 2006; Henze et al., 2008; Liao et al., 2007; Heald et al., 2008; Zhang et al., 2008c; Jiang et al., 2010c). On global scales, the total biogenic SOA (BSOA) fluxes are estimated ranging from 12 to 70 Tg/yr (Kanakidou et al., 2005). Liao et al. (2007) investigated the biogenic SOA distributions over the U.S. through updating a SOA module into a GEOS-CHEM model. It was estimated that SOA constituted up to 38% of PM2.5 in different regions of the U. S. Among those, SOA contributed from terpenes was predicted to contribute 50.5% of the biogenic SOA burden over the United States, while isoprene contributed 49.5% of the biogenic SOA burden. With the rapid economic development, China has become a major contributor to global organic aerosols (16% in year 2000) and anthropogenic VOCs emissions (Saikawa et al., 2009; Piccot et al., 1992). Global model studies also showed that there are high SOA concentrations in China (Tsigaridis and Kanakidou, 2003 and Hoyle et al., 2007). In China, applying with RAQMS model, Han et al. (2008) simulated regional organic aerosols distributions with the study period covered the summertime. High SOC concentrations were found in the forest areas of southeastern, southwestern and northeastern China. Jiang et al. (2012) investigated the seasonal variations of SOA distributions over China for a full year period using WRF/Chem. The SOA concentration was simulated using secondary organic aerosol model (SORGAM). It is estimated that the contribution of BSOA for the whole of China reached 59%, 74%, 61%, and 41% in spring, summer, autumn, and winter, respectively.

2.3 Climate change and its impact on meteorological factors

The climate system is a very complex with interacting components including the atmosphere, land surface, oceans, snow and ice, and living things. Solar radiation provides the most significant energy to drive the climate system. When the radiation balance of the Earth is changed, the climate will responds directly to such changes. It is believed that human activity is one of the important factors inducing the global climate change since 17th century. A wide range of substances including gases and aerosols are emitted into the atmosphere because of the human activity. Both gases and aerosols have contribution to climate change. The greenhouse gases including carbon dioxide (CO_2), methane (CH_4), nitrous oxide (N_2O) and dichlorodifluoromethane (CFC-12) et al. directly alter the longwave radiation from Earth back towards space. The changes in albedo due to the changes in aerosols and cloud cover have significant impact on reflecting solar radiation. The Intergovernmental Panel on Climate Change (IPCC) AR4 report presents that global CO_2 concentration increased about 100ppm from pre-industrial period to 2005; the global atmospheric concentration of CH_4 in 2005 was 1774ppb, compared to 715ppb in pre-industrial period (IPCC, 2007). Furthermore, the changes in earth surface property due to human activity activities will also influence the climate system through altering the surface albedo. According to the 4th IPCC report the global mean surface temperatures have increased $0.74\,^{\circ}C \pm 0.18\,^{\circ}C$ in the last century (IPCC, 2007). And it is predicted to increase further in the coming century.

In order to quantitative analysis the climate change in the future, IPCC prepared the Special Report on Emissions Scenarios (SRES) in the Third Assessment Report (TAR) in 2001. Emissions scenarios are defined into four scenario families (A1, A2, B1 and B2) considering different development pathways in economic, population, and technology. The 'A' corresponds to an emphasis on market forces, while 'B' denotes the world with sustainable development. The '1' or '2' denotes the economic development rates, world economic and technological convergence (Wigley et al., 2002). For example, A1 represents "a future world of very rapid economic growth, global population that peaks in mid-century and declines thereafter, and the rapid introduction of new and more efficient technologies" (IPCC, 2000). According to the different technological development characteristics in the energy system, the A1 develops into three groups: 1) fossil fuel intensive (A1FI), 2) non-fossil energy sources (A1T), 3) a balance across all sources (A1B). The projected concentrations of CO_2, CH_4 and N_2O under the six scenarios over 21st century are shown in Figure 2.2. The SRES scenarios are developed based on different region aggregations (OECD90, REF, ASIA and ALM). The OECD90 and REF regions referred to developed countries (IND), while the ASIA and ALM regions referred to developing countries (DEV) (IPCC, 2000).

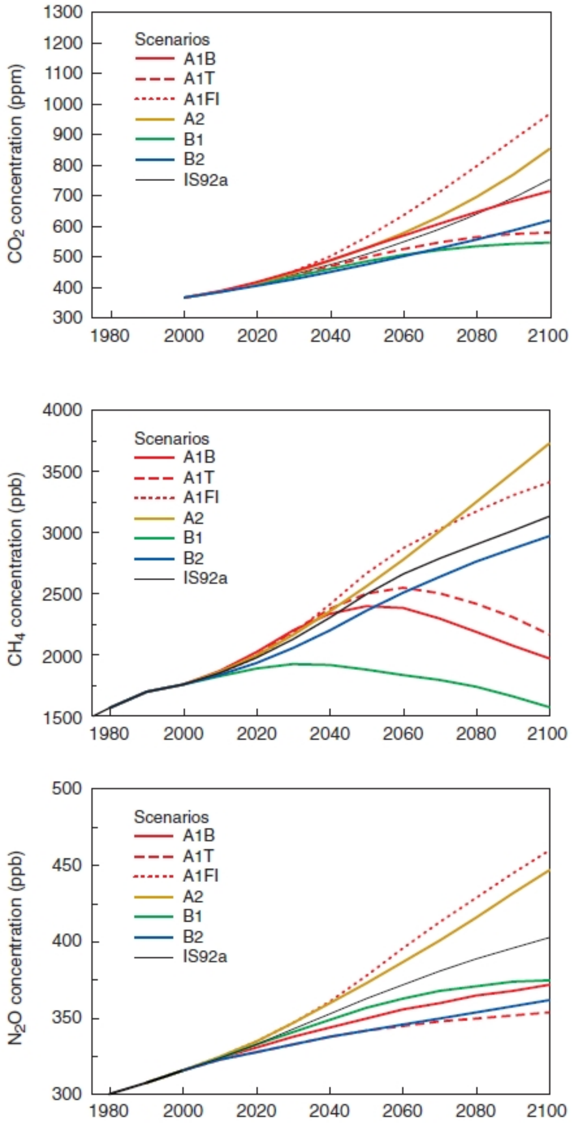

Figure 2.2 Projected changes over the 21st century in the atmospheric concentrations of CO_2, CH_4, and N_2O based on the IPCC SRES emissions scenarios (Adapted from IPCC, 2001)

Emissions scenarios are very helpful which can be used to drive GCM to develop future climate change scenarios. IPCC AR4 adopted about 20 GCM models to evaluate the future global climate change according to different future emission scenarios (IPCC, 2007). The report pointed out that there will be further warming and intense changes in the global climate system during the next 100 years due to human activities. And the trend would increase at a rate faster than those observed during the past 100 years. Briefly, the likely range for surface temperature is 1.1 °C~ 6.4 °C under six emissions scenarios at 2090~2099, compared to 1980~1999. Figure 2.3 shows the changes in annual mean surface temperature for 2046~2065 vs. 1980~1999 and 2080–2099 vs. 1980–1999 based on the scenarios A1B (top), B1 (middle) and A2 (bottom). The change patterns of temperature are basically consistent for the three SRES scenarios in these two periods. At the end of this century, simulations with B1 scenario are the coolest while simulations based on A2 scenario are the warmest. In each experiment, warming over the Northern Hemisphere is relative large than over the Southern Hemisphere, especially over northern mid- and high latitudes continents, the Arctic and along the equator in the eastern Pacific.

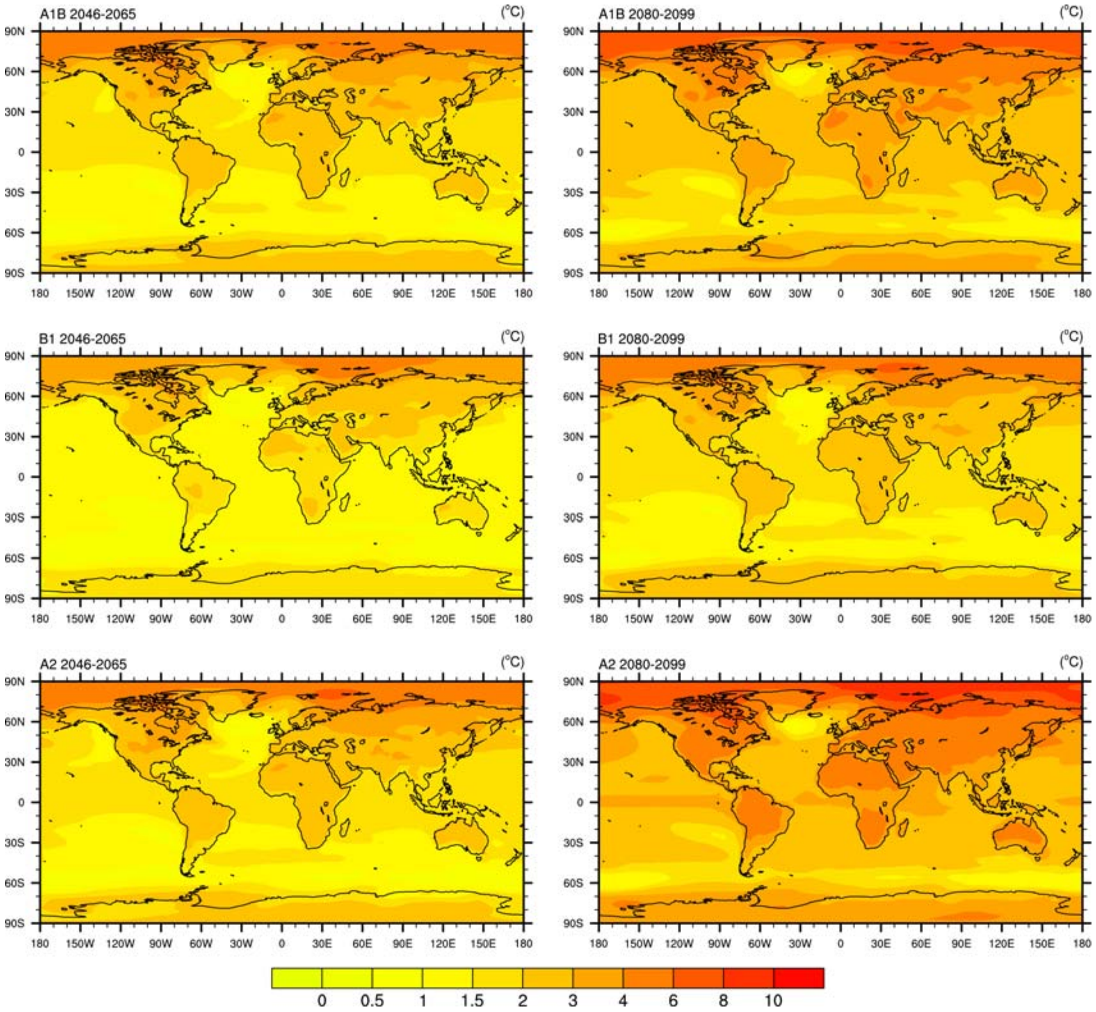

Figure 2.3 Annual mean surface air temperatures changes for 2046~2065 vs. 1980~1999 and 2080–2099 vs. 1980–1999, based on the simulation results from 20 GCMs adopted in IPCC AR4.

In response to the significant surface warming, evaporation from the ocean will increase. Higher temperature in the future allows the atmosphere to hold more water. Thus, water vapor, evaporation and precipitation are expected to increase in the future at on a global scale. The precipitation generally increases in both part of tropical areas (monsoon regimes) and high latitudes areas, with general decreases in the subtropics for the three emission scenarios (Figure 2.4). In the land region, there are dramatic reductions of precipitation the southern parts of Europe and North America. On the contrary, obvious increases are found over the northern parts of these two continents. The precipitation increases at most parts of Asia except the Middle East region. In the Southern Hemisphere, obvious reductions of precipitation are found over most parts of the land region except the middle east Africa.

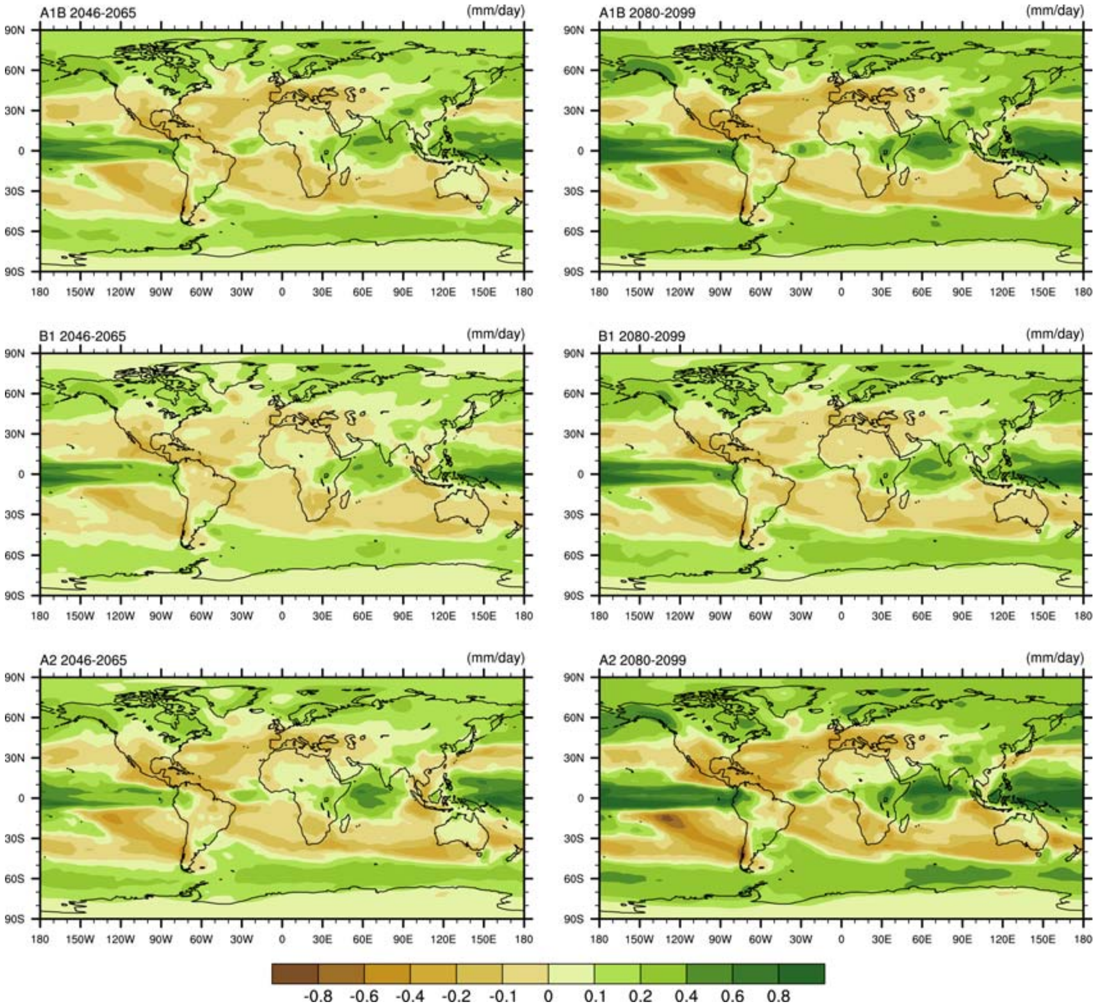

Figure 2.4 Annual mean precipitation changes for 2046~2065 vs. 1980~1999 and 2080–2099 vs. 1980–1999, based on the simulation results from 20 GCMs adopted in IPCC AR4.

The cold fronts of mid-latitudes cyclones were reported to be very useful weather system for ventilating air pollutions. The moving cold fronts in Asian can facilitate the transport of Chinese pollution to the free troposphere (Liu et al., 2003). A strong inter-annual correlation between the number of mid-latitude cyclones and the number of high-O_3 episodes were observed in the northeastern U.S. during the period of 1998 – 2006 (Leibensperger et al., 2008). It is widely accepted that future there is a reduction in the frequency of mid latitude cyclone in each hemisphere and the prevailing cyclone tracks will shift poleward (IPCC, 2007).

Regional climate model (RCM) driving by GCMs is an important downscaling technique for its higher resolution and better representation of physical processes. Over the past 20 years, with application of RCM, Chinese scientists have conducted a lot of research in predicting the future climate change in East Asia under different emission scenarios. The predicted trends in China are basically the same as the general trend in Global Climate Change in the 21th century. Based on the RegCM2 regional climate model, Gao et al. (2003a, b) simulated the climate change by doubling the CO_2 concentration in the model input. The result indicated that the surface mean temperature will increase by 2.5 ^{o}C and the precipitation will increase by 12% in China region. Jiang et al. (2008c) analyzed the trend of climate change in the next century in China region based on the emission scenarios A2, A1B and B1. And the conclusion is that the temperature would increase about 1.6 ^{o}C ~ 5 ^{o}C by the end of 21th century. The mean precipitation would increase 7.5%. Assessing these changes in South China, Huang et al. (2008) used PRECIS model developed in the

Hadley Centre for Climate Prediction and Research to investigate the changes of surface air temperature and precipitation under SRES B2 emission scenario during 2071～2100. Compared to the baseline (1961～1990), the mean surface temperature is expected to increase 2 ^{o}C ~ 4 ^{o}C. Precipitation changes have a significant seasonal variation. In summer, there will be an increment in the north part of 22 °N, while an opposite trend in the whole areas of South China. Recent studies also investigated the downscale effect of RCMs by direct comparing the results from GCM-RCM and GCM modeling system. The results showed that the projected future precipitation changes differ largely between the driving GCMs and RegCM3, with strong regional and seasonal dependence (Gao et al., 2011a; Liu et al., 2012).

2.4 How climate affects air quality

2.4.1 O_3

The impact of climate change on surface O_3 studies originated from the research of relationship between O_3 concentrations and meteorological variables, individual synoptic weather patterns since 1970s (Vukovich et al., 1977; Clark and Karl, 1982). It is widely recognized that O_3 air quality is sensitive to meteorological conditions. In the early development stage, most research started with exploring the impact of temperature on the photochemistry of O_3. A number of researches have directly pointed out that there is a positive correlation between the O_3 concentration in lower troposphere and temperature (Sillman and Samson, 1995; Aw and Kleeman, 2003). In addition to the significant role which temperature plays in causing the change of O_3 concentration, the wind, humidity, precipitation, solar radiation, cloud cover and atmospheric circulation will also influence the O_3 air quality (Dawson et al., 2007a; Steiner et al., 2006). For example, the temperature and humidity will affect the O_3 level through the impact on O_3 chemistry and biogenic emission. The transport of air pollutants will be affected by the wind patterns in the lower atmosphere. The change in precipitation is also the main factor which can affect the pollution deposition. From the above considerations, the impact of climate system on air quality can be addressed into four aspects: 1) source emissions, including biogenic emission and anthropogenic emission; 2) transformation processes; 3) transport processes; 4) removal processes.

Jacob et al. (2009) summarized three approaches used to study the impact of climate on O_3 air quality. The first method is to examine the statistic correlation between surface O_3 concentrations and meteorological variables (section 2.4.1). This method is commonly adopted to implement meteorological adjustment in analyses of long-term trends of tropospheric O_3. The obtained empirical models are also applied in air quality forecasts. The second method is based on numerical simulation by adding some perturbations of meteorological variables in regional CTM (section 2.4.2). Numerical sensitivity experiment is able to study the relative importance of physical and chemical processes that affecting O_3 concentrations. Last, a fully coupled GCM–CTM model system has been developed to investigate the impact of the changes in meteorological variables involved in climate change and also the changes in anthropogenic emissions on O_3 formation and depletion (section 2.4.3).

Correlation analysis

Correlation analysis of air quality with meteorological factors using observation data is one of the most directly approach to investigate meteorology impacts on O_3 air quality. The regression-based methods including linear regression, regression trees, and non-linear regression are the majority approaches to conduct this research. Camalier et al. (2007) developed a linear model that describes the relationship between meteorological factors and the surface O_3 concentration data collected at 39 major eastern US urban areas. The static correlations between concentration and each meteorological factor such as temperature, relative humidity, wind speed, transport distance and direction were calculated. The daily maximum temperature, mid-day average relative humidity, and transport direction were the dominant factors that influence the ground-level O_3 concentrations. Overall, the correlation analysis showed that O_3 is generally increasing with increasing temperature and decreasing with increasing relative humidity. Through a multivariable additive model, Li et al. (2010) derived the relationship between the meteorological variability and the monthly O_3 concentrations at 4 sites in south Taiwan during the period of 1997–2006. The dominant factors were wind speed, duration of sunshine and pressure.

In polluted regions, temperature is identified to be the key meteorological variable affecting O_3 concentrations. Ordonez et al. (2005) found that the serious O_3 pollution in summer 2003 in Switzerland can be explained by the warmest summer for at least 150 years. Analysis calculated by Lin et al. (2001) indicated that the probability of the maximum daily 8-h average O_3 exceed 80 ppb increased significantly with the increasing temperature and exceeded 45% when the daily maximum temperatures reaching 310K in the Northeast U.S. In Hong Kong, applied with the least squares regression analysis, the maximum hourly O_3 concentrations at Shatin showed a significant positive correlations with maximum and mean temperatures ($r = 0.6$ and 0.5, respectively) for the autumn months of 1997– 2007 (Lee et al. 2009). In mainland China, a few statistic correlation studies were performed and compared to Europe and the U.S due to lacking long trend observation. Significant correlations was also found between the near surface O_3 and temperature ($r=0.66$) at an urban site of Jinan, China, according to a recent study presented by Shan et al. (2009) using one year observational data.

While most of the studies examined the correlation between the meteorological factors and surface O_3, other studies have investigated the impact of changes in circulation patterns on air quality. Leibensperger et al. (2008) found that the extreme O_3 episode would increase due to transport changes. The decline of frequency of low-pressure systems passing through southern Canada would lengthen the stagnation events over the eastern and mid-western US which lead to the 5–10% increase of pollutant concentrations during these episodes and also the increases of episode duration from 2 to 3–4 days.

Perturbation analysis

With the development of numerical models, perturbation studies in chemical transport models start to be an active area of study since the 1990s. Meteorological variables associated with future changes in climate including temperature, atmospheric water vapor, cloud cover, solar radiation, wind speeds and mixing depths are projected to change in regional chemical transport models. These studies provide a useful method for understanding the importance of physical and chemical processes affecting pollutant concentrations. Table 2.1 summarized the possible influence on air quality in the future due to perturbing individual meteorological factor.

Table 2.1 Simulated potential changes in surface O_3 associated with meteorological parameters

Parameter	Potential changes	Reference
Temperature	consistently positive in land region	Steiner et al., 2006; Dawson et al., 2007a; Millstein et al., 2009;
Specific humidity	variable	Aw and Kleeman, 2003; Steiner et al., 2006; Dawson et al., 2007a;
Wind speed	generally negative	Baertsch-Ritter et al., 2004; Dawson et al., 2007a;
Cloud cover	generally negative	Dawson et al., 2007a;
Precipitation	weak	Dawson et al., 2007a;
Mixing height	generally negative	Dawson et al., 2007a;
Solar radiation	Weak and positive	Sillman and Samson, 1995; Dawson et al., 2007a;

Through perturbation analysis, temperature is also diagnosed to be the key meteorological factor that influencing O_3 formation in polluted regions (Sillman and Samson, 1995; Aw and Kleeman, 2003; Dawson et al., 2007a). Increasing temperature increases O_3 concentrations through chemical reaction and the increasing enhancement of biogenic emission. Using sensitivity analysis, Sillman and Samson (1995) studied the relationship between temperature and O_3 in urban, polluted rural and remote environment. O_3 concentrations would increase with the increasing temperature in polluted environments. AW and Kleeman (2003) evaluated the first-order effect of intra-annual temperature variability on air pollution in urban area. The result showed that the concentration of O_3 will enhanced with the increasing temperature in areas where complete conversion of precursor species has not yet occurred.

In response to the significant surface warming, evaporation from the ocean will increase. Thus it is predicted that there is a significant increase water vapor mixing ratio on a global average basis (Held and Soden, 2000). Steiner et al. (2006) alter the specific humidity (q, or in kg H_2O/kg air) to simulated the water vapor change in the future. The reaction between water vapor and O(1D) produces more HOx radicals into the photochemical cycle. In NO_x-limited regions, this reaction results in the destruction of O_3 production and therefore lower surface O_3. Near high anthropogenic emission regions where NO_x is in abundant supply, HO_2 reacts with NO injecting additional NO_2 to the NO-NO_2-O_3 system and resulting in additional production of O_3. Steiner et al. (2006) evaluated the effects of increasing temperature and atmospheric water vapor which will both result in a 1–5% increase in the daily peak O_3. In the same area, Millstein et al. (2009) considered the combined effect of increased temperature and water vapor concentrations on atmospheric reaction rates and biogenic emissions. The peak 1-h O_3 will increase up to 11 ppb.

Dawson et al. (2007a) performed sensitivity simulations with base case horizontal wind speed was projected to decrease or increase by 5% or 10%. The increase in wind speed led to a reduction in both exceedances and the average daily maximum 8h O_3 concentration. The average daily maximum 8h O_3 concentration tended to slightly increase at the case of 10 % reduction in wind speed. Altering the mixing height in CTM is another way to investigate the sensitivity of O_3 to ventilation effect. Dawson et al. (2007a) indicated that decreasing mixing height increased average daily maximum 8h average O_3 in more populated or polluted areas, and decreased O_3 in some less polluted or remote areas. But the increasing mixing height has the opposite effect.

There are also a few studies investigating the sensitivity of O_3 air quality to emission changes by adding perturbations in individual precursor emission in regional CTM compared to the climate effect. Anthropogenic NO_x, CO and VOCs emissions are projected to decrease to the year 2050 level in Steiner et al. (2006)'s work. Reductions in anthropogenic emissions resulted in a significant decrease of 15-20 ppb in the Bay area and surrounding Fresno of California, U.S, which is quite greater compared to the simulations with perturbing individual meteorological variables.

GCM–CTM approach

The need for a comprehensive understanding the impact of climate change on O_3 formation and depletion using coupled general circulation model (GCM) and chemical transport model (CTM) were highlighted in a number of recent studies and reviews (Jacob et al, 2009; Mickley et al., 2004; Langner et al., 2005; Lin et al., 2008a; Wu et al., 2008a; Wu et al., 2008b;). These studies are useful for understanding the complex coupling among meteorological variables associated with climate change. The general processes used for this approach are described as following. Usually, driving by the future year emission scenarios, the global climate model (GCM) offers future meteorological inputs to a global chemical transport models modeling the influence on global scale. In order to simulate the finer scale climate change, GCM can also be coupled with a regional climate and chemical transport model. In this case, global CTM can provide boundary conditions to regional CTM.

The studies using GCM-CTM approach started from the end of the last century. Scientists conducted the simulation of the effects on both global and regional scale. On global scale, Johnson et al. (1999, 2001) applied coupled global climate–chemistry models to evaluate the climate change effects on tropospheric oxidant concentrations. MOZART-2 driven by emission scenario and meteorological inputs from coupled atmosphere–ocean model was used to assess the effect of climate changes in 2100s on the chemical composition of the troposphere compared to 2000s (Brasseur et al., 2006). The studies of Stevenson et al. (2005), Liao et al. (2006) and Unger et al. (2006) were conducted under different climate scenarios to investigate the impact of future meteorology on air quality. The impact of climate processed on future atmospheric chemical composition has been investigated through a large number of global GCM–CTM models. As known to all, the results are very model dependent due to different model designs. However, despite the large variety of results found in these studies, some common results drawn from the simulations show that O_3 concentrations in the lower troposphere will decrease in remote areas due to increasing temperature and humidity under global warming conditions.

However, the global analysis can only provide information at relatively low spatial resolution. In order to evaluate the impact in urban as well as rural polluted areas, high-resolution regional air quality models are needed. Most of the regional studies considering how climate change may influence the air quality focused in the area of North America and Europe. Hogrefe et al. (2004) first applied the coupled GCM and regional climate and chemistry models to address the effect of climate change on surface O_3 concentrations in eastern United States. Results showed that the average daily maximum 8-hour O_3 concentrations will increase by 2.7, 4.2 and 5.0 ppb in each summers of 2020's, 2050's and 2080's. Jiang et al. (2008b) evaluated the impacts of climate and land use change on surface O_3 in Houston through a modeling system of a global climate model and Weather Research and Forecast model coupled with Chemistry(WRF/Chem). The afternoon O_3 concentrations were predicted consistent to increase 1 to 8 ppb over the Houston during the summertime by 2050s.

While most of the studies summarized in the above articles focused on the area of North America and Europe, only works investigated by Lin et al. (2008a) presented the effect in eastern Asia. In additional, there are no peer-reviewed studies reporting the response of O_3 air quality to climate change in China using GCM–CTM approach.

2.4.2 SOA

Aerosol is comprised of many different species including sulfate, nitrate NO_3, ammonium, EC, OC, dust and sea salt. The aerosol concentrations in the atmosphere are sensitive to the changes of temperature, humidity, wind speed, mixing depth, precipitation and also cloud cover involved in the climate change. Meteorological factors including temperature and specific humidity will affect the concentrations of semi-volatile nitrate and organic aerosols through the impact on reaction rates, aerosol thermodynamics and the amount of oxidants present. Changes in temperature also affect the biogenic VOC emissions which will further influence the concentrations of SOA. Wind speed and mixing depth have significant effects on aerosol concentrations through altering mixing and dilution process. Precipitation is also expected have a significant effect through the influence on wet deposition process. Thus, it is hard to address the impact of climate change on individual aerosol concentrations through observed correlations approach due to the complex impacts on each species. Perturbation approach and coupling GCM-CTM approach are better choice in the research on the response of aerosol concentrations to changes in meteorology and climate.

While a number of studies have revealed the complex coupling between O_3 and the changes in meteorology, knowledge on the impact of climate change and the subsequent changes in emissions on ground-level aerosol concentration are striking limited. The sensitivities of PM2.5 concentrations to individual variables including temperature, wind speed, absolute humidity, mixing height, cloud liquid water content and optical depth, cloudy area, precipitation rate, and precipitating area were examined by Dawson et al. (2007b) through perturbation approach. Temperature, wind speed, absolute humidity, mixing height, and precipitation were the main factors influencing the average PM2.5 concentrations. Due to the effect of increased gas-phase partitioning and faster gas-to-particle conversion at higher temperatures, average concentrations of total organic PM2.5 were estimated to decrease by 13 ng m^{-3} K^{-1} (Jan) and 14 ng m^{-3} K^{-1} (Jul) over land grid cells.

Scientists have applied global models to simulate the sensitivity of SOA formation to climate change and subsequent change in biogenic emission based on gas-particle partitioning theory parameterization. Liao et al. (2007) used a coupled chemistry-aerosol-climate model to investigate how SOA responds to future climate and anthropogenic emissions under the A2 scenario. They found that climate change and the increase of biogenic emissions would cause an increase of 8.6% in SOA in 2100, while the climate change and increase of anthropogenic emissions and biogenic emission would result in a 56% increase of SOA burden. The results of Heald et al. (2008) suggest that a warmer future climate without the subsequent changes in biogenic emission does not change the global mean SOA under A1B scenario. The model results also indicated that the SOA will increase 36% in 2100 due to the rising of biogenic emissions and anthropogenic emissions.

In recent years, coupled GCM and regional climate and chemical transport model have been applied to investigate the effects of potential future climate change on aerosol concentrations including SOA on regional scales (Zhang et al., 2008c; Jiang et al., 2010c). Zhang et al. (2008c) studied the responses of biogenic emission and air quality to future climate under A1B scenario in the United States. They found that climate change alone results an 18% decrease in SOA, while the combined effect of changes in climate and biogenic emissions can result in a decrease of 4% in SOA in 2050. Jiang et al. (2010c) examined the responses of SOA to future climate under A1B and A2 scenarios in the same region using CCSM3-WRF/Chem modeling system. They predicted that future temperature and biogenic emissions were about to increase over the whole U.S under both emission scenarios. The A1B emission scenario would result 5% and 26% increase in SOA burden over the southeast and Texas, while the A2 emission scenario results 8% and 11% increase in SOA burden over these two regions.

2.5 Chapter summary

In this chapter, previous studies on climate change, the impact of climate change on surface O_3 and SOA concentrations in different regions, and the three main approaches in conducting the studies are reviewed. Based on the literature review, the main gaps are identified as follow:

There is insufficient information in China to identify the impact of regional climate change on air pollution meteorology and biogenic emission. Perturbation approach is a simple diagnostic tool to complement the complex GCM–CTM simulations. Compared with perturbation approach, a CTM driven by future-climate GCM fields can simulate the changes in comprehensive physical and chemical processes due to the changes in meteorological variables caused by climate change and also the changed in emissions. It is necessary to applied GCM-CTM approach to study the sensitivity of O_3 and SOA concentrations to climate change and subsequent changes in biogenic emission for comprehensively examining this question.

Chapter 3 Methodology

This study uses air quality model system to evaluate the impact of changes in climate, biogenic emission and anthropogenic emission on surface O_3 and SOA concentrations through coupled GCM-CTM approach. The framework of the modeling system including a global climate model (GCM), regional climate and chemistry model, and emission model is shown in Figure 3.1. The detailed descriptions below will focus on each component of this modeling system.

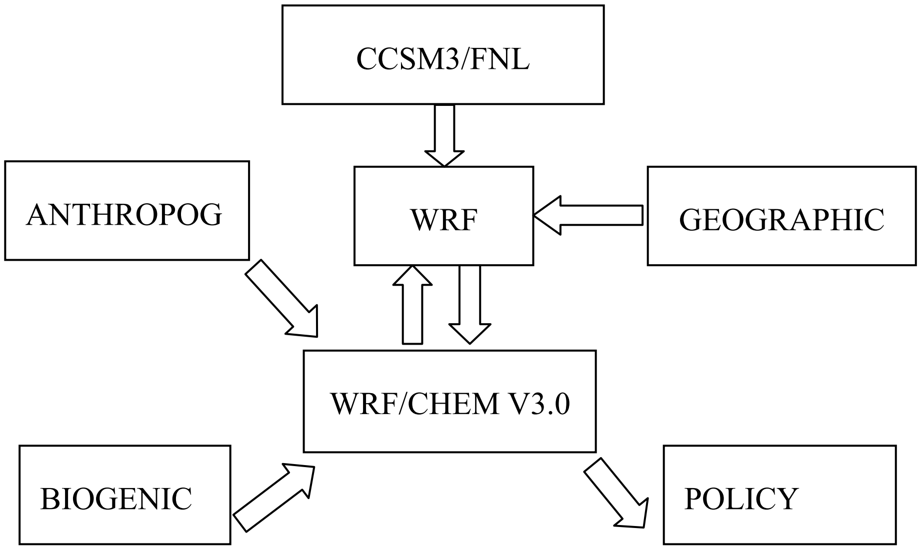

Figure 3.1 Framework of the modeling system

3.1 Model description

3.1.1 WRF/Chem model

WRF/Chem model V3.01 is used to study the impact of climate change on air quality over China. The model is developed by NOAA together with some other research institutions. At present, it is still under active development. Descriptions of WRF/Chem in detail can be found by Grell et al. (2005). The following paragraph gives a brief introduction of this model system.

In previous studies, "off-line" regional air quality modeling systems such as MM5-CMAQ were commonly used in regional atmospheric chemistry simulation. In "off-line" air quality modeling system, the modeling of meteorological processes and chemical processes are independent. Generally, regional climate models (MM5) simulate the meteorological processes and provide meteorological fields in one hour to six hour intervals to regional chemical transport models (CMAQ). However, the actual atmospheric chemical process and meteorological processes occur simultaneously. The changes in albedo due to the changes in aerosols have significant impact on reflecting solar radiation (direct effect). In the meantime, aerosol can act as cloud condensation nuclei (first-indirect effect) and therefore can affect the cloud cover, the life time of cloud and precipitation (the second indirect effect) (Zhang, 2008d). Clouds and precipitation also have a significant impact on the chemical processes. Thus, there are several disadvantages in air quality modeling system. It may ignore some meteorological processes less than the meteorological model input interval, such as cloud formation and a short precipitation process; And also it cannot simulate the feedback between the aerosol and the meteorological processes. Large amount meteorological data are need to spatially and temporally interpolated to the different coordinate systems of chemical transport model which may results some bias in the atmospheric chemistry simulation (Zhang, 2008d).

WRF/Chem is a new generation of regional air quality modeling system. It has the capability to simulate chemistry and aerosols from cloud scale to regional and global scales. The model simulates the physical and chemical processes of trace gases and aerosols simultaneously with the meteorological fields (Fast et al., 2006). Its air quality component (Chem) and meteorological component (WRF) are fully coupled “online”, i.e. its chemical and meteorological sub-models: (1) use the same horizontal and vertical coordinates, (2) use the same physical parameterization, (3) there is no temporal interpolation, and (4) it can include feedbacks between the chemical and meteorological processes. The feedback mechanism between aerosol and the meteorological processes including in WRF/Chem are shown in Figure 3.2.

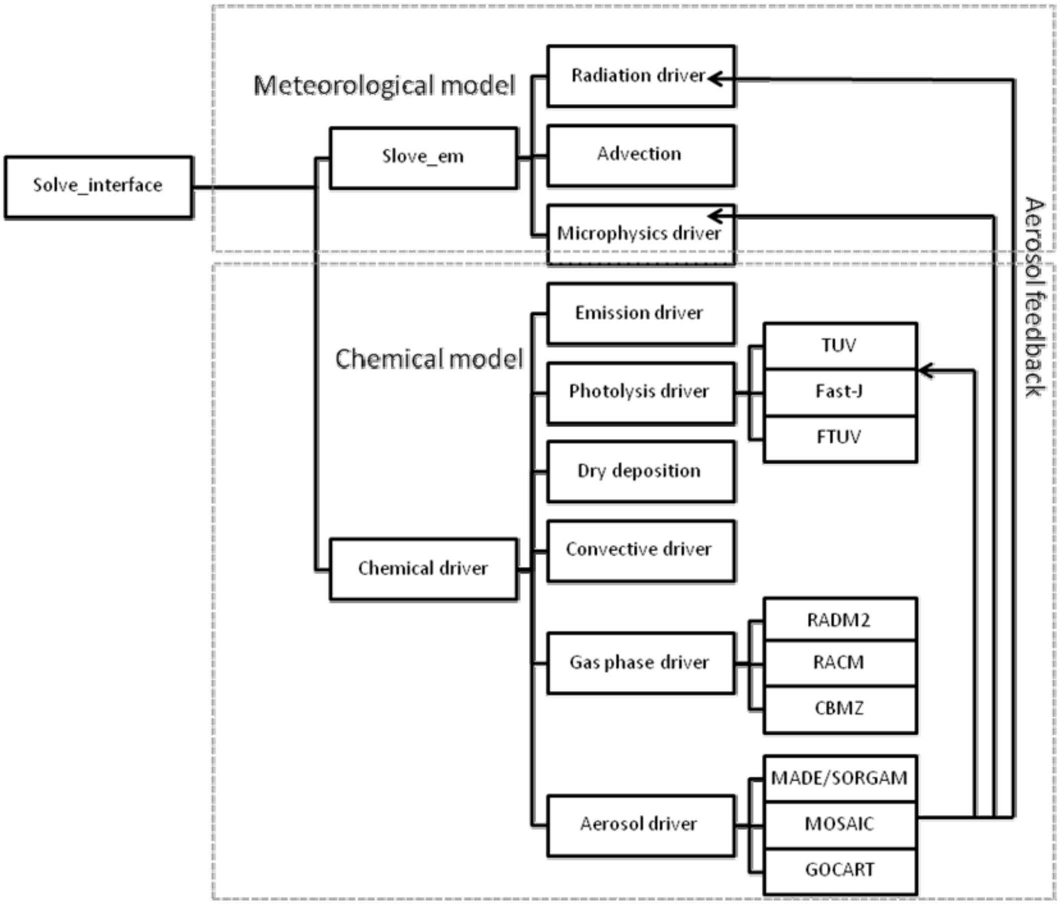

Figure 3.2 Flow diagram of WRF/Chem and the aerosol feedback mechanism on metrological process (Adapted from Jiang, 2010b)

WRF

The meteorological model WRF (Skamarock et al., 2008) is non-hydrostatic, with two dynamic cores designed to serve both operational forecasting and atmospheric research needs. It is suitable for use for a broad spectrum of applications across scales ranging from meters to thousands of kilometers. Simulations and real-time forecasting tests have indicated that the WRF model has a good performance on weather forecasts, and has broad application prospects (Steven et al., 2004; Done et al., 2004).

The dynamic core version of Advanced Research WRF (ARW) is used in this study. The technician support document for ARW can be found in http://www.mmm.ucar.edu/wrf/users/docs/arw_v3.pdf (Skamarock et al., 2008). Briefly, applying time-splitting scheme, ARW efficiently integrates the fully compressible non-hydrostatic equations of motion (Skamarock and Klemp, 2008). The equations are defined on a terrain-following sigma coordinate in vertical direction, which is written as,

$$\sigma = \frac{p_h - p_{ht}}{p_{hs} - p_{ht}}$$

where p_h is the hydrostatic component of the pressure, and p_{hs} and p_{ht} refer to values along the surface and top boundaries, respectively. Generally, we set $p_{ht} = \text{constant}$. At the surface, the value of σ is 1. And then σ decreases monotonically to 0 at the upper boundary of the model domain.

For the physical process, WRF provides many different options of physical parameterization schemes for microphysics, cumulus parameterization, surface layer, land surface model, planetary boundary layer (PBL), and radiation (Table 3.1) (Skamarock et al., 2008). The simulation of meteorological conditions in the PBL plays an important role in air quality modeling (Hu et al., 2010). In WRF/Chem v3.0, there are four different PBL schemes including Medium Range Forecast Model

(MRF), Yonsei University (YSU), Mellor–Yamada–Janjic (MYJ), and the asymmetric convective model, version 2 (ACM2). MYJ and YSU PBL scheme are two common used scheme recommended by the WRF/Chem User guide v3.0. Readers can refer to http://www.mmm.ucar.edu/wrf/users/docs/arw_v3.pdf for detail description.

Table 3.1 Physical parameterization schemes

Physics	Options
Microphysics	Kessler, Purdue Lin, WSM3, WSM5, WSM6, Eta GCP, Thompson, Goddard, Morrison
Cumulus parameterization	Kain-Fritsch, Betts-Miller-Janjic, Grell-Devenyi, Grell-3
Surface Layer	Similarity theory (MM5), Similarity theory (Eta), Similarity theory (PX)
Land-Surface Model	5-layer thermal diffusion，Noah，RUC，Pleim-Xiu
Planetary Boundary Layer	MRF, YSU, MYJ, ACM2
Longwave Radiation	RRTM, GFDL, CAM
Shortwave Radiation	GFDL, MM5 (Duhia), Goddard, CAM

Chem component

The chemistry component of WRF/Chem contains relatively comprehensive physical and chemical processes. It includes convective, advective and turbulent transport of chemicals, biogenic and anthropogenic emissions, dry and wet deposition, photolysis, gas and aqueous phase chemical transformation, aerosol chemistry and dynamics (including inorganic and organic aerosols) as well as the processes of aerosol direct and indirect effect through interaction with atmospheric radiation and microphysics. Basically, each process contains different solution schemes, which is convenient for conducting modeling studies for a large variety of scenarios. Studies (Grell et al., 2005, Tie et al., 2007) have shown that WRF/Chem has relatively good performance on modeling air pollutants concentrations, even on continuous heavy-pollution episodes (Jiang et al., 2008a).

In WRF/Chem v3.0, there are three gas-phase chemistry mechanism schemes: RADM2 (Regional Acid Deposition Model 2) (Stockwell et al., 1990), RACM (Regional Atmospheric Chemistry Mechanism) (Stockwell et al., 1997) and CBMZ (Carbon Bond Mechanism) (Zaveri and Peters, 1999). RADM2 scheme contains 156 reactions and 63 prognostic species including 21 inorganic species (14 stable species, 4 reactive intermediates, and 3 abundant stable species) and 42 organic species (26 stable species and 16 peroxy radicals). RACM is a highly improved version of the RADM2 mechanism. It has 237 reactions and 77 chemical species 21 inorganic species (14 stable species, 4 reactive intermediates, and 3 abundant stable species) and 56 organic species (32 stable species and 24 peroxy radicals). Compared with RADM2, RACM includes relatively detailed organic chemistry, such as aromatic chemistry and the oxidation mechanism for biogenic volatile organic compounds (e.g. isoprene, a-pinene, d-limonene, etc.). Hence, the reactions of the SOA precursors could be well described by RACM. CBMZ contains 55 prognostic species and 134 reactions. Based on original Carbon-Bond Mechanism (CBM-IV), CBMZ includes reactive long-lived species, revised isoprene chemistry, and optional DMS chemistry.

WRF/Chem currently contains three aerosol chemistry mechanisms GOCART (Goddard Chemistry Aerosol Radiation and Transport), MADE/SORGAM (Modal

Aerosol Dynamics Model for Europe (MADE) and Secondary Organic Aerosol Model (SORGAM)) (Ackermann et al., 1998; Schell et al., 2001) and MOSAIC (Model for Simulating Aerosol Interactions and Chemistry) (Zaveri et al., 2008). Using bulk approach, GOCART treats several aerosol types, including sulfate, dust, OC, BC and sea salt. For OC and BC, hydrophobic and hydrophilic components are considered. In MOSAIC, all major components of aerosol including SO_4, methanesulfonate (CH_3SO_3), NO_3, chloride (Cl), carbonate (CO_3), NH_4, sodium (Na), calcium (Ca), BC, primary organic mass are treated (Zaveri et al., 2008). For the treatment of aerosol size distributions, a sectional approach with discrete size bins is applied. MOSAIC offers flexibility in specifying the number of size bins, with four or eight bins commonly used. SOA module is not included in both GOCART and MOSAIC scheme. MADE simulates several major aerosol species including SO_4, NO_3, NH_4, BC, OC, sea salt, mineral dust, and aerosol water. SORGAM module considering the SOA formation has been updated into MADE by Schell et al. (2001). The aerosols size distribution in MADE/SORGAM are representing with the modal approach with three lognormal modes (Aikten, accumulation and coarse mode). Aerosol processes including nucleation, condensation and coagulation are calculated in MADE/SORGAM. For the formation of secondary aerosol particles, aerosol nucleation is the most important process which is calculated based on Kulmala et al. (1998). The formulation for the condensation process follows two steps: the production of volatile species which then condense and evaporate on ambient aerosols (Grell, et al., 2005). The coagulation process is formulated following Whitby et al.

(1991) and Binkowski and Shankar (1995).

3.1.2 CCSM model

General Circulation Model is developed to simulate the physical processes in the atmosphere, ocean, cryosphere and land surface, which is commonly used for predicting the impact of increasing greenhouse gas concentrations, such as carbon dioxide level on future climate (IPCC, 2007). It can provide reasonably climate conditions for regional climate and chemistry model to simulate the physical and chemical process.

The GCM applied to drive the regional model is the Community Climate System Model version 3(CCSM3) developed by National Center for Atmospheric Research. It is a coupled global climate model integrating four components by a flux coupler: 1) the Community Atmosphere Model version 3 (CAM3; Collins et al. 2004, 2006a), 2) the Community Land Surface Model version 3 (CLM3; Oleson et al. 2004; Dickinson et al. 2006), 3) the Community Sea Ice Model version 5 (CSIM5; Briegleb et al. 2004), and 4) the ocean is based upon the Parallel Ocean Program version 1.4.3 (POP; Smith and Gent 2002) (Collins et al., 2006b). Based on Eulerian spectral dynamical core, CCSM3 performs with triangular spectral truncation at 85, 42, and 31 wavenumbers in horizontal. The grid points in the atmosphere roughly ranges from 1.4°to 3.75° every latitude and longitude. For the vertical profile, it uses the terrain-following hybrid coordinates developed by Simmons and Burridge (1981).

A series of experiments are performed using CCSM3 including 1) twentieth-century climate experiments, 2) twenty-first century experiments, and 3) stabilization experiments for the assessment in the IPCC Fourth Assessment Report (AR4) as documented in Meehl et al. (2005). Three twenty-first century simulations are conducted from 2000 to 2100 based on Emissions Scenarios (SRES) A2, A1B and B1 provided by IPCC Special Report. These three scenarios are selected for representing a range of possible outcomes for the twenty-first century with low (B1), medium (A1B), and high (A2) emissions of greenhouse gases.

3.1.3 Biogenic Emission inventory model

In this study, the Model of Emissions of Gases and Aerosols from Nature version 2.04 (MEGAN2.04) developed by National Center for Atmospheric Research (NCAR) is applied for estimation the biogenic emission (Guenther et al., 2006). MEGAN has been fully coupled into WRF/Chem, and it was available as a WRF/Chem configuration option. MEGAN is designed for both global and regional emission modeling with the spatial resolution up to 1 km^2. It estimates the net emission rates of isoprene and other biogenic VOCs from terrestrial ecosystems into the above-canopy atmosphere according to the following expression:

$$\text{Emission} = [\varepsilon][\gamma][\rho]$$

Where ε is an emission factor which represents the emission of a compound into the canopy at standard conditions, estimated based on leaf and branch-scale emission measurements. γ is an emission activity factor that accounts for emission changes due to deviations from standard conditions and ρ is a factor that accounts for production and loss within plant canopies. The factor γ is affected by several conditions, such as leaf area index (LAI), canopy characteristic, solar angle, photosynthetic photon flux density (PPFD) transmission, air temperature, humidity, wind speed, soil moisture and so on. Emissions for each plant functional type (PFT) are calculated separately in MEGAN. The emissions are then summed to represent the total emission for a location. Compared to the earlier biogenic emission models, MEGAN has introduced several significant improvements: (1) it includes methods for characterizing and processing land cover type and density, (2) it improves simulation of canopy environment containing leaf energy balance calculations, (3) it allows light penetration through varying canopy types, and (4) it has detailed chemical speciation. Furthermore, MEGAN includes a term to account for variations in canopy production and loss of particular compounds.

3.2 CCSM2WPS

The outputs with horizontal resolution T85 (~1.41°) from the Community Climate System Model version 3.0 (CCSM3) are used to drive WRF/Chem model as in Jiang et al. (2008b). In order to prepare the initial and lateral boundaries conditions for

WRF/Chem, CCSM2WPS program is applied to convert CCSM3 outputs into regional simulation domains.

The WRF Preprocessing System (WPS) is used to convert terrestrial and meteorological data for the real time simulation of WRF/Chem. It allows the users to define the simulation domains, choose map projection, and interpolate terrestrial, meteorological data to the specified domains. There are three subprograms in WPS including GEOGRID, UNGRIB, METGRID (Figure 3.3). GEOGRID generates static geographical data including terrain, land use, soil types, and vegetation fraction. According to the variable table, UNGRIB degribs the analysis data in GRIB format (i.e., NCEP FNL Operational Global Analysis data) into an intermediate data format. The third program, METGRID, interpolates the meteorological and terrestrial data generating by GEOGRID and UNGRIB into defined domains. Since CCSM3 outputs are archiving in netCDF format, so CCSM2WPS program is needed to replace UNGRIB converting data into intermediate data format. There are three sequential programs involved in CCSM2WPS, which are READ, INTERPOLATION and WRITE.

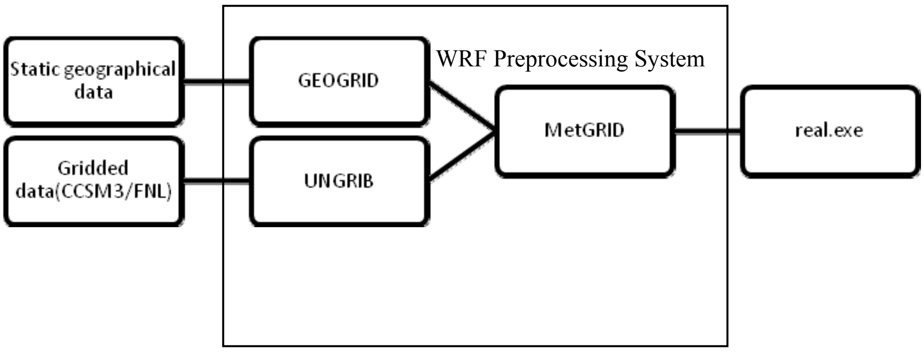

Figure 3.3 Process flow chart of WPS (Adapted from http://www.mmm.ucar.edu/wrf/users/docs/user_guide_V3/users_guide_chap3.htm)

3.2.1 READ

CCSM3 outputs are on 1.41*1.41 degree grids covering the entire world with intervals in six hours. It contains meteorological fields including two dimensional data (i.e., surface pressure, sea-level pressure, surface temperature, reference height temperature) and three dimensional data (i.e., wind, temperature, specific humidity, and geo-potential height). The meteorological variables are available on the surface and at 26 hybrid midlevels. Soil variables such as temperature and moisture are also provided by CCSM3 on 10 subsurface soil layers. The brief descriptions of 15 variables from CCSM3 outputs are included in Table 3.2. The first program, READ, is developed to interpret meteorological and soil data with netCDF format. Relative humidity is calculated through the formula involving temperature, pressure and specific humidity.

Table 3.2 Brief description of variables included in READ program

Short name	Description	Units	Layers
T	Temperature	K	26
Q	Specific humidity	Kg/Kg	26
TREFHT	Reference height temperature	K	1
TS	Surface temperature	K	1
U	Zonal wind	m/s	26
V	Meridional wind	m/s	26
Z3	Geopotential Height	m	26
PSL	Sea level pressure	Pa	1
H2OSOI	Volumetric soil water	mm3/mm3	10
TSOI	Soil temperature	K	10
PS	Surface pressure	Pa	1
PHIS	Surface geopotential	m	1
LANDFRAC	Fraction of sfc area covered by land	fraction	1
SNOWHLND	Water equivalent snow depth	kgm-2	1
ICEFRAC	Fraction of surface area covered by sea-ice	fraction	1

3.2.2 INTERPOLATE

Three dimensional meteorological data are provided at 26 vertical levels with the top model hybrid level midpoints at 3.54 hPa. In hybrid coordinate, pressure at mid-levels are defined as following,

$$\mathrm{P}_{\mathrm{k+1/2}} = \mathrm{A}_{\mathrm{k+1/2}} \times P_0 + \mathrm{B}_{\mathrm{k+1/2}} \times P_{\mathrm{s}}$$

where P_0 is a constant pressure, P_{s} is the pressure at surface, $\mathrm{A}_{\mathrm{k+1/2}}$ is the pressure hybrid coefficient at k+1/2 level and $\mathrm{B}_{\mathrm{k+1/2}}$ is the sigma coefficient. Since METGRID only accepts three dimensional data defined at pressure-levels, we need to interpolate variables from hybird coordinate to specified pressure levels. Pressure-weighted interpolation method is used to transform hybrid coordinate values to pressure values. For levels below surface pressure, it uses the ECMWF formulation as described in Trenberth et al. (1993) to interpolate temperature and geopotential height. All other variables are held constant below surface pressure equal to the values at the lowest model level.

For the soil temperature and moisture, CCSM3 provides variables at 10 subsurface soil layers below the ground (Table 3.2). In METGRID program, the soil moisture are represented by the following 4 variables 'SM000010' (soil moisture at 0-10 cm below ground layer), 'SM010040' (soil moisture at 10-40 cm below ground layer), 'SM040100' (soil moisture at 40-100 cm below ground layer), and 'SM100200' (soil moisture at 100-200 cm below ground layer) (Table 3.4). We assume that 'SM000010' is the soil moisture at 5cm below ground layer, and calculate it by interpolating from CCSM outputs at 2.8cm, 6.2cm. The transformation table for the other variables between CCSM3 and WPS are showing in Table 3.3

Table 3.3 The depth of 10 soil layers

Layers	1	2	3	4	5	6	7	8	9	10
Depth(cm)	0.7	2.8	6.2	11.9	21.2	36.6	62.0	104	173	286

Table 3.4 Summary of transformation method used in INTERPOLATE program

WRF/Chem Variables			Transform from CCSM Variables	
Short name	Description	units	Description	units
T	Temperature	K	Interpolate from Temperature (T)	K
U	U-component of the horizontal wind	m s^{-1}	Interpolate from Zonal wind(U)	m s^{-1}
V	V-component of the horizontal wind	m s^{-1}	Interpolate from Meridional wind (V)	m s^{-1}
RH	Relative humidity	%	Interpolate and transform from Specific humidity (Q)	kg kg^{-1}
HGT	Geopotential height	m	Interpolate from Geopotential Height (Z3)	M
PMSL	Sea-level pressure	Pa	Sea level pressure (PSL)	Pa
SST	Sea-surface Temperature	K	Surface temperature (TS)	K
SKINTEMP	Skin Temperature	K	Surface temperature (TS)	K
ST000010	Soil temperature from 0 to 10 cm	K	Interpolate from Soil temperature at 2nd, 3rd levels (TSOI)	K
ST010040	Soil temperature from 10 to 40 cm	K	Interpolate from Soil temperature at 5th, 6th levels (TSOI)	K
ST040100	Soil temperature from 40 to 100 cm	K	Interpolate from Soil temperature at 7th, 8th levels (TSOI)	K
ST100200	Soil temperature from 100 to 200 cm	K	Interpolate from Soil temperature at 8th, 9th levels (TSOI)	K
SM000010	Soil moisture from 40 to 100 cm	kg m^{-3}	Interpolate and transform from Volumetric soil water at 2nd, 3rd levels (H2OSOI)	mm^3 mm^{-3}
SM010040	Soil moisture from 40 to 100 cm	kg m^{-3}	Interpolate and transform from Volumetric soil water at 5th, 6th levels (H2OSOI)	mm^3 mm^{-3}
SM040100	Soil moisture from 40 to 100 cm	kg m^{-3}	Interpolate and transform from Volumetric soil water at 7th, 8th levels (H2OSOI)	mm^3 mm^{-3}
SM100200	Soil moisture from 100 to 200 cm	kg m^{-3}	Interpolate and transform from Volumetric soil water at 8th, 9th levels(H2OSOI)	mm^3 mm^{-3}
LANDSEA	Land/Sea flag (1=land, 0 or 2=sea)	proportion	Fraction of surface area covered by land (LANDFRAC)	fraction
SNOW	Water equivalent snow depth	kg m^{-2}	Water equivalent snow depth (SNOWHLND)	kg m^{-2}
SEAICE	Ice flag	proportion	Fraction of surface area covered by sea-ice (ICEFRAC)	fraction
T2	Temperature at 2 m	K	Reference height temperature (TREFHT)	K

U10	U at 10 m	m s^{-1}	The lowest level Zonal wind (U)	m s^{-1}
V10	V at 10 m	m s^{-1}	The lowest level of Meridional wind (V)	m s^{-1}
RH2	RH at 2 m	%	The lowest level of Specific humidity (Q)	kg kg^{-1}

3.2.3 WRITE

WRITE program is applied to convert CCSM data sets with netCDF format into a simple intermediate format. In the datasets with the intermediate format, the data are defined as two-dimensional arrays of real values (slab) for both 2-dimensional fields and 3-dimensional fields. So the data of 3-dimensional should be divided into 2-dimensional arrays according to the pressure level. Then the CCSM3 data are transformed into 28 layers including surface level, sea level and 26 pressure levels. Some other information should also be included in the WRTIE program when writing slab to the intermediate data. The first record (IFV) defines the format version number for WPS. In the second record, it provides the information of forecasting time, data source, variable name, units, description, vertical level, dimension in the X/Y direction, and data projection. IPROJ in the second record denotes the map projection of the data. Since the CCSM3 outputs were based on the Gaussian projection which is one of the acceptable map projection types of WPS, no additional conversion was needed. The third record specifies the information of data grid including the start location, start latitude and longitude, number of latitudes north of equator, latitude/longitude increment. The details description of the records is specified in Table 3.5.

Table 3.5 Brief description of records included in intermediate data (Adapted from http://www.mmm.ucar.edu/wrf/OnLineTutorial/Basics/IM_files/IM_wps.htm)

Short name	Description
IFV	intermediate-format version number for WPS is 5
HDATE	The time, in format "YYYY-MM-DD_HH:mm:ss" (only the first 19 characters are used)
XFCST	Forecast time (in hours) of the data in the slab
MAP_SOURCE	Source of data
FIELD	A field name. Names with special meaning are described below.
UNITS	Units describing the field in the slab.
DESC	Text description of the field in the slab.
XLVL	Pressure-level (Pa) of the data. 200100 Pa indicates surface data; 201300 Pa indicates sea-level pressure
NX	Slab dimension in the X direction
NY	Slab dimension in the Y direction
IPROJ	Flag denoting the projection.
STARTLOC	Start location of data. Could be "CENTER" or "SWCORNER". "SWCORNER" is typical.
STARTLAT	Starting latitude (degrees north)
STARTLON	Starting longitude (degrees east)
DELTALON	Longitude increment (degrees) for lat/lon grid
NLATS	Number of latitudes north of equator (for Gaussian grids)
TRUELAT2	A second extra latitude (degrees north) used for defining Lambert conformal projection
EARTH_RADIUS	Radius of the earth
SLAB	Two-dimensional array of data.

3.3 Model improvement

3.3.1 Isoprene SOA formation

SORGAM calculates the partitioning of semi-volatile organic compounds (produced during VOC oxidation) between the gas and the aerosol phase. For each parent VOC, the module assumes one or two generic oxidation products (Odum et al., 1996). SORGAM assumes that SOA compounds interact with each other and the gas/particle partitioning of these compounds occurs as an absorption process on the aerosol particle, and it can be parameterized by a quasi-ideal solution (Odum et al., 1996). For

SOA compound *i*, the saturation concentration $C_{\mathrm{sat,i}}$ can be expressed as follow:

$$C_{sat,i} = X_{i,om}\frac{\gamma_i p_i^o m_i 10^6}{RT} = X_{i,om}C^*_{sat,i}$$

where, *R* is the gas constant, *T* is the temperature, γ_i , m_i, and p_i^o are the activity coefficient, molecular weight, and saturation vapor pressure of compound *i*, respectively. Due to the lack of information, all activity coefficients γ_i are assumed to be 1. p_i^o is the function of temperature *T* and enthalpy of vaporization ΔH. $C^*_{sat,i}$ is the saturation concentration of the pure compound *i*, and $X_{i,om}$ is the mole fraction, which represents the interaction of different SOA compounds, its expression is as follow:

$$X_{i,om} = \frac{C_{aer,i}/m_i}{\sum_{j=1}^{n}(C_{aer,j}/m_j) + C_{init}/m_{init}}$$

Where $C_{aer,i}$ is the concentration of SOA compounds *i* in aerosol phase, and C_{init} represents the pre-existing absorbing aerosol materials. In thermodynamic equilibrium, the gas phase concentration just equal to the saturation concentration $C_{sat,i}$, therefore, the aerosol phase concentration of SOA compound *i* can be calculated by subtracting the gas phase concentration from its total concentration.

SORGAM treats the anthropogenic and biogenic aerosol precursors separately. In the current version of SORGAM module in WRF/Chem, eight SOA compounds are taken into account, of which four come from anthropogenic precursors and the other four come from biogenic ones. For anthropogenic SOA products, SORGAM assumes that two are from aromatics precursors, i.e. TOL (Toluene and less reactive aromatics), CSL (Cresol and other hydroxy substituted aromatics), and XYL (Xylene and more reactive aromatics), one is from higher alkanes, i.e. HC8 (Alkanes with HO rate constant greater than 6.8×10^{-12} at 298 °C and 1 atm), and another one is from higher alkenes, namely OLT (Terminal alkenes) and OLI (Internal alkenes). Biogenic SOA is represented by two surrogate compounds from the oxidation of API (a-pinene and other cyclic terpenes with one double bond), and another two species from the degradation of LIM (limonene and other cyclic diene terpenes).

Recent field and laboratory evidence demonstrated that the oxidation of isoprene can contribute to the formation of SOA in the atmosphere (Claeys et al., 2004; Kroll et al., 2005; Ng et al., 2008). Modeling studies also show that isoprene-derived SOA has significant contribution to total SOA concentration. Globally, isoprene SOA is estimated to contribute 27% to 48% of total SOA (Hoyle et al., 2007; Henze and Seinfeld, 2006). However, in SORGAM model, this SOA formation process was not included. Therefore, a parameterization scheme for the isoprene SOA formation was added in SORGAM module in WRF/Chem model in this study.

Based on chamber experiments, isoprene SOA formation can be represented by the “two product model” (Odum et al., 1996), and it could be described in two schemes for different NO_x levels, namely high-NO_x and NO_x free condition (Carlton et al., 2009). The high NO_x condition is generally with NO_x mixing ratio higher than 400 ppb (Edney et al., 2005; Kleindienst et al., 2006), which basically does not occur in ambient environment. Hence, the low NO_x condition scheme was adopted for the entire domain. In addition, isoprene oxidized by hydroxyl radical is considered as the only pathway for SOA formation (Henze and Seinfeld, 2006). The parameterization of isoprene SOA formation is as follows:

$$\text{isoprene} + \text{OH} \rightarrow \alpha_1 \text{CVISO1} + \alpha_2 \text{CVISO2}$$

$$K_{\mathrm{i}}(T) = K_{\mathrm{ref,i}} \times \exp[\frac{\Delta H_{\mathrm{vap,i}}}{R}(\frac{1}{T} - \frac{1}{T_{\mathrm{ref,}}})]$$

where α_1 and α_2 are the stoichiometric coefficients, CVISO1 and CVISO2 represents two surrogate semi-volatile products, $K_{\mathrm{i}}(T)$ is the partitioning coefficient determining the partition of semi-volatile compounds i between gas and aerosol phase. $K_{\mathrm{ref,i}}$ is the partitioning coefficient of species i at a reference temperature T_{ref}. $\Delta H_{\mathrm{vap,i}}$ is the enthalpy of vaporization. Here, α_1 and α_2 are set to 0.28 and 0.032; $K_{\mathrm{ref,1}}$ and $K_{\mathrm{ref,2}}$ are set to 0.0045 and 0.93; T_{ref} is equal to 293 K; $\Delta H_{\mathrm{vap,i}}$ is set to 42 kJ mol^{-1} (Carlton et al., 2009). It should be noted that this parameterization for isoprene SOA formation is not coupled with SORGAM, and there is no interaction between isoprene SOA and SORGAM SOA compounds.

Thus, in the modified SORGAM module, nine types of VOC are treated as the SOA precursors (Table 3.6). The SOA generated from anthropogenic VOC (TOL, XYL, CSL, HC, OLT, OLI) are called ASOA, while that from the oxidization of monoterpenes (API, LIM) and isoprene (ISOP) are considered as BSOA. ISOA and MSOA are the hypothetical products from the oxidization of API, LIM and ISOP.

Table 3.6 Types of SOA compounds included in the modified SORGAM module

Type		Precursor	Hypothetical product
ASOA		Aromatics (TOL, XYL,CSL)	SOAARO1
			SOAARO2
		Higher alkanes (HC)	SOAALK1
		Higher alkenes (OLT, OLI)	SOAOLE1
BSOA	MSOA	α-pinene (API)	SOAAPI1
			SOAAPI2
		Limonene (LIM)	SOALIM1
			SOALIM2
	ISOA	Isoprene (ISOP)	SOAISO1
			SOAISO2

3.3.2 Process analysis

O_3 mixing ratios are the net results from comprehensive physical and chemical processes. In order to estimate the individual contribution from each process, an O_3 process analysis scheme was added to Chem_driver module in WRF/Chem in this study. It can calculate the chemical contribution rate (CHEM), transport rate (TRAN) and deposition rate (DEP) at each step and each grid. CHEM is the changes of ozone concentrations due to the gas-phase chemistry. TRAN is the changes of ozone concentrations produced by processes of horizontal advection and vertical transport. DEP is an integrated contribution rate from the processes of vertical mixing, dry deposition and wet deposition. Figure 3.4 shows the flow chart of this simple process analysis scheme. For example, the CHEM are equal to the difference between the final and initial concentrations for gas-phase chemistry.

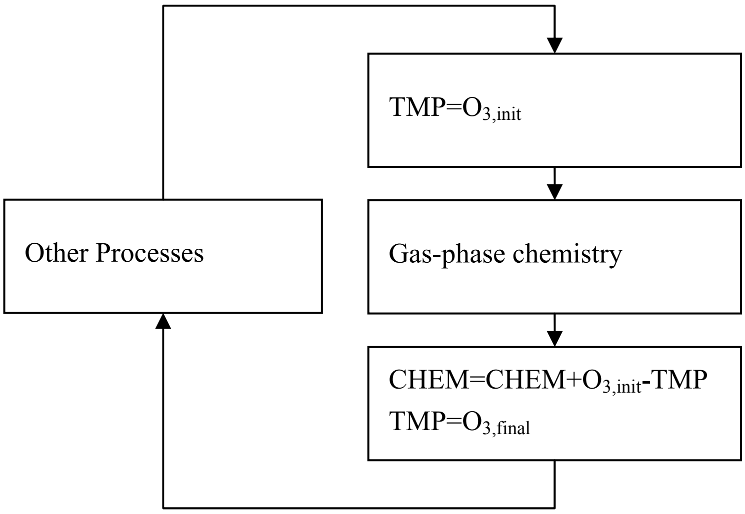

Figure 3.4 Flow chart of ozone process analysis in WRF/Chem

3.5 Model evaluation protocol

In order to evaluate the model performance, five statistical measures were selected, including the Mean bias (MB), Mean absolute error (MAE), Root mean square error(RMSE), Correlation coefficient (COE), and Hit rate (HR) (Schlünzen, 2003). For any given variable with (n) pairs of observed (O) and simulated (S) values, such as meteorological factors and air pollutant concentrations, the statistics are defined as

$$MB = \overline{S_i - O_i}$$

$$MAE = \overline{\left| S_i - O_i \right|}$$

$$RMSE = \sqrt{\frac{\sum_{i=1}^{n} (S_i - O_i)^2}{n}}$$

$$COE = \sum_{i=1}^{n} (S_i - \bar{S})(O_i - \bar{O}) / \sqrt{\sum_{i=1}^{n} (S_i - \bar{S})^2 \sum_{i=1}^{n} (O_i - \bar{O})^2}$$

$$HR = \frac{100}{n} \times \sum_{i=1}^{n} a_i$$

$$a_i = \begin{cases} 1 & \left|S_i - O_i\right| \leq threshold \\ 0 & \left|S_i - O_i\right| \leq threshold \end{cases}$$

The threshold values for the HR calculation are 2 °C for 2 meter temperature (T2), 10 % for 2 meter relatively humidity (RH2), 30 deg for 10 meter wind direction (WD10) and 1 m s^{-1} for 10 meter wind speed (WS10) (Jiang et al, 2010a).

Chapter 4 Modeling tropospheric O_3 formation over East China in springtime

4.1 Introduction

East China is one of the most polluted areas in China, especially YRD. Due to economic development, the YRD has undergoing rapid urbanization progress and became the major manufacturing center in East China. The greater YRD is surrounded by highly developed metropolitan cities, including five mega-cities Shanghai, Nanjing, Hangzhou, Ningbo, Wuxi, Suzhou, and numerous medium and small cities. Like other metropolitan areas, air pollution is of great concern in greater YRD region. Regional O_3 pollution episodes have been frequently reported in the YRD region since 1990s (Chameides et al., 1999). Continuous O_3 measurements in the YRD indicated that high O_3 mixing ratios often occurred in late spring in East China (Cheung and Wang, 2001; Wang et al., 2006a; Ran et al., 2009). However, the O_3 formation mechanisms in this region still remain uncertain. Cheung and Wang (2001) indicated that the high O_3 days were caused by favorable weather conditions, downward mixing, and local photochemical formation. The investigators also suggested that precursors from biomass burning might play an important role. Ran et al. (2009) believed that O_3 reached its maximum in spring instead of summer possibly due to the rainy season (Meiyu period) in the YRD, while Wang et al. (2006a) considered that it was attributed to summer monsoon. Therefore, it is meaningful to give a further study for the O_3 formation in this region.

In this chapter, the WRF/Chem model is applied for exploring the O_3 formation mechanisms in East China. The detailed model configuration and numerical experiments are presented in Section 4.2. In Section 4.3, the model performances focusing on meteorological fields and O_3 mixing ratios are presented, and the distribution patterns of O_3 mixing ratios and wind field on the surface and at 850 hPa are discussed, respectively. Then, the relative contributions of photochemical reactions and other processes to the O_3 formation are quantitatively investigated. Finally, three sensitivity simulations about the impacts of biogenic emissions and anthropogenic sources on the O_3 formation are conducted, and their influences are quantified. Section 4.4 summarized the chapter conclusion.

4.2 Model and Experiment

4.2.1 Model configuration

The simulation is conducted for one month of April, 2008 on a two nested domain (Figure 4.1). The outermost domain (D1, 45 km) covers the East Asia region, and the inner domain (DM2, 15 km) basically focuses on the East China region. From the ground level to the top, there are 28 vertical sigma layers to all grid meshes, with about 10 layers below AGL (Table 4.1).

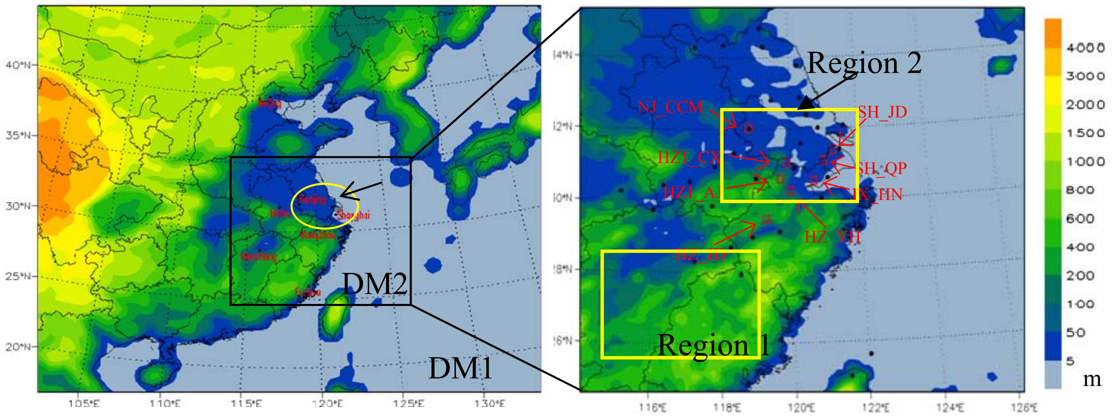

Figure 4.1 Simulation domain settings (shaded: terrain height; black point marks: meteorological stations; red square marks: O_3 observation sites; yellow box: two defined sub-regions)

Table 4.1 The grid settings, physics and chemistry options used in this study

Items	Contents
Dimensions(x, y)	81, 72/85, 82
Grid size (km)	45/15
Vertical layers	28 (1, 0.993, 0.983, 0.97, 0.954, 0.934, 0.909, 0.880, 0.835, 0.790, 0.745, 0.700, 0.621, 0.548, 0.482, 0.420, 0.364, 0.313, 0.266, 0.224, 0.185, 0.145, 0.118, 0.089, 0.063, 0.040, 0.020, 0)
Microphysics	WRF Single-Moment 5-class scheme (Hong et al., 2004)
Longwave Radiation	RRTM scheme (Mlawer et al., 1997)
Shortwave Radiation	Goddard shortwave (Chou and Suarez, 1994)
Surface Layer	Eta similarity (Janjic, 1996)
Land Surface	Noah Land Surface Model (Chen and Dudhia, 2001)
Planetary Boundary layer	Mellor-Yamada-Janjic scheme (Janjic, 2002)
Cumulus Parameterization	Grell-Devenyi ensemble scheme (Grell and Devenyi, 2002)
FDDA	Yes
Photochemical Mechanism	RACM (Stockwell et al., 1997)
Photolysis scheme	TUV (Madronich, 1987)
Aerosol Module	MADE/SORGAM (Schell et al., 2001)

In order to reduce meteorological integral errors, the National Centers for Environmental Prediction (NCEP) Final Analyses (FNL) data is assimilated to DM1 using Grid Nudging method. The FNL data has a horizontal resolution of 1°×1° and a time interval of 6 h, which is also used to generate the meteorological initial fields and lateral boundary conditions. The initial fields and lateral boundary conditions for chemical species are provided by MOZART-4 results (Emmons et al., GMD, 2010), with a 2.8°×2.8° horizontal resolution, 28 vertical levels, and 6 h time interval.

The physics parameterizations have significant effects on simulated meteorological fields, such as temperature, radiation, etc., which further affect the photochemical reactions, dry deposition and so on. Here, WRF Single-Moment 5-class scheme (WSM5, Hong et al., 2004) for microphysics, Rapid Radiative Transfer Model (RRTM, Mlawer et al., 1997) for long wave radiation, Goddard scheme (Chou and Suarez, 1994) for short wave radiation, and Mellor–Yamada–Janjic (MYJ) scheme for boundary layer scheme are adopted. Other physics options can be found in Table 4.1. Photochemical mechanism plays an important role in air quality model. In this study, RACM (Stockwell et al., 1997) is used which includes relatively detailed organic chemistry, such as aromatic chemistry and the oxidation mechanism for biogenic volatile organic compounds (e.g., isoprene, a-pinene, d-limonene, et al.). Overall, it contains 77 chemical species and 237 reactions. The photolysis frequencies of 21 photochemical reactions are calculated according to Madronich (1987).

4.2.2 Emissions

The anthropogenic emissions are obtained from the 2006 Intercontinental Chemical

Transport Experiment-Phase B (INTEX-B) inventory (Zhang et al., 2009). It is a new emission inventory for Asia with 0.5°× 0.5° horizontal resolution containing all major anthropogenic sources with the exception of biomass burning. We assume that the grid of study domains has the same emissions rates with the nearest grid of the inventory. Therefore, the inventory is interpolated to the two nested domains by looking for the nearest grid. In addition, for DM2, a supplementary emission inventory with a high resolution of 1 km × 1 km is used for the Shanghai area, which was compiled by Shanghai Environmental Monitoring Center (Wang et al., 2012). Figure 4.2a, b shows the emission rates of NO_x in DM1 and DM2, respectively. Strong emission rates are found over East China. Statistics show that the emissions in East China contribute to 20 to 25% of China's total emissions.

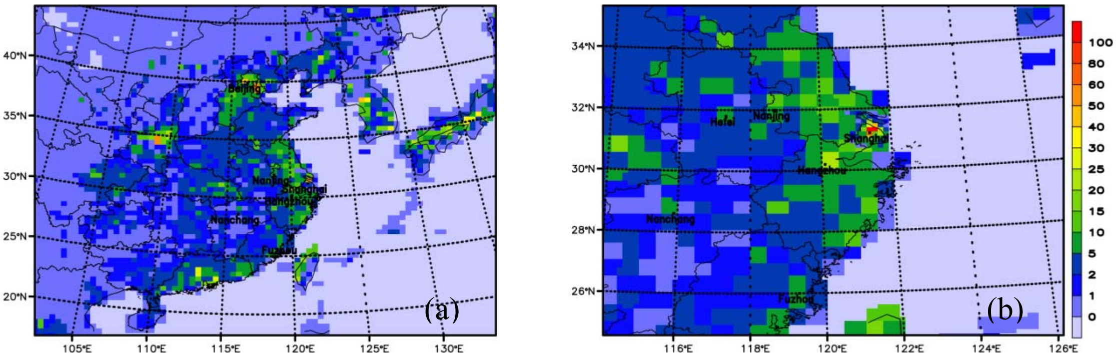

Figure 4.2 The emission rates of NO_x in a) DM1 and b) DM2 (ton $km^{-2}yr^{-1}$)

Table 4.2 Anthropogenic emissions in East China by province in 2006 (units: Gg yr^{-1})

Province	SO_2	NO_x	CO	VOC	PM10	PM2.5	BC	OC
Anhui	693	715	7986	958	757	574	84	173
Fujian	460	547	3895	701	435	337	44	127
Jiangsu	1697	1486	11326	1814	1200	881	87	186
Jiangxi	533	390	3963	463	586	400	39	76
Shanghai	618	631	1958	594	138	91	10	8
Zhejiang	1434	1106	4857	1233	806	556	36	45
Total1)	5435	4875	33985	5763	3922	2839	300	615
China total	31020	20830	166889	23247	18223	13266	1811	3217
Fraction (%)2)	17.5	23.4	20.4	24.8	21.5	21.4	16.6	19.1

1) Total of East China province (Anhui + Fujian + Jiangsu + Jiangxi + Shanghai + Zhejiang);

2) Fractions of the East China emissions to total China emissions

The emissions from biogenic sources in this study are calculated in real-time according to the simulated surface temperature and radiation, etc. by using the coupled MEGAN model (Guenther et al., 2006). The emissions are updated each half an hour. Figure 4.3 shows the mean emission rates of isoprene in DM2. High isoprene emission rates are predicted in Zhejiang, Fujian, Jiangxi, and southern Anhui provinces, while the emission rates in Shanghai, Jiangsu and most Anhui provinces are very low.

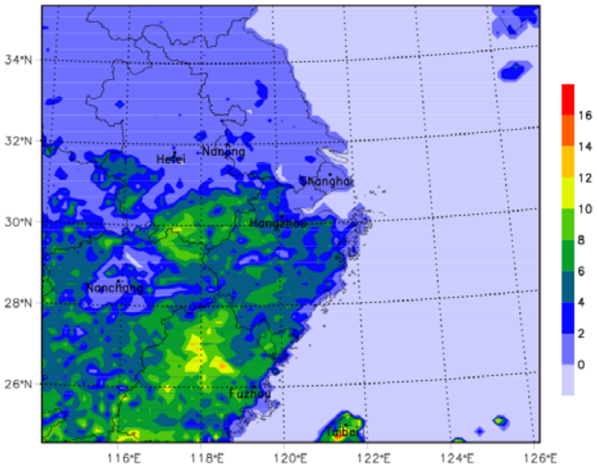

Figure 4.3 Mean emission rates of isoprene in DM2 (mol km^{-2}hr^{-1})

4.3 Results and discussions

4.3.1Model Evaluation

In this study, 4 meteorological variables observed at 33 stations over East China provided by the National Climatic Data Center (NCDC) (black dots in Figure 4.1b) were compared with DM2 simulations from 0800 LST 01 April to 1700 LST 29 April, 2008. These data sets have a time interval of 3 h. Results based on the proposed statistical measures summarized in chapter 3.5 are shown in Table 4.3. Overall, the simulated 2-m temperature (T2) and 10-m wind speed (WS10) are close to the observation data, with MB of 0.7 °C and 2.1 m s^{-1}, respectively. The COE of T2, 2-m relatively humidity (RH2), and WS10 are generally higher than 0.6, reflecting good agreements between the observation data and simulation results. The HR of 10-m wind direction (WD10) is 0.52 indicating that the model basically reproduces the trend of wind direction. In order to validate the temporal structure of the simulated temperature and winds in the East China, we selected observed ground level temperature and wind speed at four sites to compare with DM2 simulations (Figure 4.4). The variation trends of ground level temperature and wind speed are well reproduced at these four stations. However, the simulated wind speeds are generally higher than the observed at the NJ, QX and SH sites. The WRF/Chem model overestimated the surface wind speed, which has been reported in previous studies (Tuccella et al., 2012). In our study, it may be attributed to the inaccuracy in the initial and boundary conditions.

Table 4.3 Performance Statistics for four meteorological variables

Meteorological Variables	N stn 1)	Mean 2)		Δ 5)	MAE 6)	RMSE 7)	COE 8)	HR 9)
		Sim 3)	Obs 4)					
2-m Temperature (°C)	33	17.2	16.5	0.7	1.9	2.4	0.88	0.62
2-m Relative Humidity (%)	33	64	72	-8	16	20	0.61	0.55
10-m Wind Direction (deg)	33	-	-	-	-	-	0.48	0.52
10-m Wind Speed (m s^{-1})	33	5.0	2.9	2.1	2.4	2.9	0.62	0.34

1) Number of stations; 2) Mean value; 3) Simulation; 4) Observation; 5) Difference; 6) Mean absolute error; 7) Root mean square error; 8) Correlation coefficient; 9) Hit rate

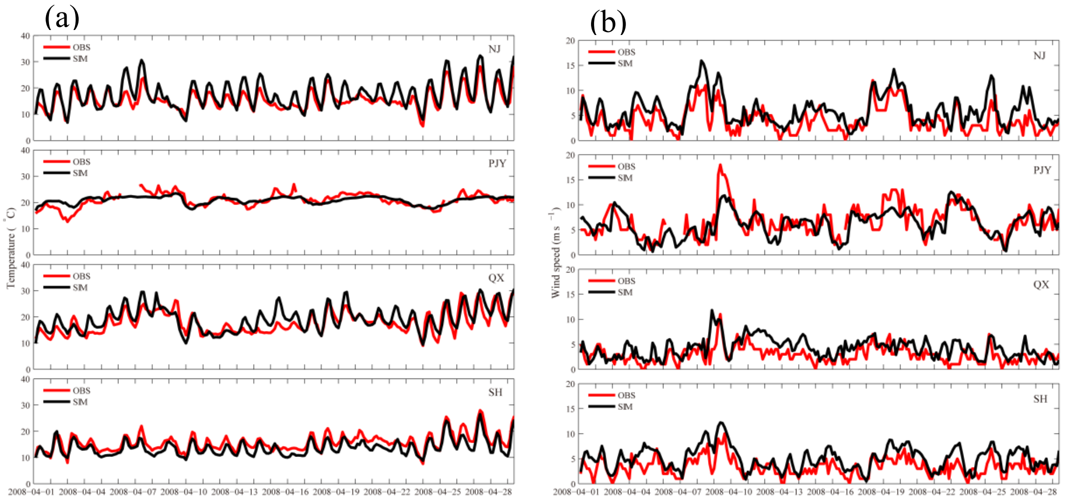

Figure 4.4 Time series of simulated and observed ground level a) temperature, b) wind speed at four sites: Nanjing (NJ), Pengjiayu (PJY), Quxian (QX), Shanghai (SH).

Hourly O_3 observation data from 0000 LST 03 April to 2300 LST 30 April, 2008 at 8 sites over the YRD are used to evaluate the O_3 modeling results. The site locations are shown in Figure 4.1, and more detailed information can be found in Table 4.4. The O_3 data of Zhejiang, Shanghai and Nanjing are provided by Zhejiang Province Environmental Monitoring Center, Shanghai Environmental Monitoring Center, and Nanjing Environmental Monitoring Center, respectively. Temporal variations of the observed and simulated hourly O_3 concentration at 8 sites are shown in Figure 4.5. It shows that the modeled results agree well with the observed ones at most sites. The correlation coefficients at the 8 sites are among 0.57 to 0.80, and the mean biases are among -12.0 to 11.3 ppb. Overall, there is a consistent variation trend of O_3 concentrations over the 8 sites during April 2008, indicating that it is a regional phenomenon for O_3 pollution. Basically, 3 episodes with relatively high O_3

concentrations are observed over the YRD, i.e. 6 – 7, 17 – 18, and 24 – 29 April. The model overestimates the O_3 peak during the episode of 6 – 7 April at most sites, and relatively well reproduces the other two episodes. The overestimation of O_3 concentrations during 6 – 7 April is probably related to the inaccuracies generated in the meteorological simulation (e.g. precipitation, temperature), as intensive precipitation and strong wind were observed during 6 – 7 April, while relatively well weather conditions are simulated, i.e. high temperatures and low humidity, and no rainfall.

Table 4.4 The information of O_3 observation sites used in this study

District	Name	ID	Lon	Lat	Type	Remarks
Hangzhou	Yuhang station	HZ_YH	119.985	30.264	suburban	located in a middle school of Yuhang town
	Jiande station	HZ_JD	119.282	29.464	urban	located at a middle school of Jiande county
Huzhou	Anji station	HZ1_AJ	119.696	30.598	rural	located in the east of Anji county
	Changxing station	HZ1_CX	119.909	31.024	suburban	located in a economic development zone of Changxing county
Jiaxing	Haining station	JX_HN	120.674	30.526	urban	Located in Haining county
Nanjing	Caochangmen station	NJ_CCM	118.748	32.058	urban	Located in the urban center of Nanjing
Shanghai	Qingpu station	SH_QP	120.978	31.093	suburban	Located by the Dianshan Lake
	Jiading station	SH_JD	121.25	31.374	urban	Located near the urban center of Jiading District

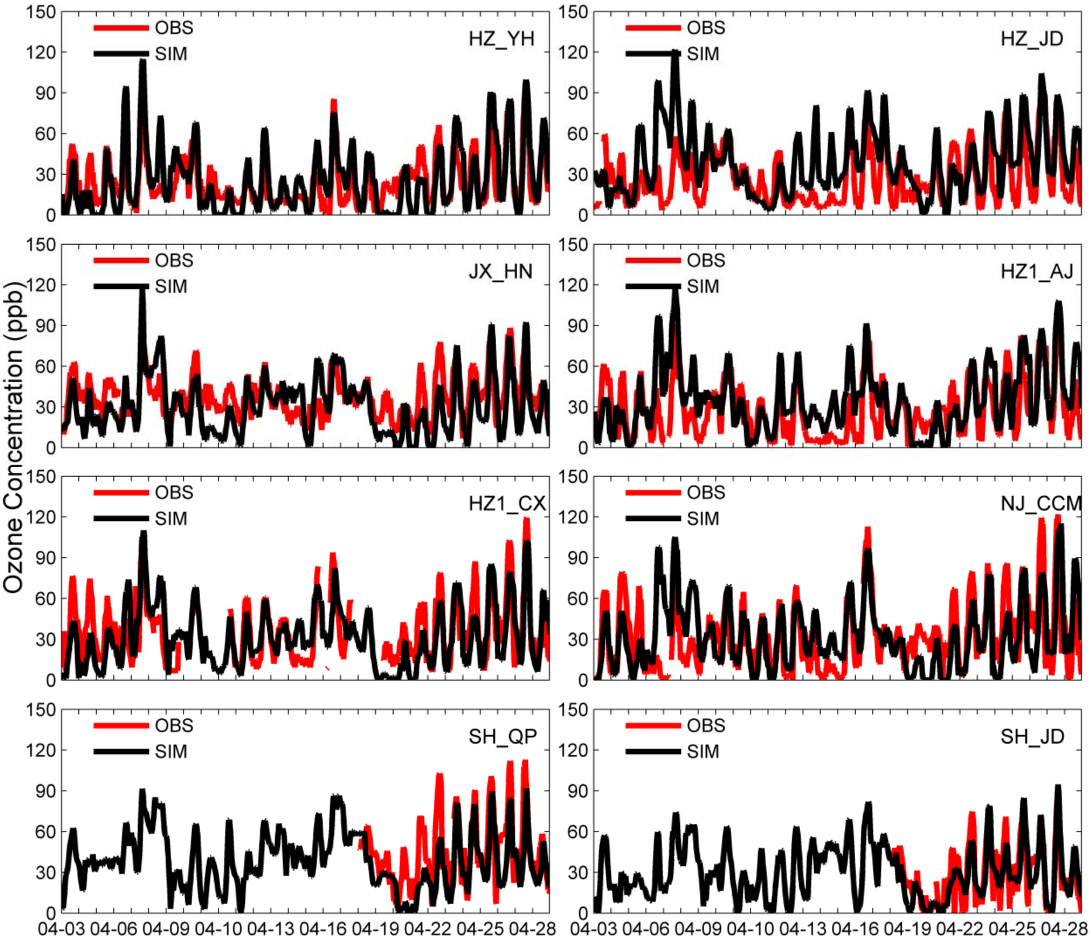

Figure 4.5 Time series of simulated and observed surface O_3 concentrations at 8 sites over YRD

Since O_3 formation is strongly related to its precursors, i.e. NO_x and VOCs (Kleinman et al., 2000), it is necessary to evaluate the model performances on these species. Unfortunately, we can’t obtain any VOCs data for evaluation in this study, and it is also difficult to obtain the NO_x data, as most environmental monitoring stations only measure the NO_2 mixing ratios in China. Hence, we further evaluate the NO_2 simulation results with the measurement data at 4 stations over the YRD (i.e. HZ_JD, HZ1_CX, JX_HN and NJ_CCM). Comparison of NO_2 concentrations at these 4 sites are illustrated in Figure 4.6. The mean bias between modeled and measured NO_2 at HZ_JD, HZ1_CX, JX_HN and NJ_CCM are 1.9, −1.0, 8.9 and −3.5 ppb, respectively, indicating that the model basically captures the NO_2 levels and distribution over the YRD. However, the correlation coefficients are relatively low, among 0.32 to 0.44. It is reasonable because the NO_x emission is highly influenced by the local emission sources such as mobile vehicles which cannot be captured by the coarse emission.

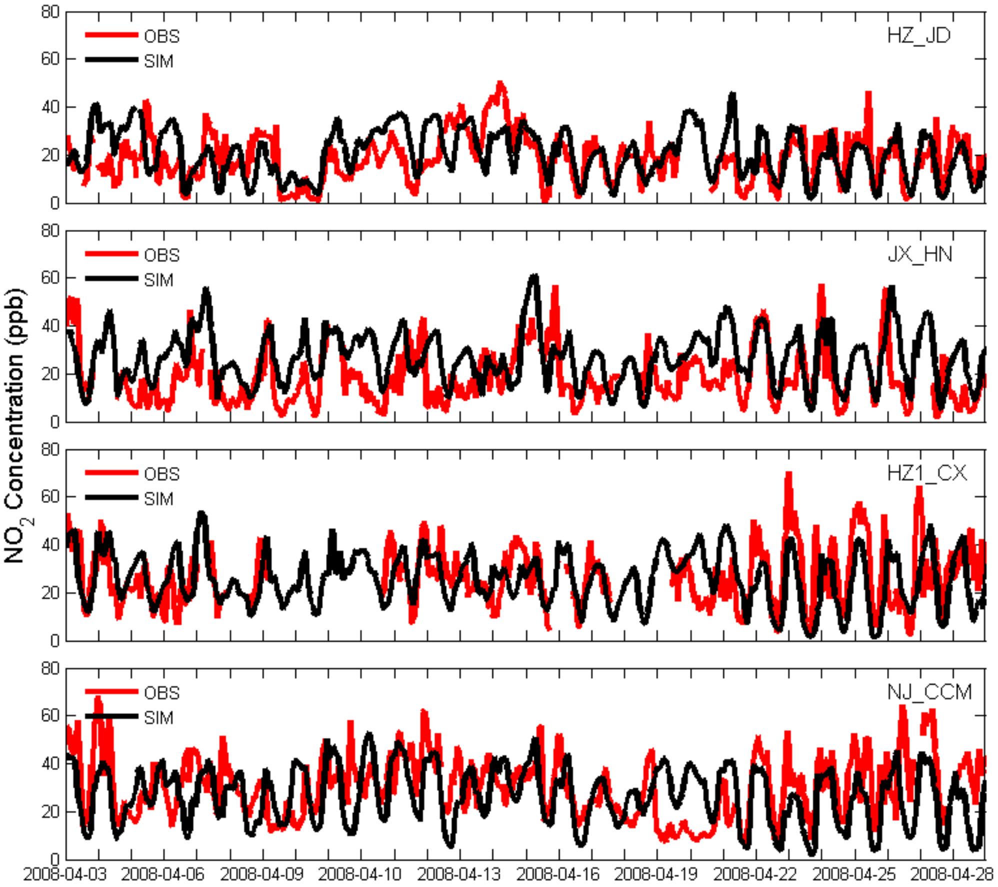

Figure 4.6 Time series of simulated and observed surface NO_2 concentrations at 4 sites over YRD

4.3.2 The distribution of O_3 mixing ratios in East China

Figure 4.7a and b shows the mean distributions of O_3 in DM2 on the surface and at 850 hPa, respectively. In order to investigate the regional transport characteristic, the wind field is also shown in Figure 4.7. On the surface, unexpectedly, the high O_3 concentrations (> 45 ppb) are located in Fujian, Jiangxi, south Anhui and southwest Zhejiang provinces, while the O_3 levels over the YRD region as well as north part of Jiangsu province are very low (< 40 ppb). Inspecting the wind field, the dominant eastern winds drove the fresh air masses from the East China Sea to the YRD region and northern Jiangsu. On the other hand, there are relatively high anthropogenic NO_x emissions (Figure 4.2) over the YRD region and northern Jiangsu, which can titrate the O_3 concentrations in this area. The winds over Fujian and Jiangxi provinces are very weak, implying that usually, the air masses over these areas are relatively stable, which are beneficial to the photochemical O_3 formation. Furthermore, the high biogenic VOCs emission rates over these areas (Figure 4.3) may be another reason to explain the high O_3 concentrations.

At 850 hPa, East China is fully controlled by the western air stream. High O_3 concentrations (> 60 ppb) occur over most East China (i.e. Jiangxi, Northern Fujian, Zhejiang, Shanghai, Southern Jiangsu, and Southern Anhui) and East China Sea, with the highest concentrations (> 70 ppb) over northeast Jiangxi and north Zhejiang. Obviously, the high O_3 is driven by western winds from East China to the East China Sea. In addition, the southwest winds over Jiangxi, Fujian, southern Anhui, and southwest Zhejiang can also drive the O_3 formed in situ to the YRD region.

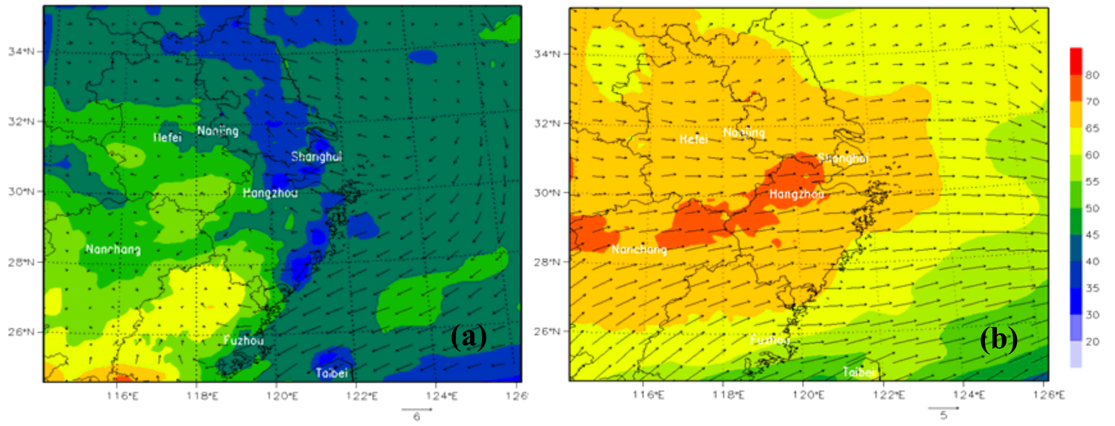

Figure 4.7 The mean distribution of simulated O_3 concentrations (shaded, ppb) and wind (vector, m s^{-1}) in DM2 during daytime (0800-1700 LST) (a, surface; b, 850 hpa)

As shown in Figure 4.5, there are high O_3 concentrations at most sites over the YRD on 7 and 29 April, so we further inspect the O_3 distributions on these two days. The O_3 patterns on the surface and at 850 hPa at 1400 LST of these two days are shown in Figure 4.8. On both days, there is a belt area with higher O_3 concentrations. On 7 April, the O_3 belt is located from northwest of East China to the YRD region, while on 29 April, the belt area is located from west of East China to the East China Sea (through the YRD). The higher O_3 mixing ratios belt on 7 April may be caused by the convergence airflow, since the southern airstream and northern one are converged on these areas, implying that the contribution from regional transport to the O_3 concentrations is significant. Meanwhile, the belt on 29 April is corresponding to a ridge of high pressure, which is located from Japan to East China (not shown). Usually, there is sunny weather (e.g. clear sky, strong solar radiation, stable boundary layer, etc.) when controlling by high pressure ridge, implying that there may be remarkable photochemical O_3 generation on that day.

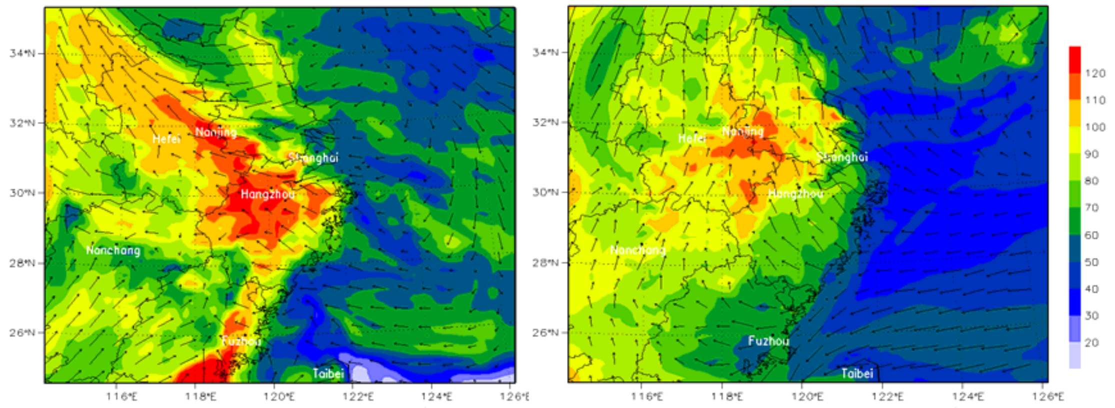

1400LST, 7 April

1400LST, 29 April

(a) surface

(b) surface

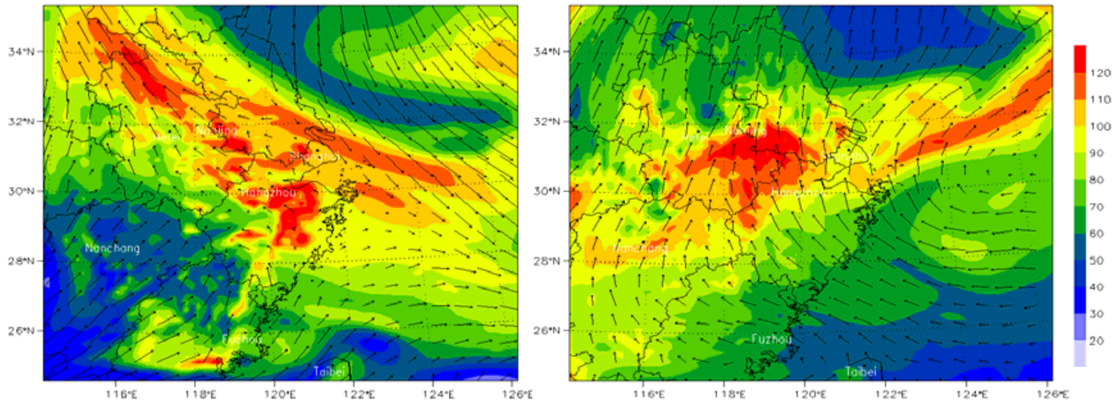

(c) 850 hPa

(d) 850 hPa

Figure 4.8 The mean distribution of simulated O_3 concentrations (shaded, ppb) and wind (vector, m s^{-1}) in DM2 at 1400 LST of two O_3 episode days.

4.3.3 Relative contributions of photochemical and physical processes

The contributions from the physical and chemical processes to ground-level O_3 concentrations have been estimated in order to analysis the mechanism of O_3 formation. Generally, the maximum hourly O_3 concentrations occur at 1400 LST every day. Hence, daily contributions to the O_3 formation are accumulated from 0800 LST to 1400 LST. Figure 4.9a, b shows the mean distribution patterns of daily accumulated chemical production rates (CHEM) and physical contribution rates (PCR) on the ground level, respectively. As shown in Figure 4.8a, the mean accumulated CHEM over the YRD region and northern Jiangsu are fully negative (< -20 ppb D^{-1}; D is defined as hours from 0800 LST to 1400 LST, same thereafter). It means the photochemical processes mainly act as a role of titrating the O_3. These significant O_3 consumptions by photochemical process result in the low O_3 mixing ratios in these areas. The mean accumulated CHEM in Jiangxi and Fujian are positive (0~20 ppb D^{-1}). Contrary to the CHEM, there are strong positive accumulated PCR (> 50 ppb D^{-1}) over the YRD and northern Jiangsu, while slight physical contributions occur in Jiangxi and Fujian provinces (Figure 4.9b). These results suggest that, on the ground level, the high O_3 mixing ratios over southern East China (i.e., Jiangxi and Fujian) are formed by local photochemical reactions, while those over the YRD region are mainly transported or diffused from surrounding areas.

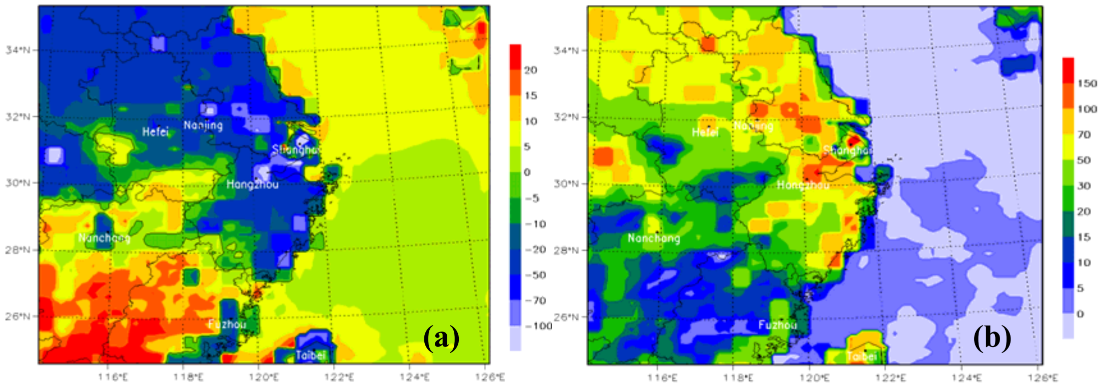

Figure 4.9 Mean distributions of daily accumulated contributions (0800-1400 LST) to O_3 formation from (a) photochemical generation and (b) physical processes on the ground level; physical processes: vertical transport + horizontal transport + dry deposition, same thereafter; unit: ppb D^{-1}.

As discussed above, southern East China and the YRD are two regions with different O_3 formation mechanisms. Therefore, two sub-regions are defined in this study (see Figure 4.1). The southern East China region [25.5 °N ~ 28.5 °N, 115 °E ~ 119 °E] is defined as Region 1, and the YRD region [30 °N ~ 32.8 °N, 118 °E ~ 122 °E] is defined as Region 2. Region 1 is a forest area, with high biogenic emissions and low anthropogenic emissions, while Region 2 is a developed area, with high anthropogenic emissions and low biogenic emissions. Figure 4.10a, b shows the daily accumulated CHEM, PCR, and net contributions during 2 ~ 30 April in Region 1 and Region 2, respectively. Basically, 3 O_3 episodes with high net contributions are captured in both regions, which lead to high O_3 mixing ratios. In Region 1, on some episode days, e.g. 4 ~ 7 April, the O_3 formation is dominated by photochemical generation, while on some other episode days e.g. 15 ~ 18 April, the photochemical and physical processes play similar roles to the O_3 formation. Overall, both photochemical and physical processes have important contributions to the O_3 formation in Region 1, with mean contributions of 11.7 and 15.0 ppb D^{-1}, respectively (Table 4.5). In Region 2, during the whole study period, the photochemical process plays a role of consuming the O_3 concentrations. The high O_3 mixing ratios may be transported from surrounding areas or vertical transported and diffused from middle and upper planetary boundary layer (PBL). The highest PCR is simulated on 7 April, consistent with the discussion in section 4.3.2 that the high O_3 mixing ratios over the YRD region are dominated by regional transport. During 24 – 29 April, the CHEMs (~ 10 ppb D^{-1}) are much lower than the other days (more than -30 ppb D^{-1}) in April, indicating more significant photochemical O_3 generation during these days, which is also consistent with the inference in the end of section 4.3.2. The mean contributions of photochemical and physical processes are -35.9 and 62.3 ppb D^{-1} respectively.

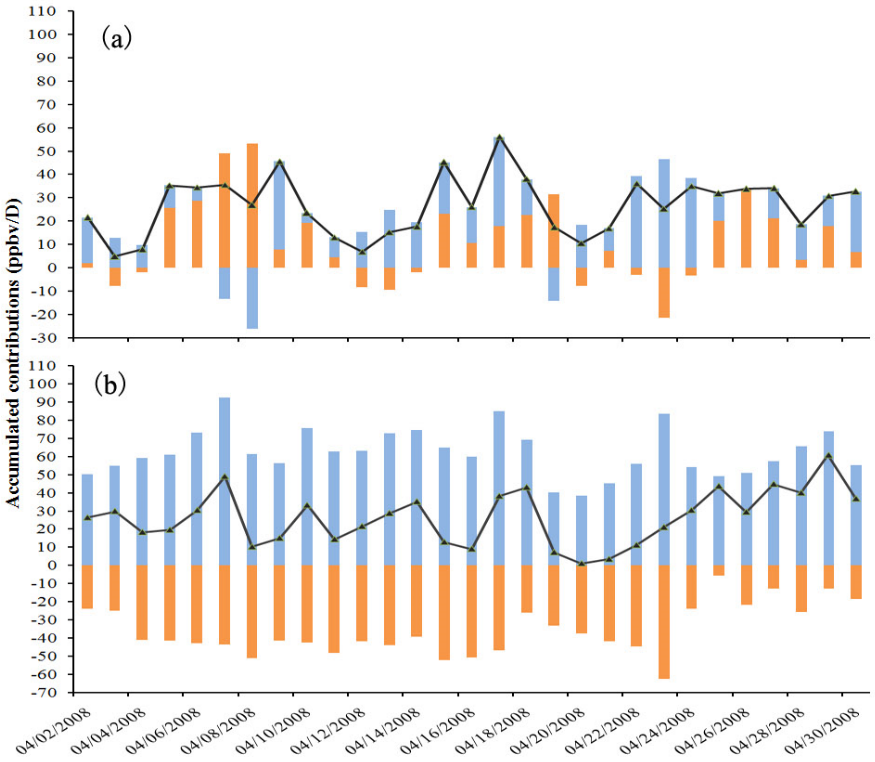

Figure 4.10 Daily accumulated photochemical production rates (0800-1400 LST) (CHEM: orange), physical processes rates (PCR: blue) and the net contributions (black lines) in two defined sub-regions (a, Region 1, southern East China region, [25.5 °N ~ 28.5 °N, 115 °E ~ 119 °E]; b, Region 2, YRD region, [30 °N ~ 32.8 °N, 118 °E ~ 122 °E])

4.3.4 The impact of biogenic and anthropogenic emissions to O_3 formation

The discussions in section 4.3.2 and 4.3.3 indicate that the high O_3 mixing ratios in Jiangxi and Fujian provinces may be related to the biogenic emissions, while the O_3 mixing ratios over the YRD region are dominated by strong anthropogenic emissions. Three additional sensitivity experiments are simulated to understand the potential contributions of biogenic emissions and anthropogenic emissions to the O_3 formation in East China: Case 1, the biogenic emissions over the East China region ([25 °N ~

35 °N, 114 °E ~ 124 °E], basically cover the DM2, same thereafter) are excluded; Case 2, the anthropogenic emission over the East China region are removed; Case 3, both biogenic and anthropogenic emissions over the East China region are removed. The other model setups of these three cases are the same as the base case (the experiment in Section 4.2).

Table 4.5 lists the mean mixing ratios of O_3 during daytime (0800 – 1700 LST) and mean accumulated contributions (0800 – 1400 LST) of photochemical and physical processes at the ground level in East China and in the two sub-regions for different study experiments. Overall, biogenic emissions increase the mean daytime O_3 mixing ratio over East China at about 2.5 ppb (Base case – Case 1), which is attributed to the increase in photochemical generation (~ 5 ppb D^{-1}). In Region 1 and Region 2, the biogenic emissions lead to an increase in accumulated CHEM at about 10.2 and 3.9 ppb D^{-1}, which result in an increase of O_3 mixing ratios of 4.8 and 2.6 ppb, respectively. These results are close with the previous studies (Wang et al., 2008), which showed that during daytime, the biogenic VOCs could increase the O_3 mixing ratios at around 5 ppb in most eastern China in summertime. The impacts of biogenic emissions to the O_3 formation are determined by the simulated biogenic species (e.g., VOCs and NO_x) concentrations, and so, it is important to evaluate the simulated biogenic VOCs concentrations. However, due to the lack of measurement data during this study period, it is impossible to directly compare the simulated and observed values. Using the same model system (WRF/Chem plus MEGAN) to simulate the biogenic VOCs concentrations, Geng et al. (2011) evaluated the modeled and observed biogenic isoprene concentrations over Zhejiang province in September 2009. Their evaluation showed that the simulated isoprene mixing ratios agree well with the observed ones when the observed isoprene mixing ratios are less than 3 ppb, but the simulation results were underestimated when the observed mixing ratios are above 3 ppb. This indicates that the simulated biogenic VOCs concentrations are reasonable to a certain extent, and the impact of biogenic emissions may be underestimated in this study.

The anthropogenic emissions play a key role to O_3 formation in East China. On average, when removing the anthropogenic sources, the accumulated CHEM increases at about 15.8 ppb D^{-1} (Base case – Case 2), but the accumulated PCR decreases at about 23.7 ppb D^{-1}, which lead to a decrease of mean daytime O_3 mixing ratios of about 4.5 ppb. Since the emissions outside of East China are the same between base case and Case 2, we could assume that there is no change in the horizontal transport/diffuse of O_3 from the outside of the East China region. Hence, the decrease in accumulated PCR should be attributed to vertical transport/diffuse, suggesting that the O_3 is mainly formed in the middle and upper PBL and then transport and diffuse to the ground level in East China. In Region 1, due to the low anthropogenic emissions, the accumulated CHEM only decreases at about 1.2 ppb D^{-1}, but the accumulated PCR decreases remarkably, with value of 11.1 ppb D^{-1}. Since the anthropogenic emissions mainly originate from the YRD and northern Jiangsu, these results indicate that the O_3 mixing ratios in forest areas could be significantly affected by the emissions from developed areas. In Region 2, when removing the anthropogenic emissions, the accumulated CHEM rises at about 40.3 ppb D^{-1}, but the PCR decreases at about 52.4 ppb D^{-1}, leading to a net decrease of 12.1 ppb D^{-1}. However, the mean daytime O_3 mixing ratios are only reduced by about 0.3 ppb, this may be related to the nighttime O_3 mixing ratios. Inspecting the daily daytime O_3 mixing ratios, in some O_3 episode days, the anthropogenic emissions contribute to more than 20 ppb to O_3 mixing ratios (not shown).

When removing both biogenic and anthropogenic emissions in East China, the O_3 mixing ratios decease to about 43 ppb in all regions (Case 3), implying that on average, about 43 ppb O_3 mixing ratios are transported through the lateral boundary from the outer domain regions as well as the background. There are still photochemical O_3 formations in all regions (3.8 ~ 8.9 ppb D^{-1}), indicating that there are obvious regional inflow of O_3 precursors from outer domain regions. Also we recognized that the combined effect of removing biogenic and anthropogenic emission is not equal to the sum results from case 1 (removing biogenic emission) and case 2 (removing anthropogenic emission) due to the nonlinear effect of photochemistry. This strongly nonlinear effect between O_3 and its precursors may also result some uncertainties in the results.

Table 4.5 Mean mixing ratios of O_3 during daytime (0800 – 1700 LST) and mean accumulated contributions (0800 – 1400 LST) of photochemical and physical processes in three concerned regions for different study experiments

	Region 1[1)]			Region 2[2)]			East China[3)]		
	CHEM[4)]	PCR[5)]	O_3[6)]	CHEM	PCR	O_3	CHEM	PCR	O_3
Base case	11.7	15.0	56.1	-35.9	62.3	44.1	-9.6	30.3	48.1
Case 1	1.5	20.9	51.3	-39.8	63.8	41.5	-14.5	32.9	45.5
Case 2	10.5	3.9	43.3	4.4	9.9	43.8	6.2	6.6	43.6
Case 3	8.9	4.2	43.0	3.8	10.1	43.6	5.2	7.0	43.3

1) Region 1, southern East China region, [25.5 °N ~ 28.5 °N, 115 °E ~ 119 °E]; 2) Region 2, YRD region, [30 °N ~ 32.8 °N, 118 °E ~ 122 °E]; 3) East China region, [25 °N ~ 35 °N, 114 °E ~ 124 °E]; 4) accumulated contributions (0800 – 1400 LST) of photochemical reactions; 5) accumulated contributions of physical processes; 6) Mean daytime (0800 – 1700 LST) O_3 mixing ratios

4.4 Conclusions

The characteristics of O_3 distributions and formations over East China in springtime (April 2008) are investigated using the WRF/Chem model. The comparison between modeled and measured meteorological fields, hourly O_3 mixing ratios, and hourly NO_2 concentrations illustrates that the model well captured the real condition.

On the ground level, the high O_3 pollution areas (> 45 ppb) are located in Fujian and Jiangxi province, while the O_3 levels over the YRD region as well as northern Jiangsu province are very low (< 30 ppb). Further investigation of the relative contributions of photochemical reactions and physical processes over East China reveals that the high O_3 mixing ratios in Jiangxi and Fujian are contributed by both local photochemical generation and regional transport, while the O_3 mixing ratios over the YRD region are transported and diffused from surrounding areas. In order to investigate the impact of local biogenic and anthropogenic emissions in East China, three additional sensitivity simulations are conducted, which show the contributions of local emissions and regional transport in East China as well as the YRD region (Region 2) and the Jiangxi and Fujian region (Region 1). On average, the biogenic emissions and anthropogenic sources may contribute 2.6 and 4.5 ppb to daytime mean O_3 mixing ratios respectively in East China, while the inflow from the outer domain and background may contribute about 43 ppb.

Chapter 5 A numerical study of the impact of climate and emission changes on surface O_3 over South China in autumn time in 2000−2050

5.1 Introduction

The aim of this chapter is to study the contributions of future climate change and emission change to surface O_3 in South China using WRF/Chem model driven by the outputs of CCSM3. South China refers to the area including the provinces of Guangdong, Hainan, Fujian, parts of Jiangxi, Hunan, Guangxi, and 2 special administrative regions (SAR): Hong Kong and Macau. In section 5.2, we describe the methodology and the input data adopted in this study. The model performance is evaluated in section 5.3. In section 5.4, future climate change and its impact to biogenic emission and surface O_3 are presented. In section 5.5, the effect of anthropogenic emission change and the combined climate change and emission change effect on O_3 formation are investigated. In section 5.6, sensitivities of surface O_3 over rural, urban and ocean regions are discussed. Section 5.7 summarizes the significant findings of this chapter.

5.2 Methodology

5.2.1. Model configuration

The WRF/Chem version 3.0 was applied to simulate the O_3 air quality in this study.

The detailed options of physical and chemical parameterization scheme used in this study are shown in Table 5.1. An Urban Canopy Model (UCM) coupled with the Noah Land Surface Model (Noah/LSM) was adopted for better simulating the urban effect on meteorological conditions and surface O_3 distribution. In the WRF/Chem model, the default U.S. Geological Survey (USGS)-based land cover data was derived from Advanced Very High Resolution Radiometer (AVHRR) observations in a 12-month period from April 1992 to March 1993 (Loveland et al., 1991). However, due to economic development, China has undergone rapid urbanization progress since 1990s. The default USGS data is too old to reflect this intensive land-cover change. So we mapped the urban land cover data acquired from the 2000 MODIS land cover product into the simulation domains to replace the default USGS data as described by Jiang et al. (2010a). For the gas phase chemistry, CBMZ was applied which contains 55 prognostic species and 134 reactions (Zaveri and Peter, 1999). Based on original Carbon Bond Mechanism (CBM-IV), CBMZ includes reactive long-lived species, revised isoprene chemistry, and optional DMS chemistry. MOSAIC was adopted as the aerosol chemistry option in simulation, with aerosol size distribution divided into eight discrete size bins (Zaveri et al., 2008). Initial and boundary conditions for the gas phase variables are using the default profiles in WRF/Chem collected from the aircraft measurements over the eastern Pacific Ocean (McKeen et al., 2002). Boundary conditions for O_3 NO_x and CO are varying with altitude. Specifically, at surface, O_3 condition is fixed at 30 ppb, and increasing exponentially to 40 ppbv at 2 km, then increasing to 150 ppb at the model top. There are no adjustments for chemical boundary conditions in the future year simulations which may result in some uncertainty in the model results.

Table 5.1 The grid settings, physics and chemistry options used in this study

Items	Contents
Dimensions(x, y)	100, 100/82,79
Grid size (km)	45/15
Vertical layers	28
Time step (s)	180
Microphysics	WRF Single-Moment 6-class scheme(Hong and Lim, 2006)
Long wave Radiation	RRTM scheme (Mlawer et al., 1997)
Shortwave Radiation	Goddard shortwave (Chou and Suarez, 1994)
Surface Layer	Moni-Obukhov scheme ((Monin and. Obukhov, 1954)
Land Surface	Noah Land-Surface Model (Chen and Dudhia, 2001)
Planetary Boundary layer	YSU scheme (Hong and Pan, 1996)
Cumulus Parameterization	Kain-Fritsch scheme (Kain, 2004)
Chemical Mechanism	CBMZ (Zaveri and Peter, 1999)
Photolysis scheme	Fast-J photolysis (Wild et al., 2000;Barnard et al., 2004)
Aerosol Module	MOSAIC using 8 sectional aerosol bins (Zaveri et al., 2008)

Two nested domains were defined in the simulation, which are shown in Figure 5.1. The outermost domain (D1) covers the most part of China region and the Korean Peninsula (5–45° N, 90–135° E), with the center point at 27.6° N, 113.1° E, horizontal grids of 100 × 100, and grid spacing of 45 km. The nested domain (D2) covers the southern part of China (15° N–28° N, 108° E–119° E), with 82 × 79 horizontal grids at 15 km grid spacing. From the ground level to the top pressure of 50 hPa, there are 28 vertical sigma layers to all grid meshes, with about 10 layers below AGL.

The NCAR CCSM3 outputs followed the A1B scenario are used to drive WRF/Chem model as in Jiang et al. (2008b, 2010c). The A1B scenario is representing a mid-line scenario for carbon dioxide emissions and economic growth compared with other SRES emission scenarios. We choose two periods of three years in 2000s (2005-2007) and 2050s (2055-2057) to provide the regional model with present and future years meteorological inputs.

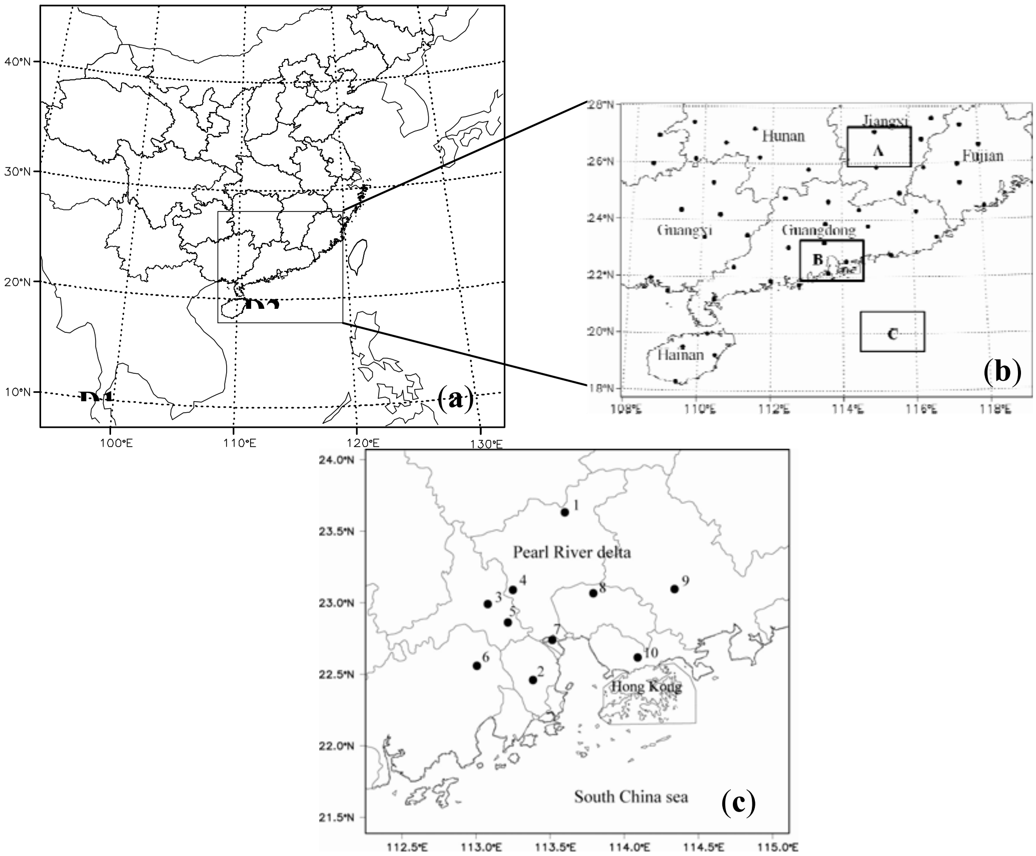

Figure 5.1 a) Simulation domain setting, b) locations of the meteorological sites for model evaluation (black point) and three selected regions (black square box), c) locations of air quality monitoring sites at PRD region: 1) Tianhu (TH), 2) Zimaling (ZML), 3) Huijingcheng (HJ), 4) Luhu (LH), 5)Shunde (SD), 6)Donghu (DH), 7) Wanqingsha (WQS), 8)Haogang (HG), 9)Xiapu (XP), and 10)Liyuan (LY)

5.2.2. Emission inventory

The anthropogenic emissions for the present year 2000s are obtained from the 2006 Intercontinental Chemical Transport Experiment-Phase B (INTEX-B) inventory (Zhang et al., 2009). It is a new emission inventory for Asia with 0.5°× 0.5° horizontal resolution developed to support INTEX-B field campaign. The emissions include sulfur dioxide (SO_2), NO_x, CO, VOCs, PM10, PM2.5, BC and OC from power, industry, residential, and transportation sectors. Emissions from ship exhaust are not included in this inventory. Biomass burning emission is not included in this inventory. The Transport and Chemical Evolution over the Pacific (TRACE-P) biomass burning emission for the year 2000 has been applied to estimate the Asia biomass burning (Streets et al., 2003). We then specified monthly variations of anthropogenic and biomass burning emissions following the work of Zhang et al. (2009) and Streets et al. (2003), respectively. Figure 5.2a shows the distributions of monthly averaged NO emissions from the major anthropogenic sources and biomass burning as well for the inner domain. Strong NO emissions (>50 mol km^{-1} hr^{-1}) were found mainly over PRD, east of Guangdong province, and coastal region of Fujian province. We estimate the future year anthropogenic emissions by multiplying the 2006 base year emission inventory with the regional growth factors for SRES A1B scenario. The growth factors in China and Southeast Asia are 1.82, 2.11, and 2.84, for CO, NOx, and NMVOC respectively, which are calculated following Wigley et al. (2002).

Biogenic emissions of O_3 precursors are computed locally using MEGAN v2.04

coupled within the WRF/Chem model (Guenther et al., 2006). Emission rates of biogenic compounds are calculated on the basis of vegetation and meteorological parameters. The vegetation parameters including plant functional type fractions, base emission rates and leaf area index with the highest resolution up to 1 km^2 are supplied by the National Center for Atmospheric Research (http://cdp.ucar.edu). Under standard conditions, as shown in Figure 5.2b, high isoprene emission rates are found in the forested regions mainly over Fujian, Hunan, and southern part of Hainan province, while the emission rates in most Guangxi, Guangdong province are relatively low. Meteorological datasets comprising 2-m temperature, surface pressure, and downward solar radiation are provided from WRF model. Climatological surface air temperature and downward solar radiation datasets are provided by CCSM monthly-mean output data of current (2005–2007) and future (2055–2057) years. Totally, hourly emissions of 138 compounds were estimated by Megan model which are grouped into 20 classes. Since the biogenic emissions are estimated based on the simulated hourly meteorological parameters, they are allowed to change in response to climate change. It should be noted that in this study the changes in NO_x from lightning and stratosphere-troposphere exchange (STE) of O_3 are not accounted in the model.

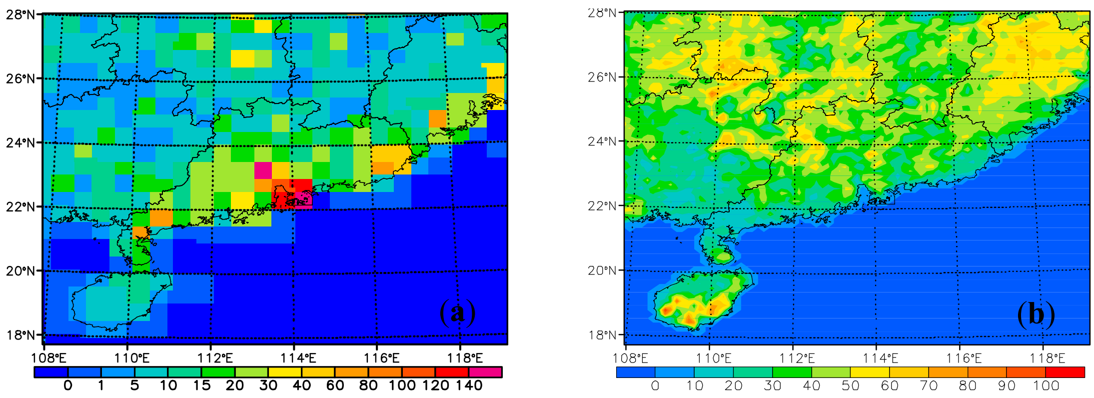

Figure 5.2 Spatial distributions of (a) daily average anthropogenic and biomass burning NO emissions in October (mol km^{-2} hr^{-1}) and (b) standard biogenic isoprene emissions generated by MEGANv2.04 (mol km^{-2} hr^{-1}).

5.2.3. Experiments design

This study conducts five cases of numerical experiments to evaluate the climate change impact, the anthropogenic emission change impact and their combined impacts on surface O_3 concentration. Different sets of simulation periods, meteorological conditions, and anthropogenic emissions are listed in Table 5.2. The control experiment CL2000EM2000 was driven by the meteorological conditions of year 2000s and the INTEX-B anthropogenic emission at 2006 with biomass burning emission obtained from TRACE-P. CL2050EM2000 was driven by the anthropogenic emissions of 2000s but with the meteorological conditions of 2050s. CL2000EM2050, CL2050EM2050 were carried out with 2050s anthropogenic emissions, but with 2000s and 2050s meteorological conditions, respectively.

Methane is a long lifetime species, which is not dynamically simulated in WRF/Chem model. Also, it is not regulated in local scales. So CH_4 concentration was not increased when conducting the "emission change" scenarios (CL2000EM2050, CL2050EM2050). However, on a global scale, methane plays an important role in determining background O_3 concentrations. We add a sensitivity experiment METH2050 to evaluate the impact of CH_4 emission change on surface O_3. The methane mixing ratio was increased to 2.90 ppm at 2056 under the A1B scenario.

Due to the limitation of computing resources, each case was run for three consecutive October (2005–2007 or 2055–2057) to represent the autumn conditions of present and future climate, since the seasonal O_3 pattern for the period 1994–2007 shows a clear autumn maximum with peaks in October (Wang et al., 2009). Each simulation starts at 0000 UST 29 September. With the initial 41 hours of the model spin-up time, simulation results of the whole October were analyzed.

Table 5.2 Five cases of numerical experiments conducted in this study

Simulation	Period	Description
CL2000EM2000	October 2005-2007	2000s CCSM3 meteorological fields and biogenic emissions; INTEX-B anthropogenic emissions;
CL2050EM2000	October 2055-2057	2050s CCSM3 meteorological fields and biogenic emissions; INTEX-B anthropogenic emissions;
CL2000EM2050	October 2005-2007	2000s CCSM3 meteorological fields and biogenic emissions; future anthropogenic emissions;
CL2050EM2050	October 2055-2057	2050s CCSM3 meteorological fields and biogenic emissions; future anthropogenic emissions;
METH2050	October 2056	2056 CCSM3 meteorological fields and biogenic emissions; INTEX-B anthropogenic emissions;2050s CH4 concentration;

5.3 Evaluation of model performance

In our study, the meteorological initial and boundary conditions of WRF/Chem are provided by a global climate model instead of reanalysis data. In order to evaluate the model performance and downscaling effect, simulation results of meteorological factors are compared with the global GCM outputs, since the CCSM3 outputs used for the comparisons have been extensively evaluated (Collins et al., 2006b).

Using sensitivity analysis (MM5-CMAQ), Wei (2012) showed that the peak O_3 concentrations would increase from 270 ppb to 301 ppb due to the rise of air temperature under a tropical cyclone scenario in PRD region. Owing to the importance of temperature on photochemical reaction and biogenic emission, the following evaluation mainly focuses on 2-m temperature (hereafter called surface temperature). Figure 5.3 shows that the large-scale spatial patterns of monthly mean surface temperature over East Asia simulated by CCSM and WRF/Chem are similar, which implies that WRF/Chem performed relatively well in the simulation of surface temperature. Also, both models show the surface temperature decreased gradually from the southeast ocean regions to the northwest China. However, we found a large local and regional variability in land regions. With WRF/Chem better resolving of key physical processes and updating with the latest high resolution geographic data, it can capture the characteristics of surface temperature in regional scale.

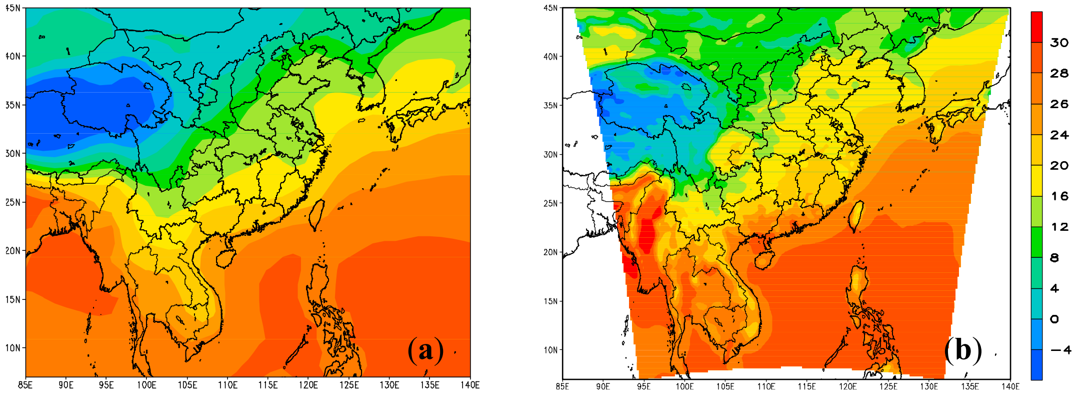

Figure 5.3 Monthly average surface temperature (°C) during October 2005–2007 from a) CCSM outputs and b) WRF/Chem outputs.

Daily mean surface temperature observed at 47 meteorological stations over South China provided by the National Climatic Data Center (NCDC) (black dots in Figure 1b) were compared with simulations in October during 2005-2007. Overall, the simulated surface temperature was slightly lower than the observed data, with mean bias of -0.63°C. The spatial pattern correlation coefficient is 0.91, reflecting good spatial agreements between the observation data and simulation results. However, there are large biases reaching as high as 1 to 2°C at the sites Jian and Ganzhou in Jiangxi province, which subsequently may result in some biases in surface O_3 concentration (Figure 5.4a). The average temporal correlation coefficient is 0.60 which indicated that the simulation basically captured the cooling trend of the surface temperature. The comparison of daily mean surface temperature at Macau (MA) and Shantou (ST) are showing in Figure 5.4b.

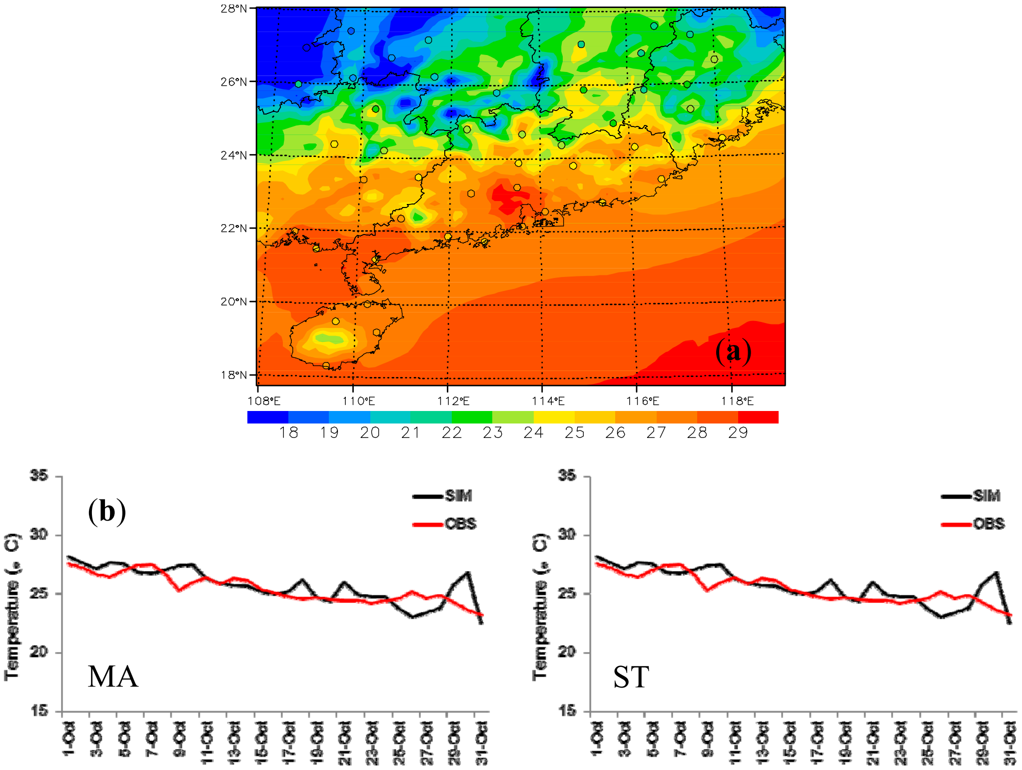

Figure 5.4 a) Simulated (shaded) and observed (dot) monthly average surface temperature (°C) in South China, b) Time series of simulated and observed surface temperature at two sites: Macau (MA) and Shantou (ST) for the October from 2005-2007.

The diurnal cycles of monthly averaged surface O_3 concentrations at 11 major sites over Hong Kong area were also evaluated. These sites are maintained by Hong Kong Environment Protection Department. The locations and the characteristics of each site can be found at http://www.epd-asg.gov.hk/english/backgd/quality.html. The result shows that the simulation well captured the diurnal cycles of surface O_3 concentrations, especially during the daytime (Figure 5.5). However, the model underestimates the O_3 concentrations at night. On average, during daytime, the simulated O_3 concentration was slightly higher than the observed data, with mean bias of 2.7 ppb. Furthermore, the monthly average O_3 concentrations at 10 sites operated by Guangdong Province Environmental Monitoring Center over PRD region (Figure 5.1c) were also evaluated. The result indicated that the model has a relatively good performance in simulating surface O_3 over PRD region, with mean bias at -0.9 ppb (Table 5.3). We also notice that the model also well captured the high O_3 at TH and XP sites.

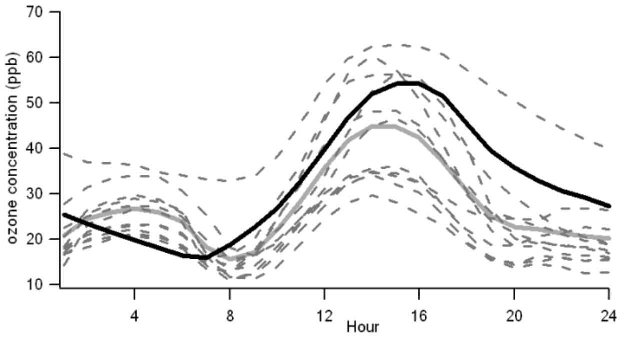

Figure 5.5 Diurnal cycles of present years O_3 concentrations in October 2005-2007 for observations at 11 stations (dotted lines), mean observed results (gray line) and the mean simulated results (black lines).

Table 5.3 Monthly average O_3 concentrations at 10 sites over PRD region during the October of 2006 and 2007

	LH	WQS	TH	LY	SD	HJ	DH	XP	HG	ZML	Mean
Obs	24.73	38.27	47.37	28.00	34.30	31.03	31.97	41.30	30.10	38.97	34.60
Sim	30.77	33.40	43.24	29.12	31.64	29.16	30.81	39.47	37.85	31.90	33.74

5.4 Climate change and its impact on O_3 air quality

5.4.1 Regional climate change

Since the meteorological factors in the planetary boundary layer have significant effects on the photochemical processes, it is necessary to analyze the changes of the meteorological factors over the period between the 2000s and the 2050s. The differences of meteorological variables including 2-m temperature, 2-m water vapor mixing ratio, planetary boundary layer height (PBL height), and 10-m wind speed were calculated based on the simulations CL2050EM2000 and CL2000EM2000 for the inner domain.

Figures 5.6a depicts the change of 2-meter temperature during 12–18 LST simulated by the regional model for October in 50 years' time. Owing to the increase of greenhouse gases, average afternoon surface temperature is predicted to increase by 1.6 °C over the entire inner domain. The highest increases of 2 to 2.8 °C occurs over the northeast and northwest area of the modeling domain, while surface temperature increases are smaller over southwest part of Guangdong province, Hainan, Guangxi and the ocean. Figure 5.6b shows that there is a significant increase of 2-m water vapor mixing ratio occurring over southern China, with the highest increase up to 2.0 g kg^{-1} over Taiwan Strait. Average near-surface water vapor is predicted to increase by 1.6 g kg^{-1} over the entire inner domain. In response to the significant surface warming, evaporation from the ocean will increase. Higher temperature in the future allows the atmosphere to hold more water. The pattern of changes in PBL height is quite similar to the spatial distribution of temperature change. The largest warming occurs over northeast and northwest area of the modeling domain results in enhanced mixing in these areas where the PBL height could increase up to 80m. The largest decrease up to 120 m in PBL height occur over areas including the Leizhou Peninsula, the eastern seaboard of Guangxi and the southeast portion of modeling domain (Figure 5.6c). A day time reduction of near-surface wind speed is predicted over Jiangxi, Fujian, Hainan and part of Guangdong, Hunan (Figure 5.6d).

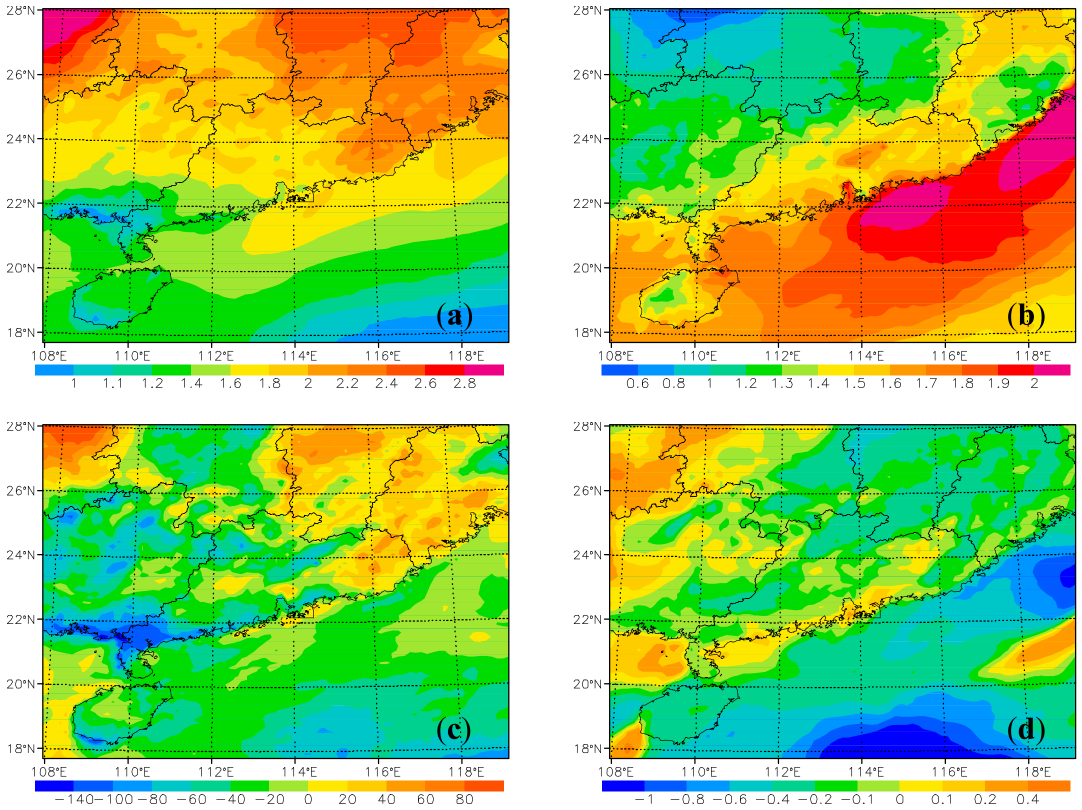

Figure 5.6 Changes in afternoon average (a) temperature (°C), (b) 2-m water vapor mixing ratio (g kg^{-1}), (c) planetary boundary layer height (m), and (d) 10-m wind speed (m/s) between CL2000EM2000 and CL2050EM2000 simulations for the month of October.

5.4.2. Changes in Surface Biogenic Emissions driven by climate change

For their contributions to the formation of surface O_3, the study of estimating biogenic emissions is of great concern at both regional and local scales. Meteorological conditions that have been known to be associated with high biogenic emissions are high radiation, high temperatures, and high relative humidity.

Our model simulates a significant increase of isoprene and monoterpenes emissions from 2000s to 2050s in response to the change of radiation and surface temperature. Figure 5.7b shows the isoprene emissions increased by 5 to 55% in October from 2000s to 2050s. The highest percentage up to 45 to 55% occurs over the northwest and northeast area of the modeling domain. Figure 5.7d shows monoterpenes also increase considerably by 5 to 40%. The predicted percentage increases in isoprene and monoterpene emissions are consistent with the results reported by Zhang et al. (2008c). They examined the sensitivity of BVOC emissions to warmer climate in future in the United States under the A1B scenario and found that the isoprene and terpene emissions are projected to increase 20–92% and 20–56% respectively by 2050s. The significant increase is largely determined by the large temperature increase and high forest coverage over this region. According to Lerdau et al. (1997) experiments, the emission rate may increase rapidly with increasing surface temperature from 15°C to 40°C. Although above 40°C, high temperature can inhibit the biogenic emission production. However there is no predicted hourly surface temperature higher than 40°C during the simulation period in this study.

On an absolute change basis, the highest increase in isoprene emissions occurs over the northeast area of the modeling domain (Jiangxi and Fujian mountain area), with an increase up to 6.5 mol km^{-2} hr^{-2} (Figure 5.7a). On average, the isoprene emissions are predicted to increase by about 1.0 mol km^{-2} hr^{-2}. The changes of monoterpenes emissions follow a pattern similar to isoprene, with the highest increase up to 2.0 mol km^{-2} hr^{-2} occurring over the Jiangxi, and Fujian mountain area (Figure 5.7c).

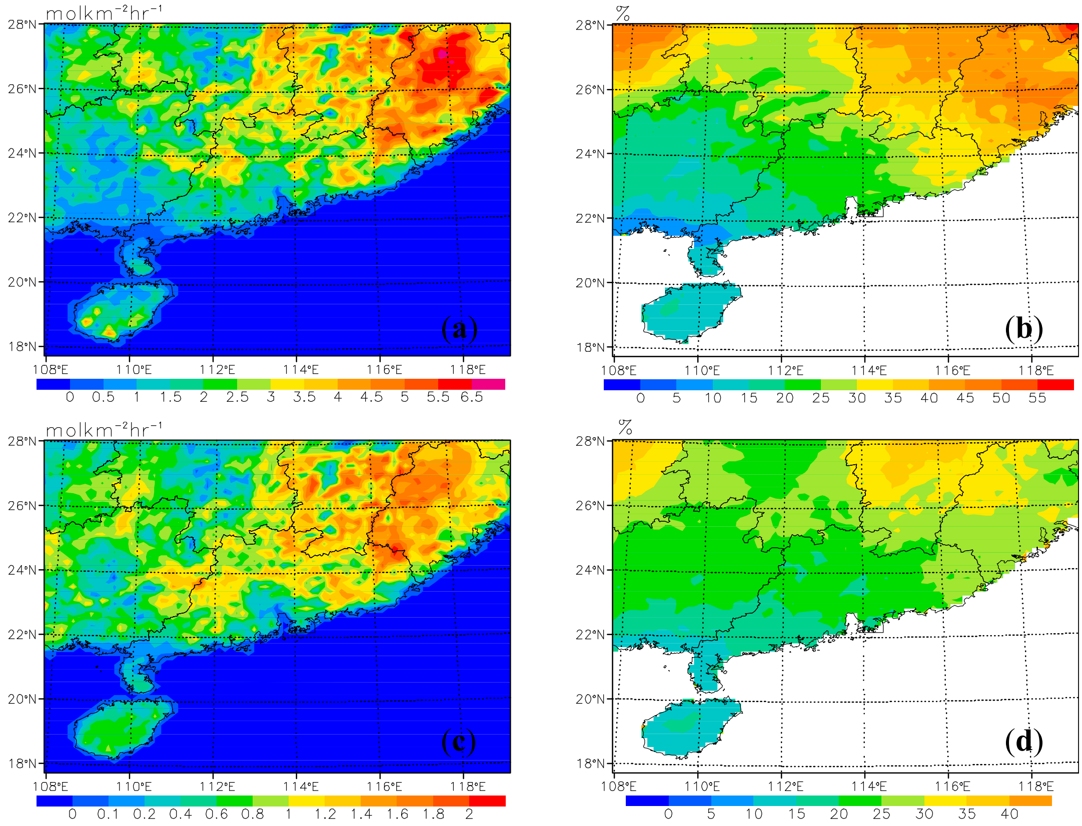

Figure 5.7 Absolute and percentage changes in emissions of isoprene (a,b) and monoterpenes (c,d) between CL2000EM2000 and CL2050EM2000 simulations for the month of October.

5.4.3. Changes in surface O_3 driven by climate change

Our model simulates a significant difference of the O_3 concentrations between the CL2050EM2000 and CL2000EM2000 within the period 12–18 LST (Figure 5.8a). In CL2050EM2000, the anthropogenic emissions at 2050s follow the same inventory at 2000s. In response to the change of meteorological variables, autumn-time afternoon O_3 concentrations change vary from –5 to 5 ppb across the inner domain. Over most parts of the land region, the surface O_3 concentration is predicted to increase by 1–5 ppb. Over the land region, the average surface O_3 concentration is predicted to increase 1.9 ppb. The regions with large increases are close to the regions with significant increase of temperature and biogenic emissions, such as the south of Jiangxi, Hunan, west of Fujian, and north of Guangdong province. The area of east Hunan and most parts of Jiangxi has the greatest magnitude of increase with concentrations increase between 3 and 5 ppb. The increases in afternoon O_3 concentrations are consistent with the 1–8 ppb increase over the Houston area estimated by Jiang et al. (2008b) using a similar model system during the summertime by 2050s. On the other hand, the largest decrease of about 4–5 ppb is found over South China Sea. Using the coupled MM5 and CMAQ model, Nolte et al. (2008) have shown that O_3 over the Pacific Ocean decrease by 1–3 ppb for the September/October period based on the A1B scenario due to increasing humidity.

The change of meteorological conditions for future climate scenario can alter the concentrations of O_3 and its precursors NO_x and VOCs through the impact on emission, chemical reactions, transport and deposition processes. Future climate changes in temperature and radiation increase the biogenic emissions up to 40% compared to present-day simulation. Thus, the isoprene mixing rations is predicted to increase 30–80 ppt over the rural forest regions (Figure 5.8c). NO_x emissions from soil increase in the 2050 climate due to higher soil temperature and moisture. The thermal decomposition rate for peroxyacetyl nitrate (PAN) is highly dependent on temperature (Sillman and Samson, 1995). Since the increasing temperature in the 2050s can enhance the decomposition rate of PAN (Figure 5.8d), there will be more NO_x and HO_x radicals reproduced to facilitate the O_3 formation (Steiner et al., 2006). Meanwhile, the decreased wind speeds near the emission source regions, over Jiangxi, Fujian, Hainan and part of Guangdong, Hunan province, are favorable for the accumulation of the O_3 precursor. Additionally, in response to elevated atmospheric moisture in the future, the reaction between water vapor and O(1D) produces more HO_x radicals into the photochemical cycle. Over clean ocean regions with low NO_x emissions, this reaction results in the destruction of O_3 production and therefore lowering surface O_3 concentration. On the contrary, near high anthropogenic emission regions where NO_x is in abundant supply, HO_2 reacts with NO injecting additional NO_2 to the NO-NO_2-O_3 system and resulting in additional production of O_3. At the same time, due to the increase of OH radicals, the reaction between NO_2 and OH creates more nitric acid over high anthropogenic emission regions (Figure 5.8b).

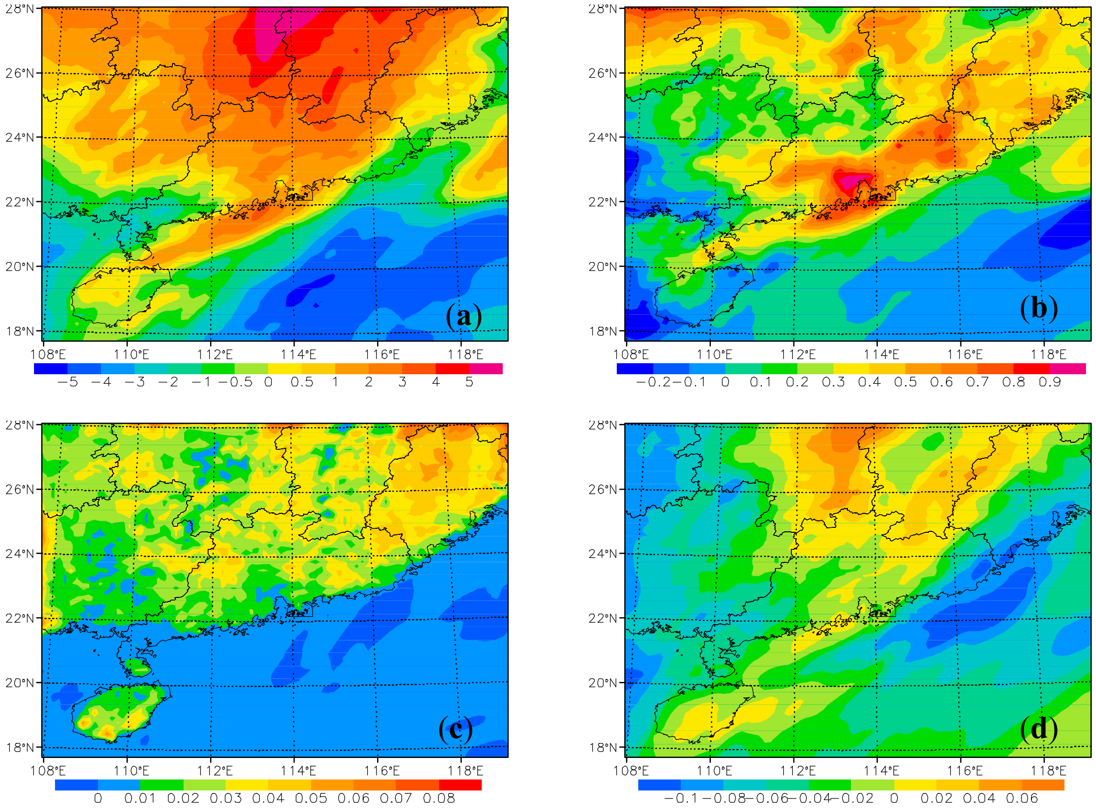

Figure 5.8 Changes in afternoon average (a) O_3 (ppb), (b) HNO_3 (ppb), (c) Isoprene (ppb), (d) PAN (ppb) between CL2050EM2000 and CL2000EM2000 simulations for the month of October.

The boundary layer O_3 budget was calculated to explore the changes in physical and chemical processes in O_3 formation between CL2000EM2000 and CL2050EM2000. Figure 5.9 shows the results of three main processes over the inner domain: O_3 gas phase chemical production (CHEM); O_3 transport (TRAN); and O_3 deposition (DEP). In response to the climate change and the subsequent increase in biogenic emission, CHEM process changes vary from –5 to 6 ppb h^{-1} in the afternoon time. The increases of O_3 production in boundary layer over 3 ppb h^{-1} induced by gas phase chemical reaction are found in PRD region and the southeast part of Hunan province. The maximum increases of CHEM process located in the area with great increase of temperature and also high anthropogenic and biogenic emissions. Over the South China Sea with low NO_x emissions, the increase of water vapor would result in a 1 to –5 ppb h^{-1} in CHEM process (Figure 5.9a). The changes in TRAN process are closely related to the variation of horizontal wind speed, wind direction. TRAN process increases 0 to 4 ppb h^{-1} over most part of the inner domain. The PRD region and southeast part of Guangdong with high anthropogenic NO_x emission have the largest decrease in O_3 transport, ranging from –1 to –7 ppb h^{-1} (Figure 5.9b). Figure 5.9c shows that the change in DEP process is between –2 and 2 ppb h^{-1}, basically there is little change in deposition process. Although the surface O_3 will increase in future, at the same time convection will also be enhanced due to warmer temperature. Increase in downward flux due to diffusion will be offset by increase in upward flux due to increase in convection activities. It can be seen that the changes in boundary layer O_3 budget was dominated by the CHEM process. The TRAN and DEP processes were relatively small compared to the CHEM process except in PRD region.

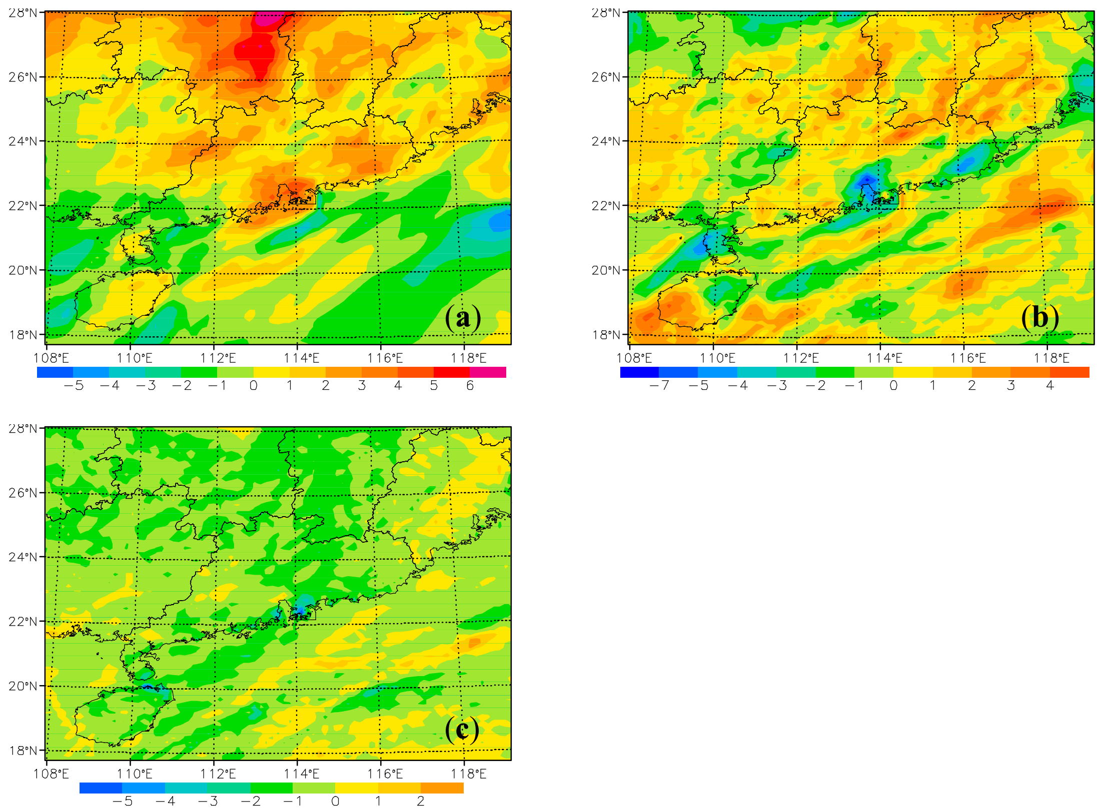

Figure 5.9 Changes in afternoon average (a) CHEM process (ppb h^{-1}), (b) TRAN process (ppb h^{-1}), (c) Dep process (ppb h^{-1}) between CL2000EM2000 and CL2050EM2000 simulations for the month of October.

5.5. Impact of anthropogenic emission change on O_3 air quality

According to IPCC SRES report, anthropogenic emissions of O_3 precursors including NO_x, CO, and VOC are projected to increase by 82%, 111%, and 184% compared to the 2000s emission level under A1B scenario in developing countries. The changes in surface O_3 due to emission change are calculated on the basis of two simulations: CL2000EM2000 and CL2000EM2050.

Figure 5.10a displays the difference in simulated O_3 mixing ratios between

CL2000EM2050 and CL2000EM2000. On average the surface O_3 is predicted to increase by 15.0 ppb over South China in the land region. The highest increases of 15 to 24 ppb occurs over west Guangdong and most parts of Guangxi province, whereas an obvious decrease about 0 to 3 ppb is found over the PRD region. There is a significant increase of surface O_3 over most of South China except PRD region. The PRD region is located in the central southern coastal part of Guangdong province including three metropolitan cities of Guangzhou, Shenzhen, Hong Kong and other seven medium and small cities. Substantial economic development leads to high air pollutant emissions in this region. Owing to the significant increase in NOx mixing ratio at 2050s level, O_3 concentrations are depressed through titration effect ($O_3 + NO = NO_2 + O_2$).

Figure 5.10b illustrates an increase in surface O_3 in the regions due to the combined effect of climate and emission changes. There is a significant increase of surface O_3 over the whole inner domain with the highest increase of 24 ppb occurring over southeast of Hunan province. On average the surface O_3 is predicted to increase by 21.3 ppb over the land region. Compared to the single anthropogenic emission effect, the combination would induce a greater increase of O_3 over land region. However, in the clean ocean area, the destruction of O_3 production due to the increase of water vapor would result in much lower enhancement.

The emission increase in CH_4 is not considered when conducting the "emission change" scenario (CL2000EM2050, CL2050EM2050). That is CH_4 concentration is kept at 170ppm in both cases. In order to examine the impact on surface O_3 due to increase in CH_4 emission, we calculated the difference between the METH2050 and CL2050EM2050 at the year 2056. Changes in autumn-time afternoon mean O_3 concentrations range from 2.5 to 6.5 ppb (Figure 5.10c). The largest increases up to 6.5 ppb are found over the regions located to the west part of PRD. On average, the increase of CH_4 induces an increase of 4.2 ppb in O_3 over the entire inner domain.

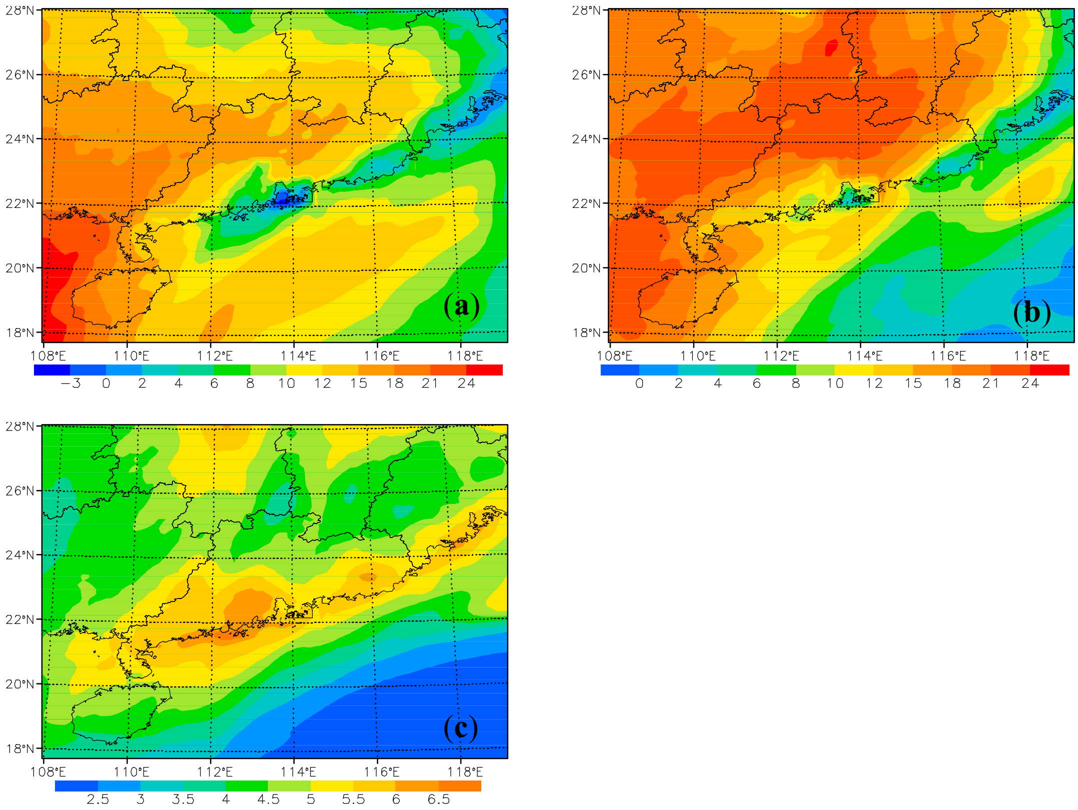

Figure 5.10 Simulated differences of afternoon average for surface O_3 a) between CL2000EM2050 and CL2000EM2000 simulations, b) between CL2050EM2050 and CL2000EM2000 simulations for the month of October, c)between METH2050 and CL2000EM2000 for the month of October at the year 2056

5.6 Sensitivity of surface O_3 over rural, urban and ocean regions

The study presented in the above subsections focused on analyzing the effects of climate and emission change on autumn time O_3 concentrations over the whole inner domain. Through the analysis we found that the impacts on surface O_3 concentration vary considerably across the inner domain. It is useful to compare the effects of climate and emission change over different landscapes. Therefore, three regions of the inner domain were selected to represent rural area, as indicated by box A, urban area, as indicated by box B (PRD), and clean ocean area, as indicated by box C (Figure 5.1b).

Figure 5.11 illustrates the spatially averaged contributions of climate change and emission change to afternoon surface O_3 for zones A, B and C. It can be seen that the effect of climate change alone in rural area (zone A) accounts for a larger increase of afternoon O_3 concentrations than in urban area (zone B). The bar chart shows that an increase of 3.9 ppb occurs over the rural area in Jiangxi province due to the effects of climate change. In PRD region (zone B), the climate change alone results in an increase of 1.5ppb in afternoon mean surface O_3 concentrations. On the contrary, there is a significant decrease of 4.5 ppb due to the effects of climate change alone in zone C. As we discussed above the significant increase of water vapor induces the destruction of O_3 production over the clean marine area.

Compared to the climate effect, the changes of anthropogenic emission result in a more significant increase of surface O_3 over all three regions. On average, the changes of anthropogenic emission contribute the increase of 11.4ppb, 6.1ppb, 12.1 ppb in zone A, zone B, and zone C, respectively. The combination effects in zone A and zone B have more influence than the emission change alone, resulting in an increase of 20 ppb and 11.4 ppb on afternoon surface O_3 concentration. The increase of surface O_3 at zone C is much lower with 4.7 ppb.

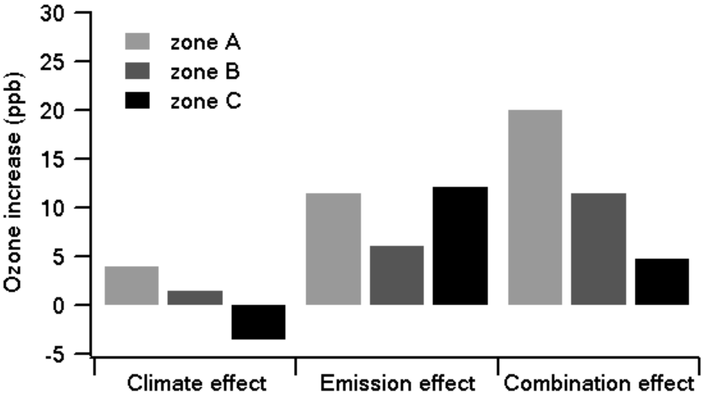

Figure 5.11 Changes in afternoon average surface O_3 concentrations induced by climate change, anthropogenic emission change, and combined change from the 2000s to the 2050s in three different regions.

5.7 Conclusions

The change of O_3 air quality due to the changes of climate and air pollutant emissions was studied by a series of numerical simulations under different meteorological and emission scenarios using WRF/Chem model. The simulations predict that on average near-surface temperature and water vapor mixing ratio are projected to increase 1.6°C and 1.6 g kg^{-1} under A1B scenario. Significant increase of biogenic isoprene and monoterpenes emission in South China due to the climate change can reach 5 to 55% and 5 to 40% respectively. In response to the change in climate and biogenic emissions, the afternoon surface O_3 mixing ratios increase 1.6 ppb over the land region in South China. Over PRD, a region of dense network of cities, the 2000-2050 climate changes increase afternoon mean surface O_3 by 1.5 ppb (zone B). The climate change induces a greater influence over rural area than over the PRD region, with an increase of 3.9 ppb in afternoon surface O_3 concentrations (zone A). 2000-2050 anthropogenic emission changes result in an increase of the surface O_3 afternoon mean by 12.8 ppb on average in the land region. The combination effect of climate and emission change would result in an increase of 18.2 ppb in land region, with the highest increase up to 24 ppb occurring over southeastern part of Hunan province.

Chapter 6 Impact of climate change on biogenic SOA over China

6.1 Introduction

As reviewed in Chapter 2, many studies have pointed out that the formation of SOA is sensitive to environment factors including temperature, relative humidity, precursors concentration, pre-existing absorbing aerosol concentration, and the concentrations of OH radical, NO_3 radical and O_3. Thus, changes in climate and subsequent changes in biogenic emissions can alter SOA concentrations in the future. Although considerable efforts have been made to investigate SOA precursors, formation processes, and properties in the last two decades, sensitivity studies of the impact of future climate change on biogenic SOA at regional scales is very limited, especially in China.

It is estimated that the annual SOA production reaches 3.05 Tg yr^{-1} over China, with about 65% contributed by biogenic SOA (BSOA) (Jiang et al., 2012). In this chapter, we mainly focus on the impact of climate change on BSOA. The objective of this study is to examine the impact of future climate change under different emissions scenarios on BSOA concentration over regional scale. In section 6.2, we introduce the model configuration and the input data adopted in this study. A module calculating the SOA formation from isoprene oxidation is added to WRF/Chem model. Then, In Section 6.3, we evaluate the model performance using available observation data. In section 6.4, the responses of BSOA to future climate change under different scenarios were investigated. Finally, the summary of this chapter are given in section 6.5.

6.2 Models and data

6.2.1 Model configurations

The modeling domain, which covers the whole China terrestrial region, Korean Peninsula, Japan on a 45 km horizontal grid, is illustrated in Figure 6.1. The options for each physics parameterization are listed in Table 6.1. For the gas phase chemistry, RACM was applied which contains relatively detailed organic chemistry, such as aromatic chemistry and the oxidation mechanism for biogenic volatile organic compounds (Stockwell et al., 1997). Hence, the reactions of the SOA precursors (see section 3.3) could be well described by RACM. Indeed, the SORGAM module was just designed for the use of RACM. Aerosol module used here was MADE/SORGAM (Schell et al., 2001). MADE can provide detailed information on the chemistry composition, size distribution and dynamic processes of inorganic aerosols, and it was coupled with SORGAM by Schell et al. (2001).

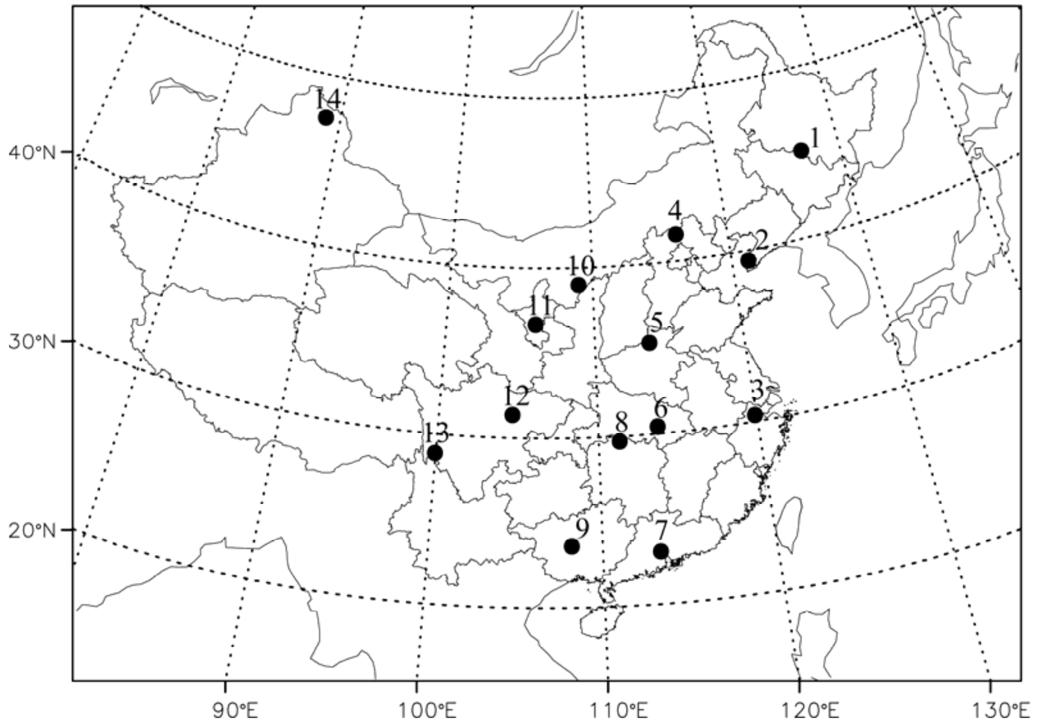

Figure 6.1 Simulation domain setting and geographical locations of the sites selected to model evaluation: 1) Longfengshan, 2) Dalian, 3) Linan, 4) Shangdianzi, 5) Zhengzhou, 6) Jinsha, 7) Panyu, 8) Taiyangshan, 9) Nanning, 10) Zhenbeitai, 11)Gaolanshan, 12) Chengdu, 13) Zhuzhang, 14) Akdala

SORGAM has been described in section 3.2. Here gives more detail information on some uncertain parameters. Enthalpy of vaporization ΔH is one of the most uncertain parameters in SOA modeling, ranging from 42 kJ mol^{-1} to 156 kJ mol^{-1} (Tsigaridis and Kanakidou, 2003; Hoyle et al., 2007; Han et al., 2008), but much lower ΔHs were estimated by Offenberg et al. (2006) (11 – 44 kJ mol^{-1}). In this study, we adopt a medium value (79 kJ mol^{-1}) for the enthalpy of vaporization, this value was also used in Tsigaridis and Kanakidou (2003). The concentration of absorbing aerosols for condensation C_{init} is another uncertain factor. Here, we consider all carbonaceous aerosols as absorbing materials. In addition, although WRF/Chem can simulate feedbacks between aerosol and meteorological processes, they were not activated in this study.

Table 6.1 The grid settings, physical and chemical options used in this study

Items	Contents
Dimensions(x, y)	135, 100
Grid size (km)	45
Microphysics	Lin et al. scheme (Lin et al., 1983)
Longwave radiation	RRTM scheme (Mlawer et al., 1997)
Shortwave radiation	Goddard shortwave (Chou and Suarez, 1994)
Surface layer	Eta similarity (Janjic, 1996)
Land surface	Noah Land Surface Model (Chen and Dudhia, 2001)
Planetary boundary layer	Mellor-Yamada-Janjic scheme (Janjic, 2002)
Cumulus parameterization	Grell-Devenyi ensemble scheme (Grell and Dévényi, 2002)
Gas-phase chemical mechanism	RACM (Stockwell et al., 1997)
Photolysis scheme	FTUV (Tie et al., 2003)
Aerosol Module	MADE/SORGAM (Schell et al., 2001)

6.2.2 Emissions

The anthropogenic emissions are obtained from the 2006 Intercontinental Chemical Transport Experiment-Phase B (INTEX-B) inventory (Zhang et al., 2009). It is a new emission inventory for Asia with 0.5°× 0.5° horizontal resolution developed to support INTEX-B field campaign. Biomass burning emission is not included in this inventory. The Transport and Chemical Evolution over the Pacific (TRACE-P) biomass burning emission for the year 2000 has been applied to estimate the Asia biomass burning (Streets et al., 2003). We then specified monthly variations of anthropogenic and biomass burning emissions following the work of Zhang et al. (2009) and Streets et al. (2003), respectively. Figure 6.2 shows the distributions of OC and non-methane VOC (NMVOC) emissions from the major anthropogenic sources and biomass burning. Strong NMVOC emissions (> 20 mol km^{-2} hr^{-1}) due to the major anthropogenic sources were found mainly over North China, YRD, and Guangdong province; and high OC emissions basically appear in the areas of North China, Sichuan Basin, and part of East China. Compared with the major anthropogenic emissions, the biomass burning emissions were insignificant in summer.

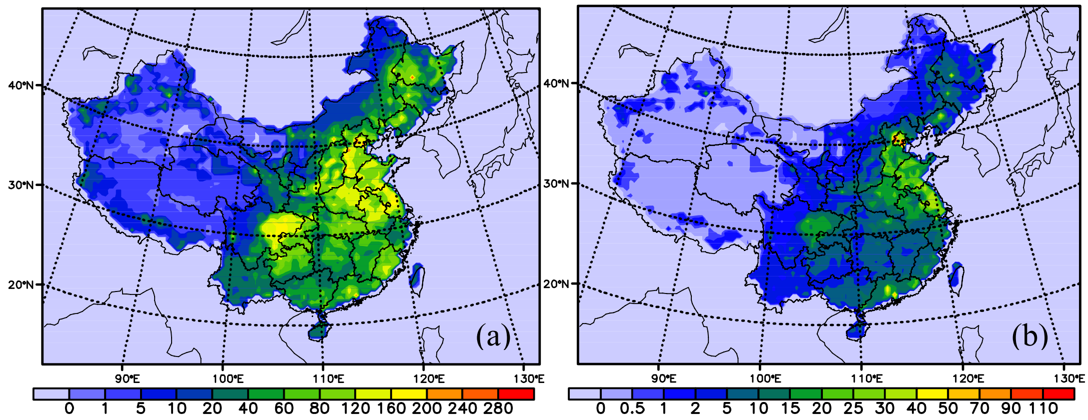

Figure 6.2 The emission rates from major anthropogenic sources in 2006 and biomass burning in 2000 in China, panel (a) is for emission rates of OC (μg m^{-2} hr^{-1}), while (b) are for emission rates of NMVOC (mol km^{-2} hr^{-1}).

Biogenic emissions in China are computed based on the vegetation and meteorological parameters using MEGAN v2.04 coupled within the WRF/Chem model (Guenther et al., 2006). The monthly-mean surface air temperature and downward solar radiation datasets are provided by CCSM monthly-mean output data of current (2005–2007) and future (2055–2057) years when the model is driven by global climate model output. Isoprene, API and LIM, calculated based on the standard isoprene emission factor, are the biogenic SOA precursors. Under standard conditions, as shown in Figure 6.3, high isoprene emission rates are found in the forested regions mainly over Northeast China, Shanxi province and 30°N south of China, while the emission rates in West China and North China are relatively low.

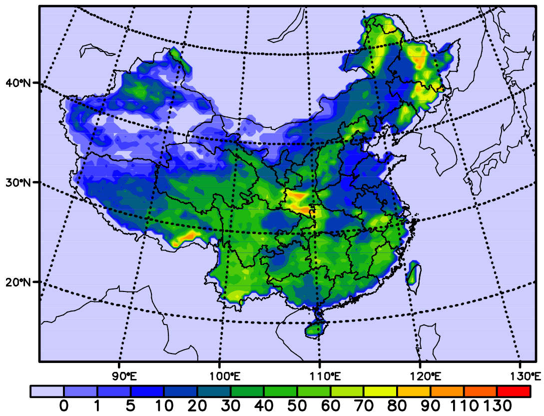

Figure 6.3 Standard biogenic isoprene emissions over China generated by MEGANv2.04 (mol km^{-2} hr^{-1}).

6.2.3 Experiment

In this study, we conducted five numerical experiments based on different combinations of model settings (Table 6.2). The first objective of this study is to investigate the model performance of the modified WRF/Chem model including the module of isoprene SOA formation. Thus, the EXP1 experiment was simulated for the whole year of 2006 to estimate the present-day SOA levels over China. In order to reduce the integration errors, simulation is carried out month by month, and the Three-Dimensional Analysis Nudging (Stauffer and Seaman, 1990) for wind fields, temperature and moisture is applied. The National Centers for Environmental Prediction (NCEP) reanalysis FNL (final) data is assimilated by Grid Nudging method.

The FNL data has a horizontal resolution of 1° × 1° and time interval of 6 hours, which is also used as the meteorological initial fields and lateral boundary conditions.

Then, applied with the modified modeling system, the effects of future climate change and the subsequent changes in biogenic emission on BSOA concentrations are investigated at regional scales. The CCSM3 outputs following A1B scenarios are selected to provide the WRF/Chem model with meteorological initial fields and lateral boundary conditions for current and future year simulation. The CTRL_A1B experiment was simulated over China under the present-day climate, emissions and chemical boundary conditions for three consecutive Julys in 2005-2007. The experiment CLFU_A1B was driven by the meteorological conditions and biogenic emissions for Julys in 2055-2057 but with present-day anthropogenic emissions and chemical boundary conditions. The differences between the CTRL and CLFU simulations are used to estimate the impacts of climate change and the subsequent changes in biogenic emission on surface BSOA formation.

IPCC has developed six families of emission scenarios (A1FI, A1B, A1T, A2, B1, B2) to represent possible future socioeconomic conditions (IPCC, 2000). The A1B scenario is representing a mid-line scenario for carbon dioxide emissions and economic growth compared with other SRES emission scenarios. In order to investigate the responses of surface SOA concentrations to different emission scenarios, experiments (CTRL_B1 and CLFU_B1) were also conducted. The meteorological boundary conditions of these two experiments are provided by the CCSM3 outputs under B1 scenarios, which is representing a baseline scenario which describes a convergent world.

Table 6.2 Five cases of numerical experiments conducted in this study

Simulation	Period	Description
EXP1	2006	2006 FNL meteorological fields and biogenic emissions; INTEX-B anthropogenic emissions;
CTRL_A1B	July 2005-2057	2000s CCSM3 A1B meteorological fields and biogenic emissions; INTEX-B anthropogenic emissions;
CLFU_A1B	July 2055-2057	2050s CCSM3 A1B meteorological fields and biogenic emissions; INTEX-B anthropogenic emissions;
CTRL_B1	July 2005-2007	2000s CCSM3 B1 meteorological fields and biogenic emissions; INTEX-B anthropogenic emissions;
CLFU_B1	July 2055-2057	2050s CCSM3 B1 meteorological fields and biogenic emissions; INTEX-B anthropogenic emissions;

6.3 Comparison with measurements

6.3.1 EC and OC concentrations

In order to evaluate the model performance, the simulated annual mean surface OC and EC concentrations are compared with observations at different sites over China in 2006 (Figure 6.4 a, b). The site locations are shown in Figure 6.1, more information can be referred to Zhang et al. (2008a). Here, the simulated OC consists of primary organic carbon (POC) and SOC. The SOC concentration was converted from SOA according to the elemental analysis results by using a high-resolution ToF-AMS. Aiken et al. (2008) measured the ratios of organic matter (OM) to OC for the SOA respectively in α-pinene/O_3, NO_x system, isoprene/NO_x system and toluene/OH, NO system, and the values were 1.58, 1.75 and 1.71, respectively. Hence, the OM/OC ratio in α-pinene/O_3, NO_x system of 1.58 was applied to the MSOA in this study, and the ratios of 1.75 and 1.71 were applied to ISOA and ASOA, respectively. The figures suggest that the model basically captured the characteristics of spatial distribution of OC and EC levels. Correlation coefficient between the measured and simulated OC is 0.78, and that for EC is 0.75. The mean simulated EC levels are basically close to the observations (7%, 4.8 versus 4.5 µg m-3), while the modeled OC concentrations are underestimated (-48%, 10.4 versus 20 µg m-3).

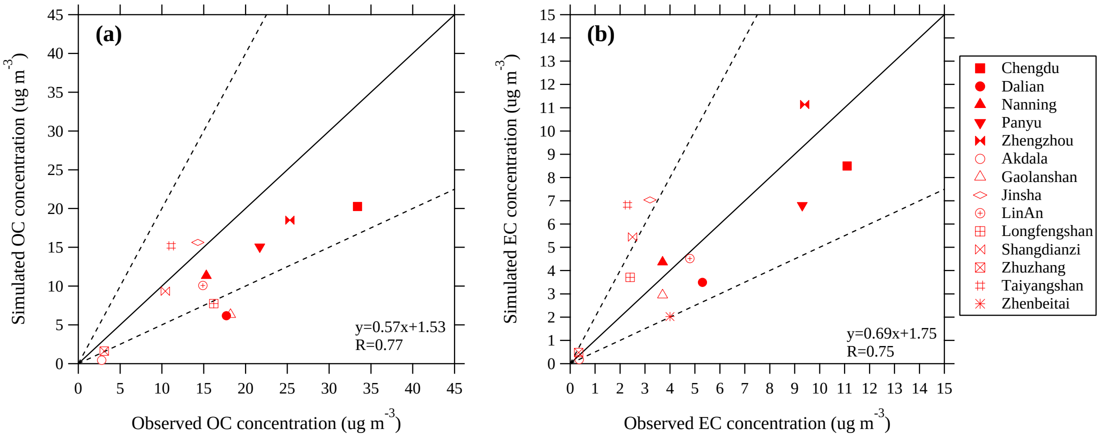

Figure 6.4 The scatter plots between simulated and observed annual mean surface concentration for OC (a) and EC (b) in several sites over China in 2006. Dashed lines represent an error of ±50%; measurement data from Zhang et al. (2008a).

Monthly mean OC and EC concentrations were further compared with the measurement at four selected sites, i.e. Chengdu (CD), Nanning (NN), Lin'an (LA) and Longfengshan (LFS) station (Figure 6.5). CD and NN are urban sites, while LA and LFS are rural stations. As shown in Figure 6.5, the characteristics of monthly variability of OC and EC are reasonably reproduced at all sites, with high levels in cold seasons (i.e. Jan, Feb, Nov, and Dec) and low concentrations in warm seasons. The mean correlation coefficients are 0.53 and 0.66, respectively. However, large deviations are also found at all sites for both OC and EC. At CD both OC and EC are basically underestimated during most months of the whole year, probably due to the low spatial resolution in emission inventories. At NN, the OC concentrations were underestimated during the warm seasons (mainly from Apr to Oct, ~ 40%), while the modeled EC concentrations were much closer with the observations. Considering that NN is located near Indo - China Peninsula, those deviations in OC may be caused by the exclusion of SOC contributions from South East Asia regions outside China. In warm seasons, there are very significant biogenic emissions in Indo - China Peninsula (Guenther et al., 2006). When summer monsoon is prevalent, biogenic emissions from Indo – China are transported into China from the south boundaries (Ding and Chan, 2005). At LA and LFS sites, the underestimation of OC concentrations mainly occurred in spring and autumn, especially in October and November (> 55%). On the other hand, due to the significant formation of SOC, the modeled OC concentrations agree well with the observed data in summer, suggesting that in spring and autumn, there may be missing OC emission sources. One possibility is the fugitive anthropogenic straw burning (Zhang et al., 2008a). The simulated EC concentrations at LA were in agreement with the measurements, while that at LFS were basically higher than the observations throughout the year. The analysis of Zhang et al. (2008a) suggested that the OC and EC at LFS site are influenced by different sources at least in some periods of a year, which may also explain the different model performance for

EC and OC at LFS in this study.

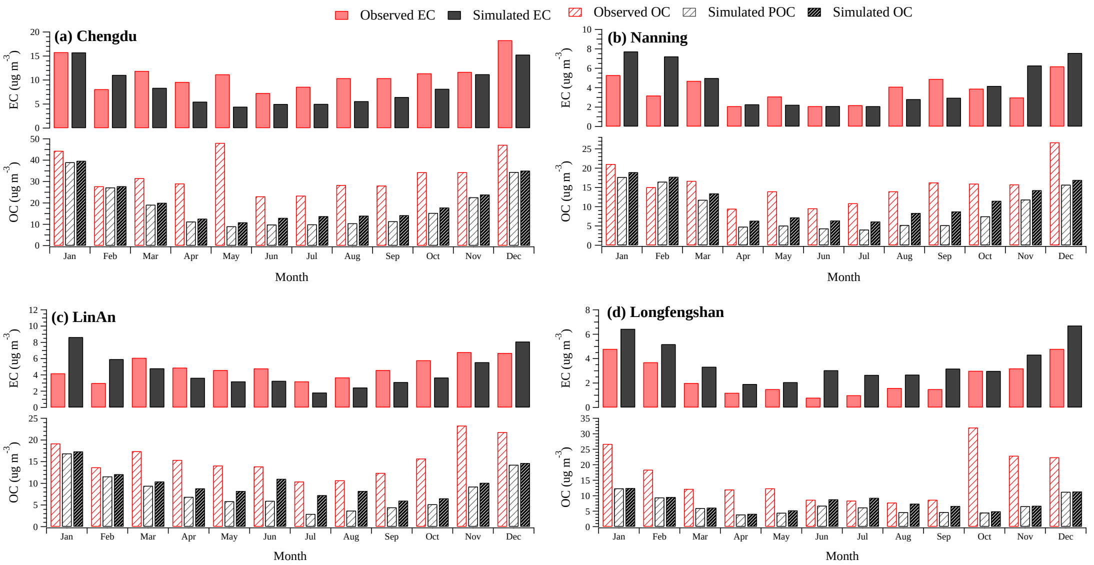

Figure 6.5 Comparison of the simulated monthly mean surface OC and EC concentrations with the measured concentrations at four selected sites over China in 2006; measurement data from Zhang et al. (2008a).

We also compared the modeled SOC to OC ratios, OC and EC concentrations in summertime with some previous studies conducted in China (Table 6.3). It can be found that the modeled SOC fractions agree well with the measurements in Guangzhou and Xiamen. However, the SOC/OC ratios (16%) are lower than the observations (26 – 59%) in Beijing (Chan et al., 2005; Dan et al., 2004; Duan et al., 2005; Lin et al., 2009b). Sun et al. (2010) adopted a Positive Matrix Factorization (PMF) method, which can explicitly distinguish POA and SOA (Zhang et al., 2005; Tsimpidi et al., 2010, Hodzic et al. 2010). The observed SOA concentrations account for 61% of total OA in Beijing during 9 to 21 Jul 2006, while the simulations only account for 20% during the same period, showing underestimation of SOC fractions in this study. However, in Sun et al. (2010)' study, the less oxidized SOA concentrations were observed to account for 16% of total OA, which is close to the simulated SOA contribution in this study (20%), indicating that only the concentrations of less oxidized SOA were reproduced in this work. Overall, the SOA concentrations in this study may be under-estimated for about 0–75%, and the negligence of chemical aging of SOA and POA should be the main reason for this underestimation.

Table 6.3 Comparison of SOC/OC, OC and EC concentrations with some previous studies for summertime conducted in China. (unit: μg m^{-3})

Region	SOC/OC	OC	EC	References	Period
Beijing, China	26 – 36%	19.2	7	Chan et al., 2005	Observed, in August 2003[b]
	37 – 59%	10.7	5.7	Dan et al., 2004	Observed, in summer 2001[b]
	53%	21.2	7.3	Duan et al., 2005	Observed, in autumn, 2002[b]
	45%	10	-	Lin et al., 2009b	Observed, in summer, 2006
	16%	14.4	11.8	This study	In summer
	61%	28.1[a]	-	Sun et al., 2010	Observed, 9Jul-21Jul, 2006[c]
	20%	19.0[a]	-	This study	9Jul-21Jul, 2006
Guangzhou, China	21 – 32%	17.5	5.4	Duan et al., 2007	Observed, in summer, 2004 – 2005[b]
	33 – 62%	9.2	4.1	Cao et al., 2004	Observed, PRD , in summer 2002[b]
	31%	7.6	3.1	This study	In summer
Xiamen, China	44%	5.6	1.5	Wang et al., 2006b	Observed, Summer 2005[b]
	30%	6.5	2.0	This study	In Summer

[a] Organic Aerosol

[b] SOA estimated by using an indirect method, i.e. the EC-tracer method (Castro et al., 1999)

[c] SOA observed directly by using high-resolution time-of-flight aerosol mass spectrometer (HR-ToF-AMS, Aiken et al., 2008)

So far, under-estimation of organic aerosols in modeling exercise is still fairly common (Pun et al., 2009; Han et al., 2008; Koo et al., 2003). Carlton et al. (2009)

gave a comprehensive summary on the potential causes. Based on the results of this study, the under-estimation may be attributed to: 1) the large uncertainty in emission inventories of primary OC and VOCs; 2) the low spatial and temporal resolution of emission inventories, especially for biomass burning emissions; 3) the exclusion of emissions from regions outside China; 4) missing SOA precursors, for example, emissions of semi-volatile organic gases, such as diesel, have been shown as an important source of organic aerosol (Robinson et al., 2007); 5) missing physical and chemical processes that contribute to SOA (e.g., liquid phase processes, Volkamer et al., 2007); 6) the limitation of model resolution. Qian et al. (2010) tested the sensitivities of modeled aerosol concentration to spatial resolution, and showed that the organic matter concentration from the simulation with 75km resolution is 50-100% less than that with 3km resolution over the central Mexico Plateau and eastern Mexico.

6.3.2 Regional distributions of biogenic emissions and SOA

Due to the seasonal variations in solar radiation, temperature and leaf area index, the emissions of BVOCs has a peak in summer. The spatial patterns of summer emission rates for biogenic isoprene, Alpha-pinene and other cyclic terpenes with one double bond (API), d-Limonene and other cyclic diene terpenes (LIM) in July, 2006 are shown in Figure 6.6. The emission rates of biogenic isoprene range up to 50 mole km^{-2} h^{-1}, and high emissions are found in the broadleaf forested regions, such as

Northeast China, Shanxi, Jiangxi, Fujian province, and southeast part of Xizang and Sichuan province. Compare with isoprene, biogenic emissions of API and LIM are relatively low. High emissions occur mainly over northeast China and 30°N south of China, with the highest value up to 3.6 mole km^{-2} h^{-1} and 1.8 mole km^{-2} h^{-1}.

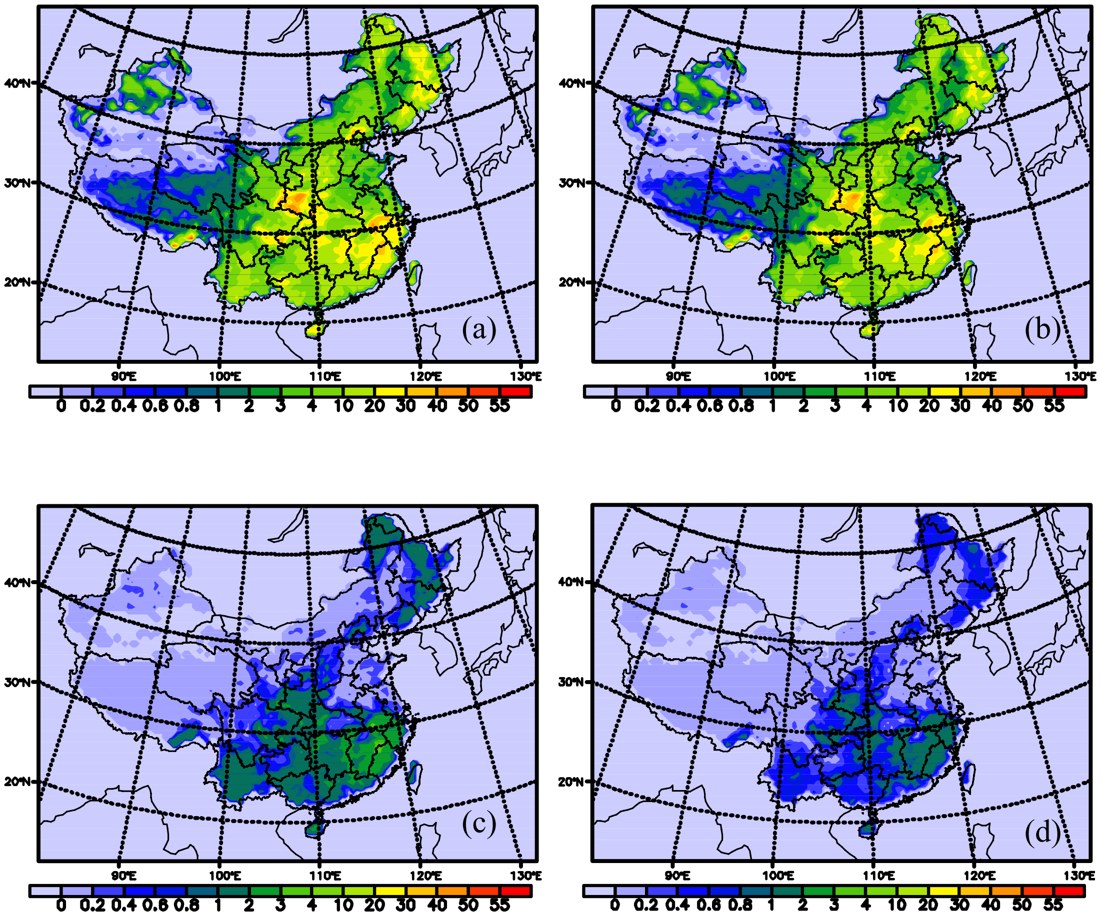

Figure 6.6 Model calculated emission rates over China for (a) BVOCs, (b) Isoprene, (c) API, and (d) LIM in July, 2006 (mole km^{-2} h^{-1}).

Figure 6.7 show the distributions of mean ground level concentration of total SOA, BSOA, ISOA and MSOA in July (Table 3.6). On the surface, the SOA concentrations range up to 8μg m^{-3} (Figure 6.7a). In summer season, the BSOA proportions in total SOA are very high, except for North China plain (Figure 6.7b). The BSOA concentrations range up to 6.5 μg m^{-3}, with the high concentrations (> 4 μg m^{-3}) mainly occurring over Jiangxi province, northeast part of Sichuan province, and south part of Anhui and Shaanxi province. Compared with the east regions, SOA concentrations over West China are relatively low (< 0.6 μg m^{-3}). It can be found that the areas around 30°N with high SOA concentrations are basically corresponding to those regions with concentrations of BVOC emissions (Figure 6.6a). The spatial distributions of ISOA are slightly different from the pattern of MSOA. Over the Shanxi province, BSOA mainly comes from the oxidation of isoprene, while over Yunnan and Jiangxi province, the contribution of monoterprenes is dominant. The spatial pattern of SOA in July is generally consistent with the distributions simulated by Han et al. (2008) in 2003 summer. However, the simulated concentrations are in general higher than those reported by Han et al. (2008), especially in Central China and North China. This may be attributed to the higher anthropogenic emissions in the latest emission inventory and a more reasonable SOA gas/particle partitioning scheme used in this study.

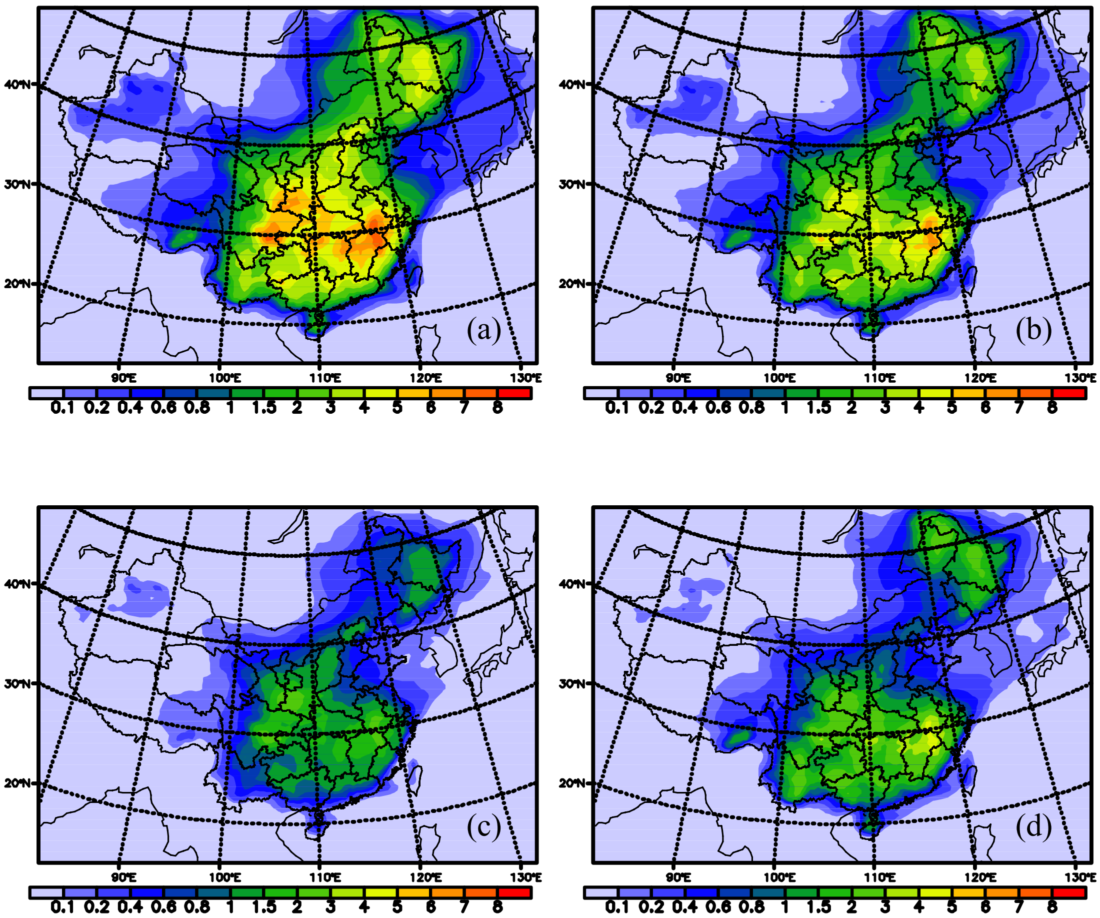

Figure 6.7 Simulated surface concentrations of (a) total SOA, (b) BSOA, (c) ISOA, and (d) MSOA in July, 2006 ($\mu g\ m^{-3}$).

6.4 Climate change and its impact on BSOA

6.4.1 Regional climate change

The changes in meteorological factors including temperature, relative humidity, planetary boundary layer height (PBLH), wind speed, precipitation and downward solar radiation have significant effects on the formation of SOA. It is necessary to analyze the changes of the meteorological factors over the period between the 2000s and the 2050s. The differences of meteorological variables including 2-m temperature, 2-m water vapor mixing ratio, PBLH, and 10-m wind speed, precipitation, net shortwave radiation were calculated based on the simulations CTRL and CLFU under two emission scenarios over China.

The simulated changes in meteorological variables for July 2000s–2050s under A1B emission scenario are illustrated in Figure 6.8. It is estimated that the average surface temperature would increase 1.5 °C over the entire China in 2050s. The largest increases over 2 °C are found over the Hunan and Sichuan province, the junction of Xizang and Xinjiang province, and northeast China. The increases are smaller over east part of Xinjiang province, Hebei, Henan, Inner Mongolia and southeast coast of China (Figure 6.8a). Average near-surface water vapor is predicted to increase by 0.9 g kg^{-1} over China. Significant increases of 2-m water vapor mixing ratio over 1.5 g kg^{-1} occur over central and southwest China (Figure 6.8b). The spatial distribution of PBLH change is quite similar to the pattern of changes in surface temperature. The largest warming occurs over central and southwest area of China results in enhanced mixing in these areas where the PBL height could increase up to 300m. The largest decrease up to 300 m in PBL height occurs over areas including Xizang, Xinjiang, Inner Mongolia (Figure 6.8c). A reduction of near-surface wind speed is predicted over West China, Inner Mongolia, part of North China, and southeast coast (Figure 6.8d). The mean precipitation is predicted to increase 0.19 mm day^{-1} over China for 2000s–2050s, a 5.4% increase from the year 2000s (Figure 6.8e). Precipitation generally increases over 30°N north of China except in Shandong, Sichuan, Xinjiang province, part of northeast China, while reductions in precipitation are predicted mainly over subtropics areas including Jiangxi, Guangdong, Guangxi province. The surface downward shortwave radiation shows a change pattern generally similar with surface temperature with increase in the Hunan and Sichuan province, the junction of Xizang and Xinjiang province, and northeast China (Figure 6.8f). It is indicated that the areas with reduction in 10-m wind speed, precipitation and increasing PBL height, surface downward shortwave radiation are generally experienced relatively large temperature increases.

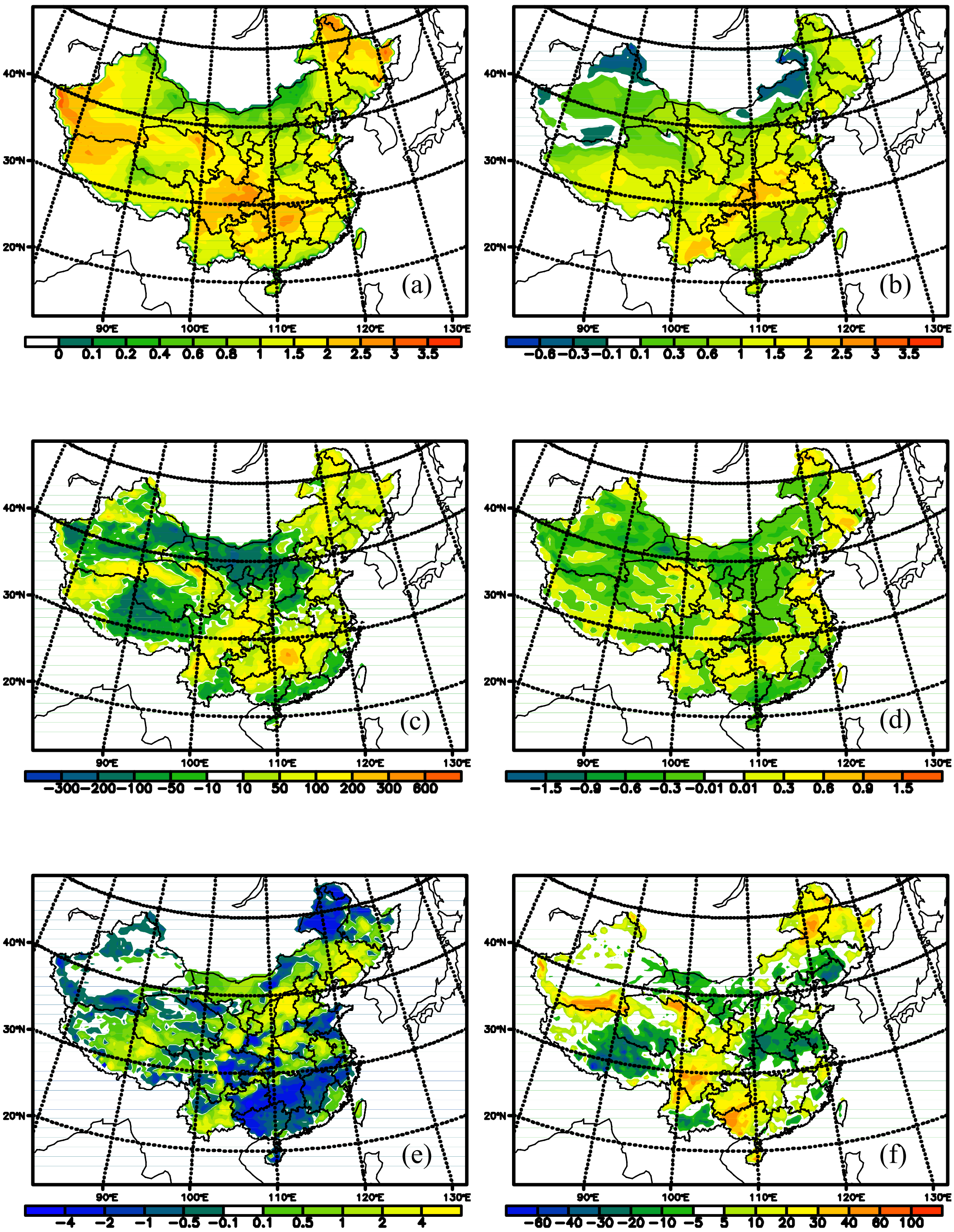

Figure 6.8 Changes in average (a) temperature (°C), (b) 2-m water vapor mixing ratio (g kg^{-1}), (c) planetary boundary layer height (m), and (d) 10-m wind speed (m s^{-1}), (e) precipitation (mm day^{-1}), (f) downward solar radiation (w m^{-2}) in July between present and future climate simulations under the A1B scenario.

The simulated changes in those six meteorological factors under B1 scenario are quite different from which under A1B scenario (Figure 6.9). The simulations predict that on average near-surface temperature and water vapor mixing ratio are projected to increase 1.2 °C and 0.3 g kg^{-1}, which is smaller than the changes under A1B scenario. This is consistent with what described in the chapter 2.3 (Figure 2.3). Under B1 scenario, areas over the Xinjiang province, the northeast and east China shows a relatively smaller warming, while North China are expected to experience more warming. The changes in water vapor mixing ratio over central and southwest China are opposite to the changes under A1B scenario. The predicted changes in wind speed, PBL height, and net downward solar radiation are also showing different patterns. The regions over Hebei, Shanxi, Henan, Chongqing, Sichuan provinces etc. with large temperature increases experience an obvious increase in wind speed, PBL height and net solar radiation. Precipitation decreases over much part of China except northwest and northeast China under B1 scenario.

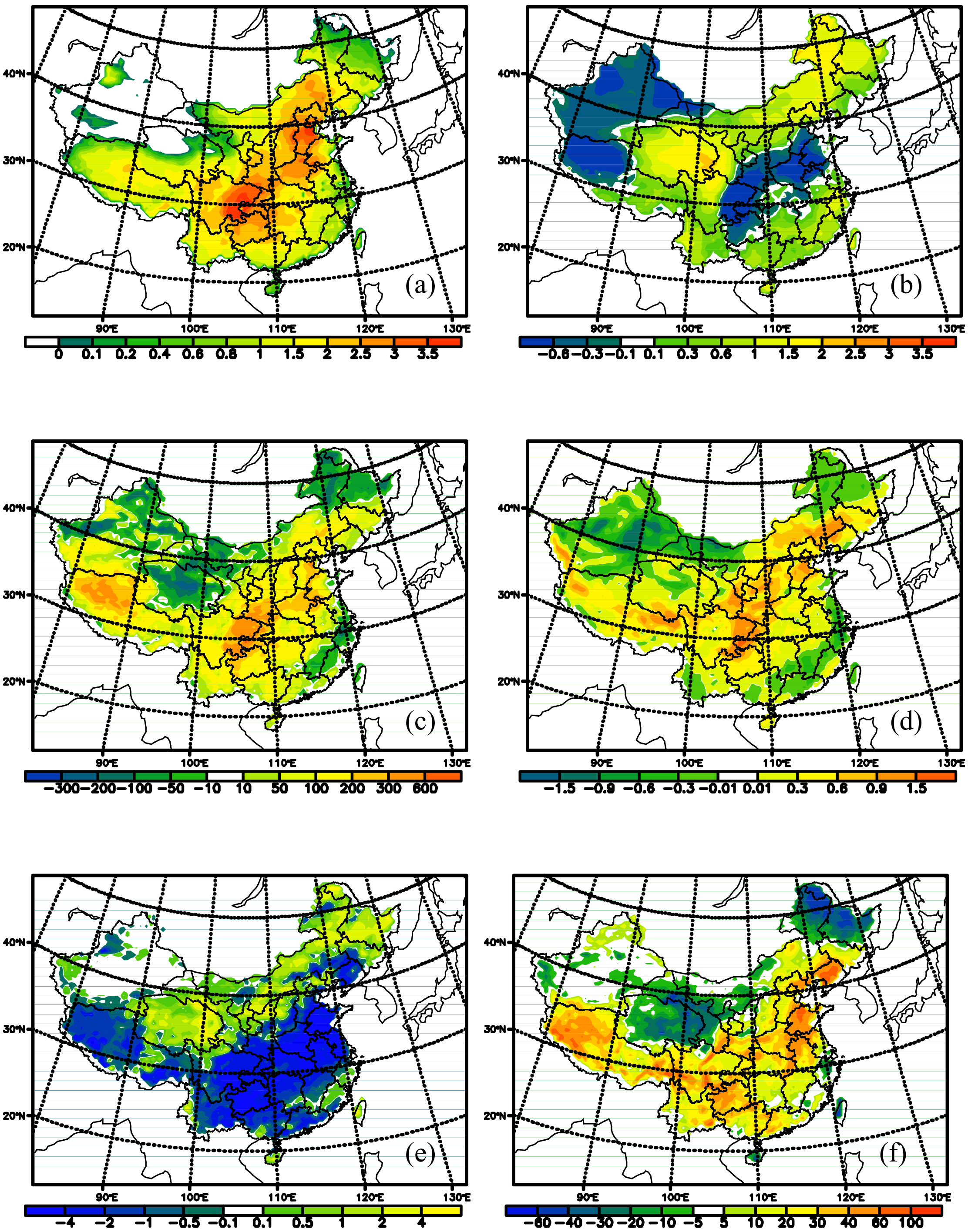

Figure 6.9 Changes in average (a) temperature (°C), (b) 2-m water vapor mixing ratio (g kg^{-1}), (c) planetary boundary layer height (m), and (d) 10-m wind speed (m s^{-1}), (e) precipitation (mm day^{-1}), (f) downward solar radiation (w m^{-2}) in July between present and future climate simulations under the B1 scenario.

Through the analysis we found that the changes in meteorological variables vary considerably across the modeling domain. Therefore, in order to quantify the changes in these meteorological variables under the A1B and B1 scenarios at different regions, six sub-regions of China including North China, Central China, South China, Northeast China, Southwest China, and West China are defined (Figure 6.10). It should be noted that Hainan and Taiwan are not included in the calculation. Under the A1B scenario, the largest temperature increases are found over Southwest China, while the smallest increases are found over North China (Table 6.4). Under the B1 scenario, the smallest temperature increase of 0.38°C occurs over West China. However, the temperature increases occurring over the North and Southwest China are larger than 2 °C. Changes in surface absolute humidity are positive in all the six sub regions, with the largest increase occurring in Southwest China under the A1B scenario. Precipitation increases over North China, Central China, Northeast China and West China, while decreases over South China and Southeast China. Under the B1 scenario, there is a significant decrease of absolute humidity in Central China which also experiences a large decrease of 55.9% in precipitation. It is indicated from the table that the changes in wind speed and PBLH are generally related to temperature changes under the two scenarios. Under A1B scenario, over West and North, the 10-m wind speed is predicted to decrease 2.11% and 1.93%, respectively. And the PBLH is also predicted to decrease over West and North which may cause by the relatively small warming in these two regions. Under B1 scenario, over the regions of North and Southwest China with large temperature increases, there are larger increases in in PBLH and 10-m wind speed. The percentage changes in downward solar radiation are relative small under A1B scenario with the largest increase occurring over West and Southwest China. However, under B1 scenario, the downward solar radiation increases larger than 9% over the Central and Southwest China.

Figure 6.10 Six sub-regions in China

Table 6.4 Regional climate changes in six sub-regions

	North	Central	South	Northeast	Southwest	West
A1B						
T2*(°C)	1.10	1.48	1.72	1.58	1.90	1.49
Q2(%)	5.56	10.42	6.63	5.96	10.97	7.97
PBLH(%)	-1.91	1.48	4.80	5.50	4.16	-1.33
WS10(%)	-2.11	0.62	-0.20	1.35	2.63	-1.93
RAIN(%)	13.42	7.30	-34.31	5.50	-1.60	4.07
SWDOWN(%)	2.71	2.70	3.81	4.21	4.58	4.99
B1						
T2(°C)	2.1	1.76	1.57	1.15	2.24	0.38
Q2(%)	2.71	-5.83	2.66	9.79	7.92	1.34
PBLH(%)	8.73	10.82	6.31	6.62	17.1	2.23
WS10(%)	10.82	4.30	1.19	3.83	10.89	-0.31
RAIN(%)	-11.82	-55.9	-41.78	12.12	-37.2	-3.91
SWDOWN(%)	4.52	9.10	6.41	-1.57	10.6	1.60

*Changes in 2-m temperature (T2), 2-m water vapor mixing ratio (Q2), planetary boundary layer height (PBLH), and 10-m wind speed (WS10), precipitation (RAIN), downward solar radiation (SWDOWN)

6.4.2 Changes in Surface Biogenic Emissions

For their contributions to the formation of BSOA, the study of estimating biogenic emissions changes is of great concern over China. Changes in meteorological conditions including solar radiation and temperatures could significantly affect biogenic emissions. In our model, biogenic emissions is calculated online based on the ‘real-time’ temperature and downward solar radiation provided from WRF model and the monthly-mean surface air temperature and downward solar radiation provided by CCSM monthly-mean output data of current (2005–2007) and future (2055–2057) years. The variables in these factors strongly affect the changes in spatial distributions of biogenic emissions. Our model simulates significant increases of isoprene and monoterpenes emissions from 2000s to 2050s under both A1B and B1 scenarios. Figure 6.11a shows the isoprene emissions increased by up to 18 mol km^{-2} hr^{-2} in July from 2000s to 2050s under A1B scenario. The highest increase occurs over 30°N south of China, part of Anhui and Shaanxi province. Figure 6.11c shows monoterpenes also increase over similar area by up to 2.7 mol km^{-2} hr^{-2}. The significant increase is largely determined by the large temperature increase and high forest coverage over these regions. The estimated increases in isoprene emissions under A1B scenario are consistent with the 0 to 20 mol km^{-2} hr^{-2} increase over the contiguous U.S. estimated by Jiang et al. (2010c) using a similar model system during the summertime by 2050s. However, the increases in monoterpenes emissions are generally larger than the estimation in Jiang et al. (2010c).Compared with the A1B scenario, increases in future biogenic isoprene emission under B1 scenario are much smaller especially in South China and Northeast China. The highest increase up to 12 mol km^{-2} hr^{-2}under the B1 scenario occurs over south part of Shaanxi province (Figure 6.11b). Figure 6.11d shows that monoterpenes also increase much smaller over 30°N south of China. Increase in both isoprene and monoterpenes emission over North China and West China are comparable under two scenarios.

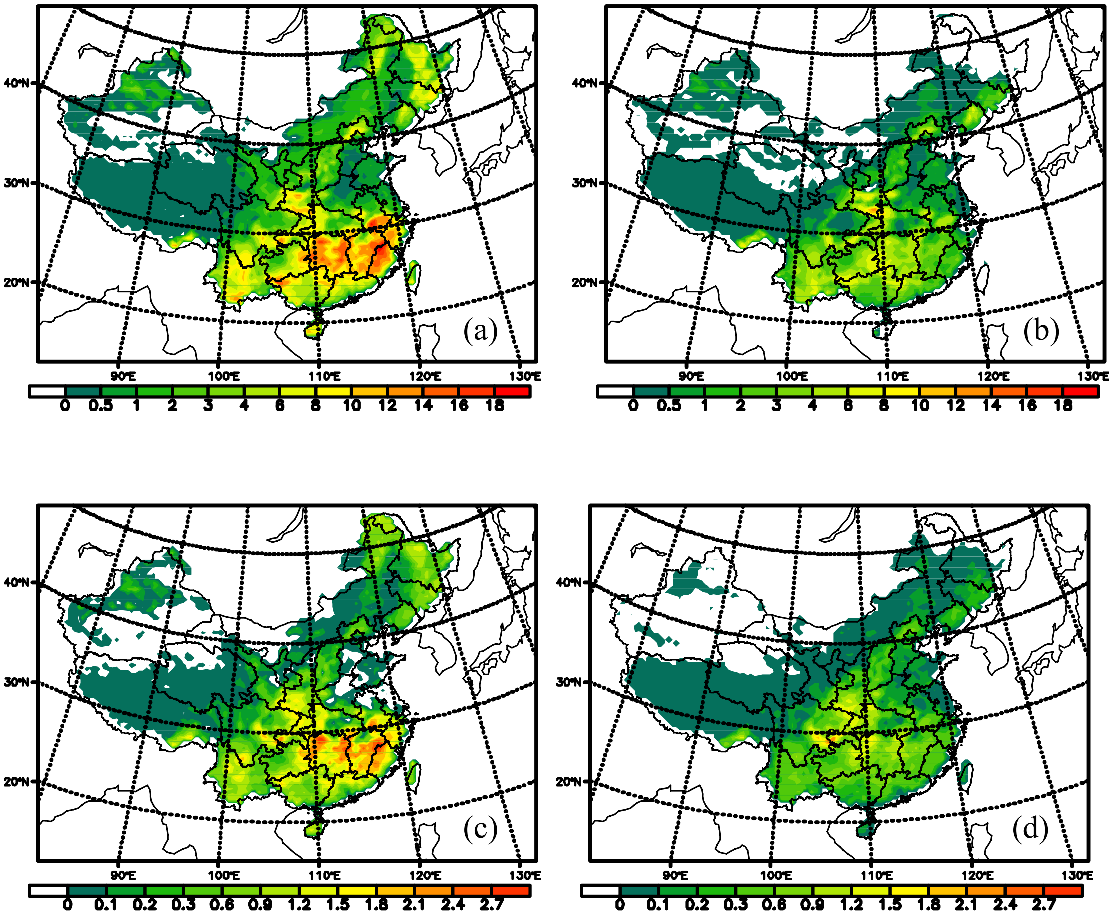

Figure 6.11 Changes in emissions of isoprene (a, b) and monoterpenes (c, d) between present and future climate simulations under A1B (a, c) and B1 (b, d) emission scenarios for the month of July.

The percentage changes in biogenic emissions under two scenarios for the six regions over China are listed in Figure 6.12. Under A1B scenario, Figure 6.12a shows the average biogenic isoprene emissions increased by 16 to 22% in July from 2000s to 2050s over six sub-regions. The percentage changes in the isoprene emissions of different regions are relatively close. The highest percentage up to 22% occurs over the Northeast China. On the contrary, under B1 scenario, the relative changes in biogenic isoprene emissions vary considerably in July from 2000s to 2050s over six sub-regions. The highest increase in percentage up to 30% occurs over the North China and Southwest China, while the smallest increase of 7% is found over Northeast China. For monoterpenes, the changes over South, Southwest, and Northeast China are relatively high under A1B scenario, with the percentage increase of 24.5%, 23.7% and 28.47%, respectively. Under B1 scenario, the percentage changes in the biogenic monoterpenes emissions over different regions are relatively close, except Southwest China (32.8%) and Northeast China (5.54%).

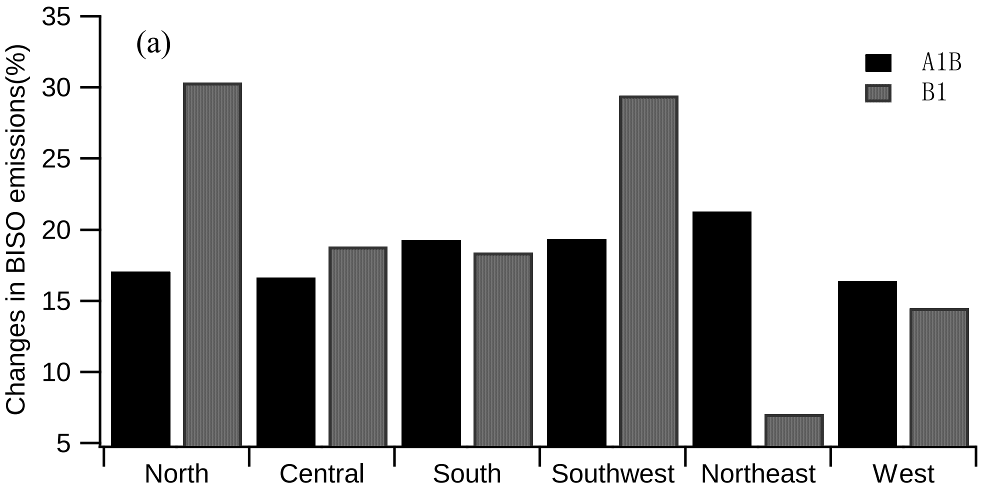

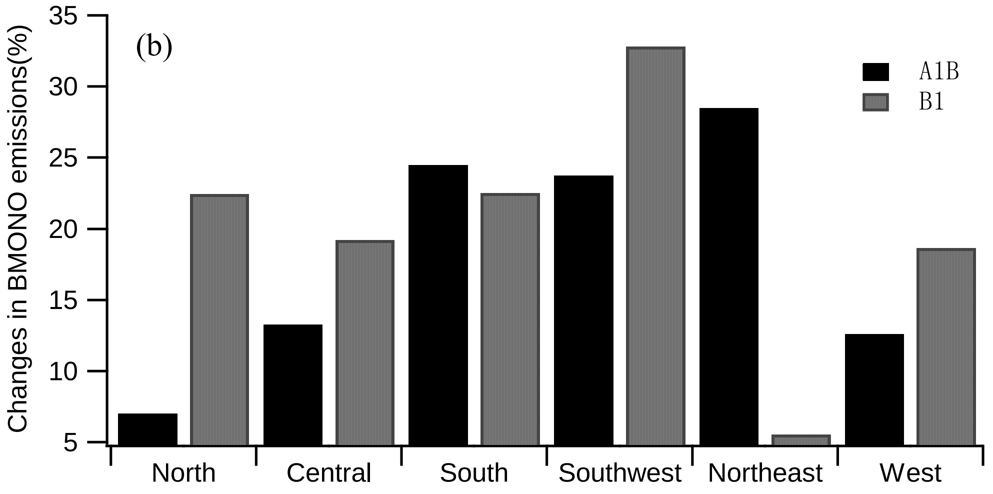

Figure 6.12 Regional biogenic emission changes in six sub-regions over China a) Biogenic isoprene, b) biogenic monoterpenes

6.4.3. Changes in Surface BSOA

Changes in meteorological factors and biogenic emissions, especially the temperature and monoterpenes changes could significantly affect BSOA concentrations. For example, the increase in temperature could decrease the partitioning coefficients and alter the gas-phase reaction rates, which would further affect the SOA formation (Jiang et al., 2010c). Hence, the increase in temperature could also result in the increase in biogenic emissions which will provide more BSOA precursors to the atmosphere.

Our model predicts a significant change of the surface BSOA concentrations ranging from –0.2 to 1.2 μg m^{-3} between the present and future climate under A1B and B1 emission scenarios over much part of China (Figure 6.13). It can be seen that the changes in surface BSOA concentration was dominated by MSOA. The changes in ISOA (–0.05 to 0.25 μg m^{-3}) were relatively small compared to the changes in MSOA concentration (0 to 1μg m^{-3}) except in West China. Under A1B emission scenario, surface BSOA concentration is predicted to increase 0.22 μg m^{-3} on average. The regions with large increases are close to the regions with significant increase of temperature and biogenic emissions, such as the South China, Central China, and Southeast China. The area of the junction of Hunan, Hubei and Jiangxi provinces has the greatest magnitude of increase with concentrations increase between 1 and 1.2 μg m^{-3}. On the other hand, the largest increase up to 1.2 μg m^{-3} is found over Sichuan and Shaanxi province under B1 scenario. The changes of BSOA over West China are relatively small under these two scenarios. The mean surface BSOA concentration is predicted to increase 0.26 μg m^{-3} under B1 scenario.

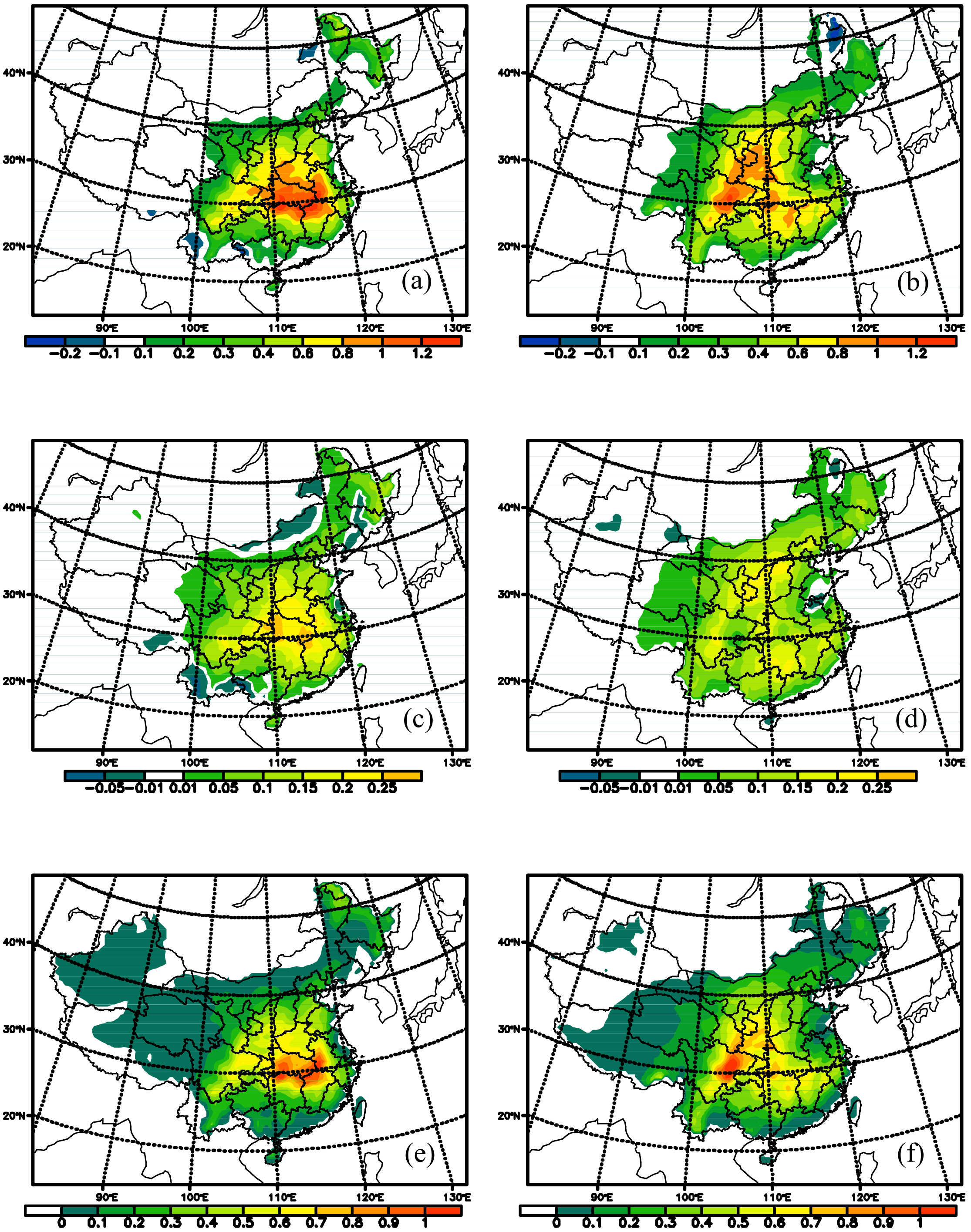

Figure 6.13 Changes in total BSOA (a, b), ISOA (c, d) and MSOA (e, f) concentrations (μg m^{-3}) between present and future climate simulations under A1B (a, c, e) and B1 (b, d, f) emission scenarios for the month of July.

The percentage changes in ISOA and MSOA concentrations under two scenarios for the five regions over China are listed in Figure 6.14. Under A1B scenario, Figure

6.14a shows the surface ISOA concentrations increased by 11 to 23% in July from 2000s to 2050s over five sub-regions. The highest increase up to 23% occurs over the Central China, while the smallest percentage increase is found over Northeast China. On the contrary, under B1 scenario, the smallest percentage increase of 12% occurs over the Central China, while the largest increase of 31% is found over North China. For MSOA, the changes over Northeast China are relatively small under both scenarios, with the percentage increase of 17.3% and 15.6% respectively (Figure 6.14b). The big increase in MSOA concentrations under B1 scenario is seen over the North China (60.6%) and Southwest China (45.5%). Different changes in 2050's biogenic isoprene and monoterpenes emissions are the main factors which cause different changes of BSOA concentrations over different regions. However, the change patterns of biogenic emissions and SOA concentrations are not always consistent. For example, the ISOA concentrations increase by 17.9% over North China which is smaller than the percentage increase (23.6%) over Central China under A1B scenario. The changes in biogenic isoprene emissions over these two regions are quite similar (around 17%). Other than biogenic isoprene emissions, differences in temperature, atmospheric oxidative capability and wind can also affect the ISOA concentrations. Although increase in ISOA precursor emissions will facilitate the ISOA formation, increase in temperature could decrease the partitioning coefficients which could further result in a reduction of ISOA concentrations. In order to separate the effect of biogenic emissions from climate change, Heald et al. (2008) conducted several sensitivity experiments using a global model and indicated that increases in biogenic emissions lead to a 26% increase in SOA concentrations and climate change individually causes a 6% increase which is much smaller.

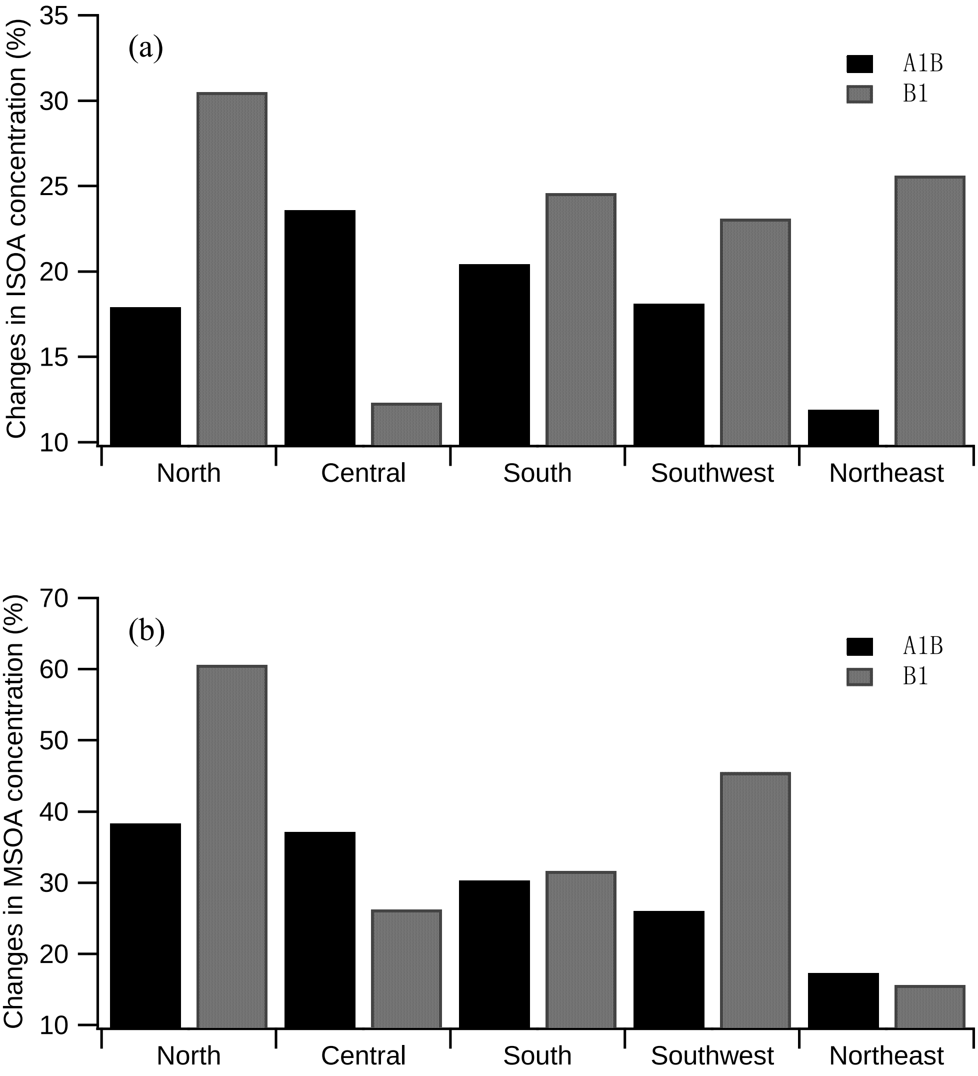

Figure 6.14 Regional BSOA concentration changes in five sub-regions over China a) ISOA, b) MSOA

6.5 Conclusion

The sensitivities of BSOA to future climate change under different scenarios are investigated through an improved modeling system. A parameterization scheme for simulating the isoprene SOA formation is updated to SORGAM module in WRF/Chem. The characteristics of SOA over China in 2006 are investigated in order to examine the performance of the modified model. Note that although uncertainties occurred in SOA simulation, the comparison between the simulated OC, EC concentrations and SOC/OC ratios with observations, and also previous studies indicated the model reasonable captured the less aged SOA levels in China, especially in summertime.

The changes in surface BSOA concentrations due to the changes of climate and biogenic emissions were studied by a series of numerical simulations under A1B and B1 scenarios. The simulations predict that on average near-surface temperature and water vapor mixing ratio are projected to increase 1.5 °C and 0.9 g kg^{-1} under A1B scenario. Significant increase of biogenic isoprene and monoterpenes emission occurs over South, Southwest, and Northeast China. In response to the change in climate and biogenic emissions, the surface BSOA concentration increases 0.22 μg m^{-3} over China, with the highest increase up 1.2 μg m^{-3} occurring over the South China and Central China. Projected changes in regional climate and the subsequent changes in biogenic emissions and BSOA concentrations are scenario dependent. In comparison with A1B, the simulations predict that on average near-surface temperature and water vapor mixing ratio are projected to increase 1.2 °C and 0.3 g kg^{-1} under B1 scenario. The mean surface BSOA concentration increases 0.26 μg m^{-3} over China. Over Southeast

China, mean surface temperature is predicted to increase 2.24°C while mean downward solar radiation is projected to increase 10.6%. Thus, a significant increase of biogenic monoterpenes emission is observed over Southwest China (32.7%). As a result, highest increases in MSOA levels were simulated over Sichuan province, with peaks exceeding 1.0 μg m^{-3}.

Chapter 7 Conclusions and future work

7.1 Conclusions

Over all, this dissertation has achieved the objectives in examining the impact of climate change on air quality over China in the future. Three specific points are summarized as follows:

First, in chapter 4, we use WRF/Chem model to study the O_3 formation mechanisms and the relative contribution of biogenic emissions and anthropogenic sources in East China. The comparison between modeled and measured meteorological fields, hourly O_3 mixing ratios, and hourly NO_2 concentrations illustrates that the modeling system was successfully constructed. On the ground level, the high O_3 mixing ratios (> 45 ppb) are located over Fujian and Jiangxi provinces. The O_3 levels over the YRD and northern Jiangsu are low (< 30 ppb). O_3 process analysis over East China reveals that the high O_3 concentrations over Jiangxi and Fujian are caused by both local photochemical generation and regional transport, while the O_3 concentrations over the YRD region are transported and diffused from surrounding areas. In addition, the contributions of biogenic and anthropogenic emissions as well as the regional transport from domain's upstream regions are discussed. On average, the biogenic and anthropogenic emissions account for 2.6 and 4.5 ppb of daytime mean O_3 mixing ratios in East China, respectively.

Second, in chapter 5, we evaluated the impact of projected changes in future climate and emissions under A1B scenario on O_3 formation over South China in autumn time. 2000-2050 climate changes and the subsequent changes in biogenic emissions result in an increase of 1.6 ppb in the afternoon surface O_3 mixing ratios over the land region in South China. In response to changes in 2000-2050 anthropogenic emission, the surface O_3 afternoon mean mixing ration would increase by 12.8 ppb on average in the land region. The combination effect of climate and emission change would result in an increase of 18.2 ppb in land region. Over PRD, a region of dense network of cities, the 2000-2050 changes in climate and increase in anthropogenic emission increase afternoon mean surface O_3 by 1.5 ppb and 6.1 ppb, respectively. The changes in climate and anthropogenic emission induce greater influence over rural area than over the PRD region, with an increase of 3.9 ppb and 11.4 ppb in afternoon surface O_3 concentrations.

Chapter 5 provides us a scope of understanding how the future climate and emission will affect the surface O_3 air quality over South China. One important conclusion is that even under very stringent pollution control measures so that emission level at 2050s is kept at 2006 level, surface O_3 concentration still increase due to climate change. The second point is that O_3 increase caused by increase in anthropogenic emission (A1B scenario) is much worse than that caused by climate change so emission control measures are mandatory. Third, O_3 control policy is not straight forward. It is indicated that when anthropogenic emissions are greatly increased, regionally O_3 increased but O_3 over metropolitan area will be reduced due to titration effect.

Third, in chapter 6, sensitivity of SOA to future summer climate over China under A1B and B1 scenarios are investigated. Projected changes in meteorological variables including temperature, water vapor, wind speed, PBLH, and precipitation are scenario dependent. A1B scenario induces a warmer and wetter climate in 2050 over China compared to B1 scenario. Specifically, under A1B scenario, the mean near-surface temperature and water vapor mixing ratio are projected to increase 1.5 °C and 0.9 g kg^{-1} under A1B scenario. Significant increase of biogenic isoprene and monoterpenes emission occurs over South, Southwest, and Northeast China under A1B. In response to the change in climate and biogenic emissions, the surface BSOA concentrations increase over China, with the highest increase up 1.2 μg m^{-3} occurring over the South China and Central China. And the simulations predict on average near-surface temperature and water vapor mixing ratio are projected to increase 1.2 °C and 0.3 g kg^{-1} under B1 scenario. Over Southeast China, mean surface temperature is predicted to increase 2.24°C while mean downward solar radiation is projected to increase 10.6%. Thus, a significant increase of biogenic monoterpenes emission is observed over Southwest China (32.7%). As a result, highest increases in MSOA levels were simulated over Sichuan province, with peaks exceeding 1.0 μg m^{-3}. Different changes in biogenic isoprene and monoterpenes emissions are the main factors which cause different changes of BSOA concentrations over different regions. However, the change patterns of biogenic emissions and BSOA concentrations are not always consistent. Other than biogenic emissions, differences in temperature, atmospheric oxidative capability and wind can also affect the SOA concentrations.

7.2 Suggestions for future research

Based on the results the current study, we find that there are still some limitations existing. Thus, a few suggestions are presented for future research as follows:

There are four components of uncertainties in the WRF/Chem modeling system. The uncertainties of the simulation results from this modeling system should be comprehensively evaluated in the future. First, high uncertainties in O_3 precursor's emissions from biogenic and anthropogenic sources could be brought to the WRF/Chem model. As reported from Zhang et al. (2009), there are high uncertainties in China's anthropogenic emissions of NOx, CO and NMVOC at 95% confidence intervals: ±31% (NOx), ±70% (CO), ±68% (NMVOC). Second, CCSM climate model is driven by emissions scenarios to provide future climate predictions to WRF/Chem. High uncertainties in the climate response and projected emissions may also be introduced in WRF/Chem simulation results. Third, the simple chemical boundary condition settings and overestimation of wind speed in boundary layer also result some bias in the simulation results. Fourth, the nonlinear effect in photochemistry may also result some uncertainties in the simulation results.

Chapter 5 provides us some understanding on how the future climate and emission will affect the surface O_3 in South China. As we all know, the simulation results are sensitive to the options of model configuration, e.g. the absence of stratosphere-troposphere exchange, no adjustments for chemical boundary conditions in the future years. These settings may bring some uncertainties to the model results. Therefore, in the future studies, more numerical experiments should be conducted to examine these issues. In this study, we accessed the impacts of climate and emission change under the A1B scenario. As demonstrated by Lin et al. (2008a), the coupled GCM-CTM predicted very different projections of regional O_3 change in response to the A1fi and B1 scenarios. In order to gain a comprehensive understanding, it is necessary to apply a serious of scenarios for similar investigation in the future. Furthermore, China is undergoing significant urbanization processes and will definitely continue to be so in future decades. The effect of future changes in land use should be taken into account.

The work in Chapter 6 reveals that future BSOA formation is sensitive to changes in temperature and biogenic emissions. Currently, the algorithm in MEGAN2.04 estimated the net BVOC emission flux is only light and temperature dependence. However, the BVOC emission is also sensitive to ambient CO_2 concentrations. The effect of future changes in CO_2 concentrations should be taken into account with new algorithm coupled in WRF/Chem model. Besides temperature and biogenic emissions, other factors including primary organic aerosol, anthropogenic emissions, partitioning coefficients, and the ambient concentrations of O_3, NO_x, and OH also influence the SOA formation. Climate change induced by greenhouse gases could significantly affect these factors in the future. Thus, additional sensitivity experiments are needed to quantify the contributions of different factors on SOA formation.

Reference

Ackermann, I.J., Hass, H., Memmesheimer, M., Ebel, A., Binkowski, F.S., U. Shankar, Modal aerosol dynamics model for Europe: Development and first applications, Atmospheric environment, 32, No.17, 2981-2999, 1998.

Aiken, A.C., Decarlo, P.F., Kroll, J.H., Worsnop, D.R., Huffman, J.A., Docherty, K.S., Ulbrich, I.M., Mohr, C., Kimmel, J.R., Sueper, D., Sun, Y., Zhang, Q., Trimborn, A., Northway, M., Ziemann, P.J., Canagaratna, M.R., Onasch, T.B., Alfarra, M.R., Prevot, A.S., Dommen, J., Duplissy, J., Metzger, A., Baltensperger, U., Jimenez, J.L., O/C and OM/OC Ratios of Primary, Secondary, and Ambient Organic Aerosols with High-Resolution Time-of-Flight Aerosol Mass Spectrometry, Environment Science and Technology, 42 (12), 4478–4485, 2008.

Alves, C.A., and Pio, C.A., Secondary organic compounds in atmospheric aerosols: speciation and formation mechanisms, Journal of the Brazilian Chemical Society, 16 (5), 1017–1029, 2005.

Anttila, P., Hyotylainen, T., Heikkila, A., Jussila, M., Finell, J., Kulmala, M., Riekkola, M. L., Determination of organic acids in aerosol particles from a coniferous forest by liquid chromatography-mass spectrometry, Journal of Separation. Science, 28, 337–346, 2005.

Avise, J., Chen, J., Lamb, B., Wiedinmyer, C., Guenther, A., Salathé, E., and Mass, C.: Attribution of projected changes in summertime US ozone and PM2.5 concentrations to global changes, Atmos. Chem. Phys., 9, 1111-1124, 2009.

Aw, J. and Kleeman, M. J., Evaluating the first-order effect of intraannual temperature variability on urban air pollution, Journal of Geophysiccal Research, 108, 4365, 2003.

Baertsch-Ritter, N., Keller, J., Dommen, J., Prevot, A.S.H., Effects of various meteorological conditions and spatial emission resolutions on the ozone concentration and ROG/NOx limitation in the Milan area (I), Atmospheric Chemistry and Physcis, 4, 423–438, 2004.

Barnard, J.C., Chapman, E.G., Fast, J.D., Schmelzer, J.R., Schlusser, J.R., Shetter., R.E., An evaluation of the FAST-J photolysis algorithm for predicting nitrogen dioxide photolysis rates under clear and cloudy sky conditions, Atmospheric Environment, 38, 3393-3403, 2004.

Bell, M. L., Dominici F., Samet J. M., A meta-analysis of time-series studies of ozone and mortality with comparison to the National Morbidity, Mortality, and Air Pollution Study, Epidemiology, 16,436–445, 2005.

Binkowski, F.S., and Shankar, U., The regional particulate matter model, 1. mode desription and preliminary results, Journal of Geophysical research, 100, 26191-26209, 1995.

Brasseur, G. P., Schultz, M., Granier, C., Saunois, M., Diehl, T., Botzet, M., Roeckner, E., and S.Walters., Impact of climate change on the future chemical composition of the global troposphere, Journal of Climate, 19, 3932–3951, 2006.

Briegleb, B.P., Bitz, C.M., Hunke, E.C., Lipscomb, W.H., Holland, M.M., Schramm, J.L., Moritz, R.E., Scientific description of the sea ice component in the Community Climate System Model, Version Three. Tech. Rep. NCAR/TN- 463+STR, National Center for Atmospheric Research, Boulder, CO, 78 pp, 2004.

Camalier, L., Cox, W., Dolwick, P., The effects of meteorology on ozone in urban areas and their use in assessing ozone trends, Atmospheric Environment 41, 7127–7137, 2007.

Cao, J.J., Lee, S.C., Chow, J.C., Watson, J.G., Ho, K.F., Zhang, R.J., Jin, Z.D., Shen, Z.X., Chen, G.C., Kang, Y.M., Zou, S.C., Zhang, L.Z., Qi, S.H., Dai, M.H., Cheng, Y., Hu, K., Spatial and seasonal distributions of carbonaceous aerosols over China, Journal of Geophysical Research, 112, D22S11, 2007.

Cao, J.J., Lee, S.C., Ho, K.F., Zou, S.C., Fung, K., Li, Y., Watson, J.G., Chow, J.C., Spatial and seasonal variations of atmospheric organic carbon and elemental carbon in Pearl River Delta Region, China, Atmospheric Environment, 38, 4447–4456, 2004.

Castro, L.M., Pio, C.A., Harrison, R.M., Smith, D.J.T., Carbonaceous aerosol in urban and rural European atmospheres: estimation of secondary organic carbon concentrations, Atmospheric Environment, 33, 2771–2781, 1999.

Carlton, A.G., Wiedinmyer, C., Kroll, J.H., A review of Secondary Organic Aerosol (SOA) formation from isoprene, Atmospheric Chemistry and Physics, 9, 4987-5005, 2009.

Chameides, W.L., Li, X., Tang, X.Y., Zhou, X.J., Luo, C., Kiang, C.S., St John, J., Saylor, R.D., Liu, S.C., Lam, K.S., Wang, T., Giorgi, F., Is ozone pollution affecting crop yields in China?, Geophysical Research Letters 26, 867-870, 1999.

Chan, C.K., and Yao, X.H., Air pollution in Mega cities in China, Atmospheric Environment, 42, 1–42, 2008.

Chan, C.Y., Xu, X.D., Li, Y.S., Wong, K.H., Ding, G.A., Chan, L.Y., Cheng, X.H., Characteristics of vertical profiles and sources of PM2.5, PM10 and carbonaceous species in Beijing, Atmospheric and Environment, 39, 5113–5124. 2005.

Chen, F., and Dudhia J., Coupling an advanced land-surface/hydrology model with the Penn State/NCAR MM5 modeling system. Part I: model description and implementation, Monthly Weather Review, 129, 569–585, 2001.

Cheung, V. T. F., and Wang, T., Observational study of ozone pollution at a rural site in the Yangtze Delta of China, Atmospheric Environment, 35, 4947–4958, 2001.

Chou, M.D., and Suarez, M.J., An efficient thermal infrared radiation parameterization for use in general circulation models, NASA Technical Memorandum, 104606, 3, 85pp. 1994.

Claeys, M., Graham, B., Vas, G., Wang, W., Vermeylen, R., Pashynska, V., Cafmeyer, J., Guyon, P., Andreae, M.O., Artaxo, P., Maenhaut W., Formation of secondary organic aerosols through photooxidation of isoprene, Science, 303, 1173–1176, 2004.

Clark, T. L., and Karl, T. R., Application of prognostic meteorological variables to forecasts of daily maximum one hour ozone concentration in the northern United States, Journal of Applied Meteorology, 21. 1662-1671, 1982.

Cocker, D.R., Clegg, S.L., Flagan, R.C., Seinfeld, J.H., The effect of water on gas-particle partitioning of secondary organic aerosol. Part I: alpha-pinene/ozone system, Atmospheric Environment, 35(35), 6049-6072, 2001a.

Cocker, D.R., Mader, B.T., Kalberer, M., Flagan, R.C., Seinfeld, J.H., The effect of water ongas-particle partitioning of secondary organic aerosol: II. m-xylene and 1,3,5-trimethylbenzene photooxidation systems, Atmospheric Environment, 35(35), 6073-6085, 2001b.

Collins, W.D., and Coauthors, Description of the NCAR Community Atmosphere Model (CAM3). Tech. Rep. NCAR/TN-464STR, National Center for Atmospheric Research, Boulder, CO, 226 pp, 2004.

Collins, W.D., and Coauthors, The formulation and atmospheric simulation of the Community Atmosphere Model version 3 (CAM3), Journal of Climate, 19, 2144–2161, 2006a.

Collins, William D., and Coauthors, The Community Climate System Model Version 3 (CCSM3), Journal of Climate ,19, 2122–2143, 2006b.

Dan, M., Zhuang, G.S., Li, X.X., Tao, H.R., Zhuang, Y.H., The characteristics of carbonaceous species and their sources in PM2.5 in Beijing, Atmospheric Environment, 38, 3443–3452, 2004.

Dawson, J.P., Adams, P.J., Pandis, S.N., Sensitivity of ozone to summertime climate in the Eastern USA: a modeling case study, Atmospheric Environment, 41, 1494–1511, 2007a.

Dawson, J.P., Adams, P.J., Pandis, S.N., Sensitivity of PM2.5 to climate in the Eastern US: a modeling case study, Atmospheric Chemistry and Physics, 7, 4,295–4,309, 2007b.

DeCarlo, P. F., Kimmel, J. R., Trimborn, A., Northway, M. J., Jayne, J. T., Aiken, A. C., Gonin, M., Fuhrer, K., Horvath, T., Docherty, K. S., Worsnop, D. R., Jimenez, J. L., Field-deployable, high-resolution, time-of-flight aerosol mass spectrometer, Analysis Chemistry, 78, 8281–8289, 2006.

Decesari, S., Facchini, M. C., Matta, E., Lettini, F., Mircea, M., Fuzzi, S., Tagliavini, E., Putaud, J.-P., Chemical features and seasonal variation of fine aerosol water-soluble organic compounds in the Po Valley, Italy, Atmospheric Environment, 35, 3691 – 3699, 2001.

Dickinson, R.E., Oleson, K.W., Bonan, G., Hoffman, F., Thornton, P., Vertenstein, M., Yang, Z.L., Zeng, X., The Community Land Model and its climate statistics as a component of the Community Climate System Model, Journal of Climate, 19, 2302–2324, 2006.

Ding Y.H. and Chan J.C.L., The East Asian summer monsoon: an overview, Meteorology and Atmospheric Physics, 89, 117–142, 2005.

Ding, A. J., Wang, T., Thouret, V., Cammas, J.-P., N´ed´elec, P., Tropospheric ozone climatology over Beijing: analysis of aircraft data from the MOZAIC program, Journal of Geophysical Research, 8(1), 1–13, 2008.

Done, J., Davis, C.A., Weisman, M., The next generation of NWP: Explicit forecasts of convection using the Weather Research and Forecasting (WRF) model, Atmospheric Science Letter, 5, 110–117, 2004.

Drewnick, F., Hings, S. S., DeCarlo, P. F., Jayne, J. T., Gonin, M., Fuhrer, K., Weimer, S., Jimenez, J. L., Demerjian, K. L., Borrmann, S., Worsnop, D. R., A new Time-of-Flight Aerosol Mass Spectrometer (ToF-AMS) – instrument description and first field deployment, Aerosol Science and Technology, 39, 637–658, 2005.

Duan, F.K., He, K.B., Ma, Y.L., Jia, Y.T., Yang, F.M., Lei, Y., Tanaka, S., Okuta, T., Characteristics of carbonaceous aerosols in Beijing, China, Chemosphere, 60, 355–364, 2005.

Duan, J.C., Tan, J.H., Cheng, D.X., Bi, X.H., Deng, W.J., Sheng, G.Y., Fu, J.M., Wong, M.H., Sources and characteristics of carbonaceous aerosol in two largest cities in

Pearl River Delta Region, China, Atmospheric Environment, 41, 2895 – 2903, 2007.

Edney, E.O., Kleindienst, T.E., Jaoui, M., Lewandowski, M., Offenberg, J.H., Wang,W., Claeys, M., Formation of 2-methyl tetrols and 2-methylglyceric acid in secondary organic aerosol from laboratory irradiated isoprene/NOx/SO2/air mixtures and their detection in ambient PM2.5 samples collected in the eastern United States, Atmospheric Environment, 39, 5281–5289, 2005.

Emberson, L., Ashmore, M., Murray, F., Air Pollution Impacts on Crops and Forests, A Global Assessment Imperial College Press, London, U.K, 2003.

Emmons, L.K., Walters, S., Hess, P.G., Lamarque, J.F., Pfister, G.G., Fillmore, D., Granier, C., Guenther, A., Kinnison, D., Laepple, T., Orlando, J., Tie, X., Tyndall, G.,Wiedinmyer, C., Baughcum, S.L., Kloster, S., Description and evaluation of the Model for Ozone and Related chemical Tracers, version 4 (MOZART-4), Geoscientific Model Development, 3, 43–67, 2010.

Fan, S. J., Wang, B. M., Tesche, M., Engelmann, R., Althausen, A., Liu, J., Zhu, W., Fan, Q., Li, M. H., Ta, N., Song, L. L., Leong, K. C., Meteorological conditions and structures of atmospheric boundary layer in October 2004 over Pearl River Delta area, Atmospheric Environment, 42, 6174–6186, 2008.

Fast, J.D., Gustafson Jr., W.I., Easter, R.C., Zaveri, R.A., Barnard, J.C., Chapman, E.G., Grell, G.A., Peckham S.E., Evolution of ozone, particulates, and aerosol direct radiative forcing in the vicinity of Houston using a fully coupled meteorology-chemistry-aerosol model, Journal Geophysical Research, 111, D21305, 2006.

Gao, X. J., Zhao, Z. C., Ding, Y. H., Huang, R.H., Giorgi, F., Climate change due to greenhouse effects in China as simulated by a regional climate model part I: evaluation of the model simulations, Acta Meteorologica Sinica, 61(1), 20—28, 2003a.

Gao, X. J., Zhao, Z. C., Ding, Y. H., Huang, R.H., Giorgi, F., Climate change due to greenhouse effects in China as simulated by a regional climate model part Ⅱ: climate change, Acta Meteorologica Sinica, 61(1), 29—38, 2003b.

Gao, X., Shi, Y., Giorgi, F., A high resolution simulation of climate change over China, Science China Earth Science, 54:462–472, 2011a.

Gao, Y., Liu, X.H., Zhao, C., Zhang, M.G., Emission controls versus meteorological conditions in determining aerosol concentrations in Beijing during the 2008 Olympic Games, Atmospheric Chemistry and Physics,11, 12437–12451, 2011b.

Geng, F., Tie, X., Guenther, A., Li, G., Cao, J., Harley, P., Effect of isoprene emissions from major forests on ozone formation in the city of Shanghai, China, Atmospheric Chemistry and Physics, 11, 10449-10459, 2011.

Grell, G. A., and Dévényi, D., A generalized approach to parameterizing convection combining ensemble and data assimilation techniques, Geophysical Research Letter., 29(14), 1693, 2002.

Grell G.A., Peckham S.E., Schmitz R., Mceen S.A., Fully coupled "online" chemistry within the WRF model: description and application, Atmospheric Environment, 39, 6957–6975, 2005.

Guenther, A., Karl, T., Harley, P., Wiedinmyer, C., Palmer, P.I., Geron, C., Estimates of global terrestrial isoprene emissions using MEGAN (Model of Emissions of Gases and Aerosols from Nature), Atmospheric Chemistry and Physics 6, 3181–3210, 2006.

Guo, H., Jiang, F., Cheng, H.R., Simpson, I.J., Wang, X.M., Ding, A.J., Wang, T.J., Saunders, S.M., Wang, T., Lam, S.H.M., Blake, D.R., Zhang, Y.L., Xie, M., Concurrent observations of air pollutants at two sites in the Pearl River Delta and the implication of regional transport, Atmospheric Chemistry and Physics, 9, 7343-7360, 2009.

Han, Z., Zhang, R., Wang, Q., Wang, W., Cao, J.J., Xu, J., Regional modeling of organic aerosols over China in summertime, Journal of Geophysical Research, 113, D11202, 2008.

He, Y. J., Uno, I., Wang, Z. F., Pochanart, P., Li, J., and Akimoto, H., Significant impact of the East Asia monsoon on ozone seasonal behavior in the boundary layer of Eastern China and the west Pacific region, Atmospheric Chemistry and Physics, 8, 7543-7555, 2008.

Heald, C.L., D.K. Henze, L.W. Horowitz, Feddema, J., Lamarque, J.F., Guenther, A., Hess, P.G., Vitt, F., Seinfeld, J.H., Goldstein, A.H., Fung, I., Predicted change in global secondary organic aerosol concentrations in response to future climate, emissions, and land use change, Journal of Geophysical Research, 113, D05211, 2008.

Held, I.M., and Soden, B.J., Water vapor feedback and global warming, Annual Review Energy Environment, 25, 441–475, 2000.

Henze, D. K., Seinfeld, J. H., Ng, N. L., Kroll, J. H., Fu, T.-M., Jacob, D. J., and Heald, C. L., Global modeling of secondary organic aerosol formation from aromatic hydrocarbons: high- vs. low-yield pathways, Atmospheric Chemistry and Physics, 8, 2405-2420, 2008.

Henze, D.K., and Seinfeld, J.H., Global secondary organic aerosol from isoprene oxidation, Geophysical Research Letters, 33, L09812, 2006.

Hogrefe, C., Lynn, B., Civerolo, K., Ku, J.Y., Rosenthal, J., Rosenzweig, C., Goldberg, R., Gaffin, S., Knowlton, K., Kinney, P.L., Simulating changes in regional air pollution over the eastern United States due to changes in global and regional climate and emissions, Journal of Geophysical Research 109, D22301, 2004.

Hong S.Y., and Lim J.O.J., The WRF Single-Moment 6-Class Microphysics Scheme (WSM6), Journal of the Korean Meteorological Society 42, 129–151, 2006.

Hong, S.Y., Dudhia, J., Chen, S.H., A revised approach to ice microphysical processes for the bulk parameterization of clouds and precipitation, Monthly Weather Review, 132, 103–120, 2004.

Hong, S.Y., and Pan, H.L., Nonlocal boundary layer vertical diffusion in a Medium-Range Forecast model, Monthly Weather Review, 124, 2322–2339, 1996.

Hoyle, C.R., Berntsen, T., Myhre, G., Isaksen, I.S.A., Secondary organic aerosol in the global aerosol – chemical transport model Oslo CTM2, Atmospheric Chemistry and Physics, 7, 5675–5694, 2007.

Hu, X.M., Nielsen-Gammon, J.W., Zhang, F.Q., Evaluation of Three Planetary Boundary Layer Schemes in the WRF Model, Journal of Applied Meteorology and Climatology, 49, 1831–1844, 2010.

Huang, J.P., Fung, J.C.H., Lau, A.K.H., Qin, Y., Numerical simulation and process analysis of typhoon-related ozone episode in Hong Kong, Journal of Geophysical Research, 110, D05301, 2005.

Huang, J.P., Fung, J.C.H., Lau, A.K.H., Integrated processes analysis and systematic meteorological classification of ozone episodes in Hong Kong, Journal of Geophysical Research, 111, D20309, 2006.

Huang, X. Y., Wen Z. P., Du Y. D., Xu Y. L., Scenario analyses on the changes of future surface air temperature and precipitation in south China, Journal of Tropical Meteorology, 24(3), 2008.

Intergovernmental Panel on Climate Change (IPCC), Special Report on Emissions Scenarios : a special report of Working Group III of the Intergovernmental Panel on Climate Change, edited by Nakicenovic, N., Swart, R., Cambridge University Press, New York, 2000.

Intergovernmental Panel on Climate Change (IPCC), Climate Change 2001: The

Scientific Basis—Contribution of Working Group I to the Third Assessment Report of the Intergovernmental Panel on Climate Change, edited by Houghton J.T., Ding, Y., Griggs D.J., Noguer, M., van der Linden, P.J., Dai, X., Maskell, K., and Johnson, C.A., Cambridge University Press, New York, 2001.

Intergovernmental Panel on Climate Change (IPCC), Climate Change 2007: The Physical Scientific Basis. Contribution of Working Group I to the Fourth Assessment Report of the Intergovernmental Panel on Climate Change, edited by Solomon, S., Qin, D., Manning, M., Chen, Z., Marquis, M., Averyt, K.B., Tignor, M., Miller, H.L., Cambridge University Press, New York, 2007.

Jacob, D. J., Winner, D. A., Effect of climate change on air quality, Atmospheric Environment, 42, 51-63, 2009.

Jacob, D.J., Logan, J.A., Yevich, R.M., Gardner, G.M., Spivakovsky, C.M., Wofsy, S.C., Munger, J.W., Sillman, S., Prather, M.J., Rodgers, M.O., Westberg, H., Zimmerman, P.R., Simulation of summertime ozone over North America, Journal of Geophysical Research, 98, 14797-14816, 1993.

Janjic, Z.I., Nonsingular Implementation of the Mellor–Yamada Level 2.5 Scheme in the NCEP Meso model, NCEP Office Note, No. 437, 61 pp, 2002.

Janjic, Z.I., The surface layer in the NCEP Eta Model, Eleventh Conference on Numerical Weather Prediction, Norfolk, VA, American Meteorological Society, Boston, MA, 354–355, 19–23 August, 1996.

Jeffries, H.E., and Crouse R., Scientific and Technical Issues Related to the Application of Incremental Reactivity, report prepared for Western States Petroleum Association, Glendale, CA, September 17, 1990.

Jiang, F., Guo, H., Wang, T.J., Cheng, H.R., Wang, X.M., Simpson, I.J., Ding, A.J., Saunders, S.M., Lam, S.H.M., Blake D.R., An ozone episode in the Pearl River Delta: Field observation and model simulation, Journal of Geophysical Research, 115, D22305, 2010a.

Jiang F., Liu Q., Huang X.X., Wang T.J., Zhuang B.L., Xie M., Regional Modeling of Secondary Organic Aerosol over China by Using WRF/Chem, Journal of Aerosol Science, 43, 57–73, 2012.

Jiang F., Wang T.J., Wang T.T., Xie M., Zhao H., Numerical modeling of a continuous photochemical pollution episode in Hong Kong using WRF–chem., Atmospheric Environment, 42, 8717-8727, 2008a.

Jiang, F., Study on the spatial and temporal distributions of secondary organic aerosols

(SOA) over China and its radiative effects, Nanjing: Nanjing University, 2010b.

Jiang, X. Y., Yang, Z. L., Liao, H., Wiedinmyer, C., Sensitivity of biogenic secondary organic aerosols to future climate change at regional scales An online coupled simulation, Atmospheric Environment, 44, 4891-4907, 2010c.

Jiang, X.Y., Wiedinmyer, C., Chen, F., Yang, Z.L., Lo, J. C.F., Predicted impacts of climate and land use change on surface ozone in the Houston, Texas, area, Journal of Geophysical Research 113, D20312, 2008b.

Jiang, Z. H., Zhang, X., Wang, J. J., Projection Of climate change in China in the 21st century By IPCC-AR4 Models, Geographical Research, 27(4), 2008c.

Johnson, C. E., Stevenson, D. S., Collins, W. J., Derwent, R. G., Relative role of climate and emissions changes on future tropospheric oxidant concentrations, J. Geophys. Res. 104, 18631–18645, 1999.

Johnson, C. E., Stevenson, D. S., Collins, W. J., Derwent, R. G., Role of climate feedback on methane and ozone studied with a coupled ocean-atmosphere-chemistry model, Geophys. Res. Lett., 28, 1723–1726, 2001.

Johnson, K., Carruthers, D., Girnary, S., Athanassiadou, M., Baker, J. Johnson, C., The Local Impact of Climate Change on Air Quality, Report to the Department of Environment Food and Rural Affairs, 2005.

Jonsson, Å. M., Hallquist, M., Ljungström, E., The effect of temperature and water on secondary organic aerosol formation from ozonolysis of limonene, Δ3-carene and α-pinene, Atmospheric Chemistry and Physics, 8, 6541-6549, 2008.

Kain, J. S., The Kain–Fritsch convective parameterization scheme: An update, Journal of Applied Meteorology, 43, 170–181, 2004.

Kanakidou, M., Seinfeld, J.H., Pandis, S.N., Barnes, I., Dentener, F.J., Organic aerosol and global climate modeling: A review. Atmospheric Chemistry and Physics, 5, 1053–1123, 2005.

Kleindienst, T.E., Conver, T.S., McIver, C.D., Edney E.O., Determination of secondary organic aerosol products from the photooxidation of toluene and their implications in ambient PM2.5, Journal of Atmospheric Chemistry, 47(1), 79 – 100, 2004.

Kleindienst, T.E., Edney, E.O., Lewandowski, M., Offenberg, J.H., Jaoui, M., Secondary organic carbon and aerosol yields from the irradiations of isoprene and -pinene in the presence of NOx and SO2, Environmental Science and Technology, 40, 3807–3812, 2006.

Kleindienst, T.E., Lewandowski, M., Offenberg, J.H., Jaoui, M., Edney E.O., Ozone-isoprene reaction: Re-examination of the formation of secondary organic aerosol, Geophysical Research Letter, 34, L01805, 2007.

Kleinman, L. I., The dependence of tropospheric ozone production rate on ozone precursors, Atmospheric Environment, 39, 575–586, 2005.

Kleinman, L.I., Daum, P.H., Imre, D.G., Lee, J.H., Lee, Y.N., Nunnermacker, L.J., Springston, S.R., Weinstein-Lloyd, J., Newman, L., Ozone production in the New York City urban plume, Journal of Geophysical Research, 105, 14495-14512, 2000.

Koo, B.Y., Ansari, A.S., Pandis, S.N., Integrated approaches to modeling the organic and inorganic atmospheric aerosol components, Atmospheric Environment, 37 (4), 4757–4768, 2003.

Kotianova, P., Matisova, E., Puxbaum, H., Lehotay, J., Analysis of organic compounds in aerosols. A review, Chemia Analityczna, 49, 833–844, 2004.

Kroll, J.H., Ng, N.L., Murphy, S.M., Flagan, R.C., Seinfeld, J.H., Secondary organic aerosol formation from isoprene photooxidation under high-NOx conditions, Geophysical Research Letters, 32, L18808, 2005.

Kulmala, M., Laaksonen, A., Pirjola, L., Parameterization for sulphuric acid/water nucleation rates, Journal of Geophysical research, 103, 8301-8307, 1998.

Kwok, R. H. F., Fung, J. C. H., Lau, A. K. H., Fu, J. S., Numerical study on seasonal variations of gaseous pollutants and particulate matters in Hong Kong and Pearl River Delta Region, Journal of Geophysical Research, 115, D16308, 2010.

Lam, K. S., Wang, T. J., Chan, L. Y., Wang, T., Harris, J., Flow patterns influencing the seasonal behavior of surface ozone and carbon monoxide at a coastal site near Hong Kong, Atmospheric Environment, 35, 3121–3135, 2001.

Lam, K.S., Wang, T.J., Wu, C.L., Li, Y.S., Study on an ozone episode in hot season in Hong Kong and transboundary air pollution over Pearl River Delta region of China, Atmospheric Environment 39, 1967-1977, 2005.

Lamsal, L.N., Martin, R.V., Padmanabhan, A., van Donkelaar, A., Zhang, Q., Sioris, C.E., Chance, K., Kurosu, T.P., Newchurch, M.J., Application of satellite observations for timely updates to global anthropogenic NOx emission inventories, Geophysical Research Letter, 38, L05810, 2011.

Lane, T.E., Donahue, N.M., Pandis, S.N., Effect of NOx on secondary organic aerosol concentrations, Environment Science and Technology, 42(16), 6022-6027, 2008.

Langner, J., Bergstrom, R., Foltescu, V., Impact of climate change on surface ozone and deposition of sulphur and nitrogen in Europe. Atmospheric Environment, 39, 1129–1141, 2005.

Lee, A., Goldstein, A.H., Keywood, M.D., Gao, S., Varutbangkul, V., Bahreini, R., Ng, N.L., Flagan, R.C., Seinfeld, J.H., Gasphase products and secondary aerosol yields from the ozonolysis of ten different terpenes, Journal of Geophysical Research, 111, D07302, 2006a.

Lee, A., Goldstein, A.H., Kroll, J.H., Ng, N.L., Varutbangkul, V., Flagan, R.C., Seinfeld, J.H., Gas-phase products and secondary aerosol yields from the photooxidation of 16 different terpenes, Journal of Geophysical Research, 111, D17305, 2006b.

Lee, Y.C., Wenig, M., Yang, X., The emergence of urban ozone episodes in autumn and air temperature rise in Hong Kong, Air Quality, Atmosphere and Health, 2, 111-121, 2009.

Leibensperger, E. M., Mickley, L. J., and Jacob, D. J., Sensitivity of US air quality to mid-latitude cyclone frequency and implications of 1980–2006 climate change, Atmospheric Chemistry and Physcis, 8, 7075-7086, 2008.

Lelieveld, J., and F. J. Dentener, What controls tropospheric ozone?, Journal of Geophysical Research, 105, 3531 – 3551, 2000.

Lerdau, M., Guenther, A., Monson, R., Plant production and emission of volatile organic compounds, Bioscience, 47(6), 373-383, 1997.

Li, H.C., Chen K.S., Huang C.H., Wang H.K., Meteorologically adjusted long-term trend of ground-level ozone concentrations in Kaohsiung County, southern Taiwan, Atmospheric Environment, 44(29), 3605-3608, 2010.

Li, J., Wang, Z., Akimoto, H., Gao, C., Pochanart, P., Wang, X., Modeling study of ozone seasonal cycle in lower troposphere over east Asia, Journal of Geophysical Research, 112, D22S25, 2007.

Liao, H., Chen, W.T., Seinfeld, J.H., Role of climate change in global predictions of future tropospheric ozone and aerosols, Journal of Geophysical Research, 111, D12304, 2006.

Liao, H., Henze, D.K., Seinfeld, J.H., Wu, S., Mickley, L.J., Biogenic secondary organic aerosol over the United States: comparison of climatological simulations with observations, Journal of Geophysical Research 112, D06201, 2007.

Lin, C.Y.C., Jacob, D.J., Fiore, A.M., Trends in exceedances of the ozone air quality standard in the continental United States, 1980–1998, Atmospheric Environment, 35, 3217–3228, 2001.

Lin, J., Nielsen, C.P., Zhao, Y., Lei, Y., Liu, Y., Mcelroy, M.B., Recent changes in particulate air pollution over China observed from space and the ground: effectiveness of emission control, Environmental Science and Technology, 44, 7771–7776, 2010.

Ling, Z.H., Guo, H., Zheng, J.Y., Louie, P.K.K., Cheng, H.R., Jiang, F., Cheung, K., Wong, L.C., Feng, X.Q., Establishing a conceptual model for photochemical ozone pollution in subtropical Hong Kong, Atmospheric Environment, 76, 208–220, 2013.

Lin, J.T., Patten, K.O., Hayhoe, K., Liang, X.Z., Wuebbles, D.J., Effects of future climate and biogenic emissions changes on surface ozone over the United States and China, Journal of Applied Meteorology and Climatology 47, 1888–1909, 2008a.

Lin, M., Holloway, T., Oki, T., Streets, D. G., and Richter, A., Multi-scale model analysis of boundary layer ozone over East Asia, Atmospheric Chemistry and Physics, 9, 3277-3301, 2009a.

Lin, P., Hu, M., Deng, Z., Slanina, J., Han, S., Kondo, Y., Takegawa, N., Miyazaki, Y., Zhao, Y., Sugimoto, N., Seasonal and diurnal variations of organic carbon in PM2.5 in Beijing and the estimation of secondary organic carbon, Journal of Geophysical Research, 114, D00G11, 2009b.

Lin, W., Xu, X., Zhang, X., Tang, J., Contributions of pollutants from North China Plain to surface ozone at the Shangdianzi GAW Station, Atmospheric Chemistry and Physics, 8, 5889–5898, 2008b.

Lin, Y.L., Farley, R.D., Orville, H. D., Bulk parameterization of the snow field in a cloud model, Journal of Climate and Applied Meteorology, 22, 1065–1092, 1983.

Liu S.Y., Gao W., Liang Z.X., A regional climate model downscaling projection of China future climate change, Climate dynamics, doi: 10.1007/s00382-012-1632-5, 2012.

Liu, H. Y., Jacob, D. J., Chan, L. Y., Oltmans, S. J., Bey, I., Yantosca, R. M., Harris, J. M., Duncan, B. N., Martin, R. V., Sources of tropospheric ozone along the Asian Pacific Rim: An analysis of ozonesonde observations, Journal of Geophysical Research, 107(D21), 4573, 2002.

Liu, H.Y., Jacob, D.J., Bey, I., Yantosca, R.M., Duncan, B.N., Sachse, G.W., Transport pathways for Asian combustion outflow over the Pacific: interannual and seasonal variations, Journal of Geophysics Research, 108, 8786, 2003.

Loveland, T.R., Merchant, J.W., Ohlen, D.O., Brown, J.F., Development of a landcover characteristics database for the conterminous U.S, Photogrammetric Engineering and Remote Sensing 57, 1453-1463, 1991.

Luo, C., John, J.C. St., Zhou, X., Lam, K.S., Wang, T., Chameides, W. L., A nonurban ozone air pollution episode over eastern China: observations and model simulations, Journal of Geophysical Research, 105(D2), 1889–1908, 2000.

Madronich, S., Photodissociation in the atmosphere, 1, actinic flux and the effects of ground reflections and clouds, Journal of Geophysical Research, 92, 9740–9752, 1987.

Mauderly, J.L., and Chow, J.C., Health Effects of Organic Aerosols. Inhalation Toxicology, 20 (3), 257–288, 2008.

McKeen, S. A., Wotawa, G., Parrish, D. D., Holloway, J. S., Buhr, M. P., Hubler, G., Fehsenfeld, F. C., and Meagher, J. F., Ozone production from Canadian wildfires during June and July of 1995, Journal of Geophysical Research 107(D14), 4192, 2002.

Meehl, G.A., Covey, C., McAvaney, B., Latif, M., Stouffer, R. J., The Coupled Model Intercomparison Project, Bulletin of the American Meteorological Society, 86, 89–93, 2005.

Mickley, L.J., Jacob, D.J., Field, B.D., Rind, D., Effects of future climate change on regional air pollution episodes in the United States, Geophysical Research Letter, 31, 24, L24103, 2004.

Millstein, D.E., Harley, R.A., Impact of climate change on photochemical air pollution in Southern California, Atmospheric Chemistry and Physics, 9, 11, 3745-3754, 2009.

Mlawer E.J., Taubman S.J., Brown P.D., Iacono M.J., Clough S.A., Radiative transfer for inhomogeneous atmosphere: RRTM, a validated correlated-k model for the longwave, Journal of Geophysical Research, 102 (D14), 16663–16682, 1997.

Monin, A.S., Obukhov, A.M., Basic laws of turbulent mixing in the surface layer of the atmosphere, Contributions of the Geophysical Institute of the Slovak Academy of Sciences, 151, 163–187, 1954.

Murphy, D.M., Cziczo, D.J., Hudson, P. K., Thomson, D. S., Carbonaceous material in aerosol particles in the lower stratosphere and tropopause region, Journal of Geophysical Research, 112, D04203, 2007.

Ng, N.L., Chhabra, P.S., Chan, A.W.H., Surratt, J.D., Kroll, J.H., Kwan, A.J., McCabe, D.C., Wennberg, P.O., Sorooshian, A., Murphy, S.M., Dalleska, N.F., Flagan, R.C., Seinfeld, J.H., Effect of NO_x level on secondary organic aerosol (SOA) formation from the photooxidation of terpenes, Atmospheric Chemistry and Physics, 7(19), 5159-5174, 2007.

Ng, N.L., Kwan, A.J., Surratt, J.D., Chan, A.W.H., Chhabra, P.S., Sorooshian, A., Pye, H.O.T., Crounse, J.D., Wennberg, P.O., Flagan, R.C., Seinfeld, J.H., Secondary organic aerosol (SOA) formation from reaction of isoprene with nitrate radicals (NO_3), Atmospheric Chemistry and Physics, 8, 4117–4140, 2008.

Nolte, C.G., Gilliland, A.B., Hogrefe, C., Mickley, L.J., Linking global to regional models to assess future climate impacts on surface ozone levels in the United States, Journal of Geophysical Research, 113, D14307, 2008.

NRC, Committee on Tropospheric Ozone: Rethinking the Ozone Problem in Urban and Regional Air Pollution, 1991.

Odum, J.R., Hoffmann, T., Bowman, F., Collins, D., Flagan, R.C., Seinfeld, J.H., Gas/particle partitioning and secondary organic aerosol yields. Environment Science and Technology, 30, 2580–2585, 1996.

Odum, J.R., Jungkamp, T.P.W., Griffin, R.J., Forstner, H.J.L., Flagan R.C., and Seinfeld, J.H., Aromatics, reformulated gasoline, and atmospheric organic aerosol formation, Environmental Science and Technology 31(7), 1890-1897, 1997.

Offenberg, J.H., Kleindienst, T.E., Jaoui, M., Lewandowski, M., Edney, E.O., Thermal properties of secondary organic aerosols, Geophysical Research Letters, 33, 2006.

Oleson, K.W., Bonan, G.B., Levis, S., Thornton, P., Vertenstein, M., Yang, Z., Dai, Y., Bosilovichm, M., Dickinson, R., Dirmeyer, P., Hoffman, F., Houser, F., Houser, P., Niu, G., Zeng, X., Technical description of the Community Land Model (CLM), Tech. Rep. NCAR/TN-461STR, National Center for Atmospheric Research, Boulder, CO, 174 pp, 2004.

Ordonez, C., Mathis, H., Furger, M., Henne, S., Hoglin, C., Staehelin, J., Prevot, A.S.H., Changes of daily surface ozone maxima in Switzerland in all seasons from 1992 to 2002 and discussion of summer 2003, Atmospheric Chemistry and Physics, 5, 1187–1203, 2005.

Pandis, S.N., Harley, R.A., Cass, G.R., Seinfeld, J.H., Secondary organic aerosol formation and transport. Atmospheric Environment, 26, 2269–2282. 1992.

Pankow, J.F., An absorption model of gas/particle partitioning involved in the formation of secondary organic aerosol, Atmospheric Environment, 28, 189-193, 1994.

Piccot, S.D., Watson, J.J., Jones, J.W., Global inventory of volatile organic compound emissions from anthropogenic sources, Journal of Geophysical Research, 97, 9897–9912, 1992.

Polidori, A., Turpin, B. J., Davidson, C. I., Rodenburg, L. A., Maimone, F., Organic PM2.5: Fractionation by polarity, FTIR spectroscopy, and OM/OC ratio for the Pittsburgh aerosol, Aerosol Science and Technology, 42, 233–246, 2008.

Presto, A.A., Hartz, K.E.H., Donahue, N.M., Secondary organic aerosol production from terpene ozonolysis. 2. Effect of NO_x concentration, Environmental Science and Technology, 39(18), 7046-7054, 2005.

Pun, B.K., Balmori, R.T.F., Seigneur, C., Modeling wintertime particulate matter formation in central California, Atmospheric Environment, 43, 402–409, 2009.

Qian, Y., Gustafson Jr., W.I., Fast, J.D., An investigation of the sub-grid variability of trace gases and aerosols for global climate modeling, Atmospheric Chemistry and Physics, 10, 6917-6946, 2010.

Ran, L., Zhao, C., Geng, F., Tie, X., Tang, X., Peng, L., Zhou, G., Yu, Q., Xu, J., Guenther, A., Ozone photochemical production in urban Shanghai, China: analysis based on ground level observations, Journal of Geophysical Research, 114, D15301, 2009.

Robinson, A.L., Donahue, N.M., Shrivastava, M.K., Weitkamp, E.A., Sage, A.M., Grieshop, A.P., Lane, T.E., Pierce, J.R., Pandis, S.N., Rethinking organic aerosols: semivolatile emissions and photochemical aging, Science, 315, 1259–1262, 2007.

Saikawa, E., Naik, V., Horowitz, L.W., Liu, J.F., Mauzerall D.L., Present and potential future contributions of sulfate, black and organic carbon aerosols from China to global air quality, premature mortality and radiative forcing, Atmospheric Environment, 43, 2814–2822, 2009.

Sax, M., Zenobi, R., Baltensperger, U., Kalberer, M., Time resolved infrared spectroscopic analysis of aerosol formed by photo-oxidation of 1,3,5-trimethylbenzene and -pinene, Aerosol Science and Technology, 39, 822–830, 2005.

Schell B., Ackermann, I.J., Hass, H., Binkowski, F.S., Ebel, A., Modeling the formation of secondary organic aerosol within a comprehensive air quality model system, Journal of Geophysical research, 106, 28275-28293, 2001.
Schlünzen, K.H., and Katzfey, J.J.: Relevance of sub-grid-scale land-use effects for mesoscale model, Tellus, 55A, 232–246 (2003).

Shan, W., Yin, Y., Zhang, J., Ji, X., Deng, X., Surface ozone and meteorological conditions in a single year at an urban site in central-eastern China, Environmental Monitoring Assessment, 151, 127–141, 2009.

Sillman, S., and Samson, F. J., Impact of Temperature on Oxidant Photochemistry in Urban, Polluted Rural and Remote Environments, Journal of Geophysical Research, 100, 11497–11508, 1995.

Sillman, S., Logan, J. A., Wofsy, S. C., The sensitivity of ozone to nitrogen oxides and hydrocarbons in regional ozone episodes, Journal of Geophysical Research, 95, 1837-1851, 1990.

Simmons, A.J., and Burridge, D.M., An Energy and Angular-Momentum Conserving Vertical Finite-Difference Scheme and Hybrid Vertical Coordinates, Monthly Weather Review, 109, 758–766, 1981.

Skamarock, W.C. and Klemp, J.B., A time-split non-hydrostatic atmospheric model for weather research and forecasting applications. Journal of Computer Physics, 227, 3465-3485, 2008.

Skamarock, W.C., Klemp, J.B., Dudhia, J., Gill, D.O., Barker, D.M., Duda, M.G., Huang, X.Y., Wang, W., Powers, J.G., A Description of the Advanced Research WRF version 3, NCAR Tech. Note NCAR/TN-475+STR, 113 pp, 2008.

Smith, R. D., and P. R. Gent, Reference manual for the Parallel Ocean Program (POP) ocean component of the Community Climate System Model (CCSM2.0 and 3.0), Tech. Rep. LA-UR-02-2484, Los Alamos National Laboratory, 2002.

Song, C., Zaveri, R.A., Alexander, M.L., Thornton, J.A., Madronich, S., Ortega, J.V., Zelenyuk, A., Yu, X.Y., Laskin, A., Maughan, D.A., Effect of hydrophobic primary organic aerosols on secondary organic aerosol formation from ozonolysis of α-pinene, Geophysical Research Letter, 34, L20803, 2007.

Staehelin, J., Harris, N.R.P., Appenzeller, C., Eberhard, J., Ozone trends: A review, Reviews of Geophysics, 39, 231 – 290, 2001.

Stauffer, D.R., and Seaman, N.L.: Use of four-dimensional data assimilation in a limited-area mesoscale model, Part I: Experiments with synoptic-scale data. Mon.

Wea. Rev., 118, 1250–1277 (1990).

Steiner, A. L., Tonse, S., Cohen, R. C., Goldstein, A. H. and Harley, R. A., Influence of future climate and emissions on regional air quality in California, Journal of Geophysical Research, 111, D18, 2006

Steven, E.K., Benjamin, S.G., McGinley, J.A., Brown, J.M., Schultz, P., Szoke, E.J., Smirnova, T.G., Shaw, B.L., Birkenheuer, D., Albers, S., Peckham, S.E., & Grell, G.A. Real-time applications of the WRF model at the Forecast Systems Laboratory, In: 84th AMS Annual Meeting, Seattle, USA, January 10–15, 2004.

Stevenson, D., Doherty, R., Sanderson, M., Johnson, C., Collins, B., Derwent, D., Impacts of climate change and variability on tropospheric ozone and its precursors, Faraday Discussions, 130, 1–17, 2005.

Stockwell, W.R., Kirchner, F., Kuhn, M., Seereld, S., A new mechanism for regional atmospheric chemistry modeling, Journal of Geophysical Research, 102, 25847–25879, 1997.

Stockwell, W.R., Middleton, P., Chang, J.S., Tang, X., The secondgeneration regional acid deposition model chemical mechanism for regional air quality modeling, Journal of Geophysical Research 95, 16343–16367, 1990.

Strader R., Lurnmann, F., Pandis, S.N., Evaluation of secondary organic aerosol formation in winter, Atmospheric Environment, 33, 4849-4863, 1999.

Streets D.G., Yarber K.F., Woo J.H., Carmichael G.R., Biomass burning in Asia: annual and seasonal estimates and atmospheric emissions, Global Biogeochemical Cycles, 17, 1099, 2003.

Sun, J.Y., Zhang, Q., Canagaratna, M.R., Zhang, Y.M., Ng, N.L., Sun, Y.L., Jayne, J.T., Zhang, X.C., Zhang, X.Y., Worsnop, D.R., Highly time-andsize-resolved characterization of submicron aerosol particles in Beijing using an aerodyne aerosol mass spectrometer, Atmospheric Environment, 44, 131－140, 2010.

Thornton, J.A., Wooldridge, P.J., Cohen, R.C., Martinez, M., Harder, H., Brune, W.H., Williams, E.J., Roberts, J.M., Fehsenfeld, F.C., Hall, S.R., Shetter, R.E., Wert, B.P., Fried, A., Ozone production rates as a function of NO_x abundances and HO_x production rates in the Nashville urban plume, Journal of Geophysical Research,107(D12), 4146, 2002.

Tie, X., Madronich, S., Walters, S., Zhang, R., Rasch, P., Collins, W., Effect of clouds on photolysis and oxidants in the troposphere, Journal of Geophysical Research, 108(D20), 4642, 2003.

Tie, X.X., Madronich, S., Li, G.H., Ying, Z.M., Zhang, R.Y., Garcia, A.R., Lee-Taylor, J., Liu, Y.B., Characterizations of chemical oxidants in Mexico City: A regional chemical dynamical model (WRF-Chem) study, Atmospheric Environment, 41, 1989–2008, 2007.

Trenberth, K.E., Berry J.C., Buja, L.E., Vertical interpolation and truncation of model-coordinate data, NCAR/TN-396+STR, 1993.

Tsigaridis, K. and Kanakidou, M., Global modeling of secondary organic aerosol in the troposphere: A sensitivity analysis, Atmospheric Chemistry and Physics, 3, 1849–1869, 2003.

Tuccella, P., Curci, G., Visconti, G., Bessagnet, B., Menut, L., Park, R. J., Modeling of gas and aerosol with WRF/Chem over Europe: Evaluation and sensitivity study, Journal of Geophysical Research, 117, D03303, 2012.

Unger, N., Shindell, D. T., Koch, D. M., Amann, M., Cofala, J., Streets, D. G., Influences of man-made emissions and climate changes on tropospheric ozone, methane, and sulfate at 2030 from a broad range of possible futures, Journal of Geophysical Research, 111, D12313, 2006.

Volkamer, R., Martini, F.S., Molina, L.T., Salcedo, D., Jimenez, J.L., Molina, M.J., A missing sink for gas-phase glyoxal in Mexico City: Formation of secondary organic aerosol, Geophysical Research Letters, 34, 2007.

Vukovich F. M., Bach W. D., Crissman B. W., King W. J., On the relationship between high ozone in the rural surface layer and high pressure system, Atmospheric Environment, 11, 967-983, 1977.

Wagener, S., Langner, M., Hansen, U., Moriske, H.J., Endlicher, W., Spatial and seasonal variations of biogenic tracer compounds in ambient PM10 and PM1 samples in Berlin, Germany, Atmospheric Environment, 47, 33–42, 2012.

Wang, H.X., Zhou, L.J., Tang, X.Y., Ozone concentrations in rural regions of the Yangtze Delta in China, Journal of Atmospheric Chemistry 54, 255–265, 2006a.

Wang, J., Zhuang, M.Z., Yang, H.B., Zhang, X.M., Cao, C., Huang, Z., Characteristics of organic and element carbon aerosols in PM10 in Xiamen, Environment Chemistry, 25(4), 518– 519, 2006b.

Wang, Q.G., Han, Z.W., Wang, T.J., Zhang, R.J., Impacts of biogenic emissions of VOC and NOx on tropospheric ozone during summertime in eastern China, Science of the Total Environment, 395, 41-49, 2008.

Wang, S.X., Zhao, M., Xing, J., Wu, Y., Zhou, Y., Lei, Y., He, K.B., Fu, L.X., Hao, J.M., Quantifying the air pollutants emission reduction during the 2008 Olympic Games in Beijing, Environmental Science & Technology 44, 2490-2496, 2010a.

Wang, T., Cheung, V. T. F., Anson, M., Li, Y. S., Ozone and related gaseous pollutants in the boundary layer of eastern China: Overview of the recent measurements at a rural site, Geophysical Research Letter, 28, 2373–2376, 2001.

Wang, T., Guo, H., Blake, D. R., Kwok, Y. H., Simpson, I. J., Li, Y. S., Measurements of trace gases in the inflow of South China Sea background air and outflow of regional pollution at Tai O, Southern China, J. Atmospheric Chemistry, 52, 295–317, 2005a.

Wang, T., Wei, X. L., Ding, A. J., Poon, C. N., Lam, K. S., Li, Y. S., Chan, L. Y., and Anson, M., Increasing surface ozone concentrations in the background atmosphere of Southern China, 1994–2007, Atmospheric Chemistry and Physics, 9, 6217-6227, 2009.

Wang, T.J., Jiang, F., Deng, J.J., Shen, Y., Fu, Q.Y.,Wang, Q., Fu, Y., Xu, J.H., Zhang, D.N., Urban air quality and regional haze weather forecast for Yangtze River Delta region, Atmospheric Environment, 58, 70–83, 2012.

Wang, X., Zhang, Y., Hu, Y., Zhou, W., Lu, K., Zhong, L., Zeng, L., Shao, M., Hu, M., Russell, A.G., Process analysis and sensitivity study of regional ozone formation over the Pearl River Delta, China, during the PRIDE-PRD2004 campaign using the Community Multiscale Air Quality modeling system. Atmospheric Chemistry Physics, 10, 4423-4437, 2010b.

Wang, X.M., Carmichael G, Chen D.L., Tang Y.H., Wang T.J., Impacts of different emission sources on air quality during March 2001 in the Pearl River Delta (PRD) region, Atmospheric Environment, 39(29), 5227–5241, 2005b.

Wang, Z.Y., Hao, L.Q., Zhang, W.J., Chemical processes on the formation of secondary organic aerosols, Progress in Chemistry 17 (4), 732–739, 2005c.

Wei, X.L., Li, Y.S., Lam, K.S., Wang, A.Y., Wang, T.J., Impact of biogenic VOC emissions on a tropical cyclone-related ozone episode in the Pearl River Delta region, China, Atmospheric Environment 41, 7851-7864, 2007.

Wei, X.L., Liu, Q., Lam, K.S., Wang, T. J., Impact of precursor levels and global warming on peak ozone concentration in the PRD region of China, Advances in Atmospheric Science, 29(3), 635–645, 2012.

Whitby, E.R., McMurry, P.H., Shankar, U., Binkowski, F.S., Modal aerosol dynamics modeling, Rep. 600/3-91/020, Atmospheric Research and Exposure Assessment Laboratory, US Environmental Protection Agency, Research Triangle Park, NC, 1991. (Available as NTIS PB91- 1617291AS from National Technical Information Service, Springfield, VA).

Wigley, T. M. L., Smith, S. J., Prather, M. J., Radiative forcing due to reactive gas emissions, Journal of Climate, 15(18), 2690– 2696, 2002.

Wild, O., Zhu, X., Prather, M.J., Fast, J., Accurate simulation of in- and below-cloud photolysis in tropospheric chemical models, Journal of Atmospheric Chemistry, 37, 245-282, 2000.

Wu, S., Mickley, L.J., Jacob, D.J., Rind, D., Streets, D.G., Effects of 2000–2050 changes in climate and emissions on global tropospheric ozone and the policy-relevant background ozone in the United States, Journal of Geophysical Research, 113, D18312, 2008a.

Wu, S., Mickley, L.J., Leibensperger, E.M., Jacob, D.J., Rind, D., Streets, D.G., Effects of 2000–2050 global change on ozone air quality in the United States, Journal of Geophysical Research, 113, D06302, 2008b.

Xu, X., Lin, W., Wang, T., Yan, P., Tang, J., Meng, Z., Wang, Y., Long-term trend of surface ozone at a regional background station in eastern China 1991–2006: enhanced variability, Atmospheric Chemistry and Physics, 8, 2595–2607, 2008.

Yu, S., Bhave, P. V., Dennis, R. L., and Mathur, R., Seasonal and regional variations of primary and secondary organic aerosols over the Continental United States, Semi-empirical estimates and model evaluation, Environment Science and Technology, 41, 4690–4697, 2007

Zaveri, R. A., and Peters, L.K., A new lumped structure photochemical mechanism for large-scale applications, Journal of Geophysical Research104, 30387–30415, 1999.

Zaveri, R.A., Easter, R.C., Fast, J.D., Peters, L.K., Model for simulating aerosol interactions and chemistry (MOSAIC), Journal Geophysical Research, 113, D13204, 2008.

Zhang Q., Streets D.G., Carmichael G.R., He K., Huo H., Kannari A., Klimont Z., Park, I.S., Reddy, S., Fu, J.S., Chen, D., Duan, L., Lei, Y., Wang, L.T., Yao, Z.L., Asian emissions in 2006 for the NASA INTEX-B mission, Atmospheric Chemistry and Physics, 9, 5131–5153, 2009.

Zhang, J., Wang, T., Chameides, W.L., Cardelino, C., Kwok, J., Blake, D.R., Ding, A., So, K.L., Ozone production and hydrocarbon reactivity in Hong Kong, Southern China. Atmospheric Chemistry and Physics 7, 557-573, 2007a.

Zhang, Q., Streets, D.G., He, K.B., Wang, Y.X., Richter, A., Burrows, J.P., Uno, I., Jang, C.J., Chen, D., Yao, Z.L., Lei Y., NO_x emission trends for China, 1995–2004: the view from the ground and the view from space, Journal of Geophysical Research, 112, D22306, 2007b.

Zhang, X.Y., Wang, Y.Q., Zhang, X.C., Guo, W., Gong, S.L., Carbonaceous aerosol composition over various regions of China during 2006, Journal of Geophysical Research, 113, D14111, 2008a.

Zhang, Y. H., Hu, M., Zhong, L. J., Wiedensohler, A., Liu, S. C., Andreae, M. O., Wang, W., Fan, S. J., Regional integrated experiments on air quality over Pearl River Delta 2004 (PRDIEPRD2004): Overview, Atmospheric Environment, 42, 6157–6173, 2008b.

Zhang, Y., Hu, X.M., Leung, L.R., Gustafson Jr.,W.I., Impacts of regional climate change on biogenic emissions and air quality, Journal of Geophysical Research, 113, D18310, 2008c.

Zhang, Y., Online Coupled Meteorology and Chemistry models: History, Current Status, and Outlook, Atmospheric Chemistry and Physics, 8, 2895-2932, 2008d.

Zheng, J.Y., Zhong, L.J., Wang, T., Louie, P.K.K., Li, Z.C., Ground-level ozone in the Pearl River Delta region: Analysis of data from a recently established regional air quality monitoring network, Atmospheric Environment 44, 814-823, 2010.